

**Development of Cost-Effective Membrane-Electrode-Assembly (MEA) for
Direct Borohydride Fuel Cells**

DISSERTATION

Presented in Partial Fulfillment of the Requirements for the Degree of
Doctor of Philosophy in the Graduate School of
The Ohio State University

By

Jia Ma, B.Eng., M.S.

Graduate Program in Materials Science and Engineering

The Ohio State University

2012

Dissertation Committee:

Professor Yogeshwar Sahai, Advisor

Professor Rudy Buchheit

Professor Yunzhi Wang

Copyright by

Jia Ma

2012

Abstract

A DBFC is an electrochemical device that generates electrical energy by electro-oxidation of borohydride ion (BH_4^-) and electro-reduction of an oxidant. Usually, a DBFC employs an alkaline solution of sodium borohydride (NaBH_4) as the fuel, and oxygen or hydrogen peroxide as the oxidant. DBFCs are considered attractive energy suppliers because of their high electrochemical activity, open circuit potential, energy storage capacity, and power performance at ambient temperature. The key component of a DBFC is membrane-electrode-assembly (MEA). To facilitate the successful commercialization of DBFCs, high-performance and cost-effective MEA must be developed. This research attempts to develop an effective MEA of a DBFC using low-cost materials.

An active single fuel cell system was set up and optimized, and this provides platform to investigate MEA performance. Borohydride ions undergo electro-oxidation readily on non-precious electrocatalyst materials, which provides a solution to reduce DBFC cost. Ni-based composite was employed as anode electrocatalyst. High power performance and reasonable stability were achieved by a DBFC with the prepared Ni-based composite anode catalyst. Different co-catalysts (palladium on carbon and platinum on carbon), anode substrates (carbon paper and Ni foam) were employed and compared. Ni foam was

found to be an effective anode substrate which facilitates mass transport and extends electrochemical active area.

An important constituent of an electrochemical energy conversion or storage device is electrode binder. Polymers, particularly Nafion[®] ionomer, are generally employed as electrode binders in various types of fuel cells. To replace expensive Nafion[®] material, alternative electrode binders were developed based on polyvinyl alcohol (PVA) and chitosan. Both PVA and chitosan are low-cost materials, and chitosan is derived from a natural abundant biopolymer. Both PVA and chitosan chemical hydrogel were prepared and found to be efficient as electrode binder in DBFCs in terms of electrode stability and yielding high electrochemical performance.

In addition, membrane electrolytes based on PVA and chitosan were developed. A PVA chemical hydrogel membrane was prepared and employed in a DBFC using oxygen as oxidant, and this cell achieved a peak power density a little higher than that using Nafion[®] membranes. A chitosan hydrogel membrane was prepared by covalently cross-linking chitosan with glutaraldehyde homogeneously. A chitosan membrane was also heterogeneously modified with sulfuric acid/sulfate, phosphate, or triphosphate. A chitosan-based DBFC gave significantly superior power performance and comparable stability and efficiency to a Nafion[®]-based DBFC.

Various studies have demonstrated that a DBFC is able to give high power performance with low-cost MEA materials. The use of Ni-based anode, polymer chemical

hydrogel electrode binder and membrane electrolyte based on PVA or chitosan would reduce cost of DBFC and thus may help its commercialization.

Dedication

This document is dedicated to my family.

Acknowledgements

The completing of a dissertation would not have been possible without the help of numerous people. Thus my sincere gratitude goes to my family, my friends, and my companions and superiors at the Ohio State University for their love and support over the last few years.

I sincerely thank my esteemed advisor, Dr. Yogeshwar Sahai, for leading me to the area of fuel cell and electrochemistry that is of great interest to myself. I express my deepest gratitude to him for his painstaking tutelage, expert guidance, continuous encouragement and inspiration, during the course of my graduate study. The financial assistance provided by the Third Frontier Fuel Cell Program of State of Ohio is gratefully acknowledged. The collaboration and financial support from ITN Energy Systems of Littleton Colorado is also deeply appreciated.

I wish to thank Dr. Rudy Buchheit, Dr. Yunzhi Wang, Dr. Ji-Cheng Zhao, Dr. Xiaodong Sun, who served as my candidacy exam, or dissertation committee members, for their perspective comments and insightful criticism of my work. I extend my thanks to Dr. Suliman Dregia, Dr. Henk Verweij, Dr. James Williams for their invaluable help in my candidacy exam and on various other occasions.

My graduate research has been made more efficient and also extensive with the support of many MSE faculty, staff and graduate students. Thus, my special thanks go out to Dr.

Jianjun Guan and Zhenqing Li for their help in polymer characterization and helpful suggestions; Dr. John Lannutti and Carol Lee for their help in mechanical test; Dr Nitin Padture and his graduate students for their help in electrodeposition; Dr. Krenar Shqau and Dr. Lanlin Zhang for their help in setting up Keithley instrument and related software; my former colleague and labmate, Dr. Nurul A. Choudhury, for his assistance in lab work in strenuous times and valuable discussions of my research; Dr. Belinda L. Hurley for her help in Gamry electrochemical system and analytical spectroscopy; Dr. Gordon Renkes for his help in infrared spectroscopy; Mr. Steve Bright for his help in conducting TGA, DSC, XRD measurements; and Mr. Ken Kushner and Mr. Ross Baldwin for their help in lab facilities.

My graduate studies would not have been the same without the social and academic support provided by many MSE colleagues. I am particularly thankful to Mark Cooper, Mei Wang, Ning Zhou, Hongqing Sun, Lin Li, Li Sun, Kun Piao, Yuan Zhang, Yang Guo, Liu Cao, Tengfei Jiang, Huang Lin, Xiaoji Li, Yufeng Zheng, for their help in my candidacy exam, graduate courses and in various other ways. I am also thankful to my friends, Siwei Cao, Jing Yang, Huimin Wang, Meng Tong, Lang Qin, Meimei Liu. We not only studied, but also relaxed, and entertained well together.

Finally, heartfelt thanks go to my parents, Quan Zheng and Xiaobin Ma, who give me unlimited and unselfish love and affection throughout my life. Whatever I have to go through, they are my biggest comfort. My thank also goes to my dearest lifelong buddy, Baobi, whom I share my laugh and tear with. I am also grateful to my beloved husband,

Zhenchao Sun, and my lovely daughter, Fumei Sun, who give me the desire to become a smart, sophisticated, elegant and capable woman. And I wish someday I will get there.

Vita

February, 1984Born - Dalian, China

July, 2006B.E. Fine Chemical Engineering,
Dalian University of Technology, China

June, 2010M.S. Materials Science and Engineering,
The Ohio State University, USA

January, 2008 - PresentGraduate Research Associate,
Materials Science and Engineering,
The Ohio State University, USA

Publications

1. Jia Ma, Yogeshwar Sahai, Rudolph G. Buchheit, Evaluation of Multivalent Phosphate Cross-linked Chitosan Biopolymer Membrane for Direct Borohydride Fuel Cells, *Journal of Power Sources*, 202, 2012, 18– 27.
2. Jia Ma, Nurul A. Choudhury, Yogeshwar Sahai, Rudolph G. Buchheit, A High Performance Direct Borohydride Fuel Cell Employing Cross-linked Chitosan Membrane, *Journal of Power Sources*, 196, 2011, 8257-8246.

3. Jia Ma, Nurul A. Choudhury, Yogeshwar Sahai, Rudolph G. Buchheit, Direct Borohydride Fuel Cells Employing Low-cost Polyvinyl Alcohol Hydrogel Membrane Electrolyte and Nickel-based Anode Catalyst, *Fuel Cells*, 11, 2011, 603–610.
4. Jia Ma, Yogeshwar Sahai, Rudolph G. Buchheit, Direct Borohydride Fuel Cell Using Ni-based Composite Anodes, *Journal of Power Sources*, 195, 2010, 4709-4713.
5. Jia Ma, Nurul A. Choudhury, Yogeshwar Sahai, A Comprehensive Review of Direct Borohydride Fuel Cells, *Renewable and Sustainable Energy Reviews*, 14, 2010, 183-199.
6. Jia Ma, Yogeshwar Sahai, Cost-effective Materials for Direct Borohydride Fuel Cells, *ECS transaction*, 42, 2011 (in print).
7. Nurul A. Choudhury, Jia Ma, Yogeshwar Sahai, Rudolph G. Buchheit, High Performance Polymer Chemical Hydrogel-based Electrode Binder Materials for Direct Borohydride Fuel Cells, *Journal of Power Sources*, 196, 2011, 5817-5822.
8. Yogeshwar Sahai, Jia Ma, Development of Direct Borohydride Fuel Cell, Extended abstract in Proceedings of 2009 China-North America Workshop on Fuel Cell Science & Technology, August 13-15, 2009, Shanghai, China, 61-62.
9. Dongping Wang, Mei Wang, Xiuna Wang, Rong Zhang, Jia Ma, Licheng Sun, Influence of the Built-in Pyridinium Salt on Asymmetric Epoxidation of Substituted Chromenes Catalysed by Chiral (pyrrolidine salen) Mn (III) Complexes, *Journal of Molecular Catalysis A: Chemical*, 270, 2007, 278-283.

10. Dongping Wang, Mei Wang, Rong Zhang, Xiuna Wang, Aiping Gao, Jia Ma, Licheng Sun, Asymmetric Epoxidation of Styrene and Chromenes Catalysed by Dimeric Chiral (pyrrolidine salen) Mn(III) Complexes, *Applied Catalysis A: General*, 315, 2006, 120-127.

Fields of Study

Major Field: Materials Science and Engineering

Table of Contents

Abstract	ii
Dedication	v
Acknowledgements	vi
Vita	ix
List of Figures	xvii
List of Tables	xxiii
Chapter 1 Introduction	1
Chapter 2 Literature Review	10
2.1 Direct borohydride fuel cells	10
2.1.1 Properties of sodium borohydride	10
2.1.2 Reactions occurring in DBFC	11
2.1.2.1 Reactions occurring at anode	11
2.1.2.2 Reactions occurring at cathode	15
2.1.3. Electrode	17
2.1.3.1 Anode catalyst materials	17
2.1.3.2 Cathode catalyst materials	23
2.1.3.3 Catalyst supporting materials	27

2.1.4 Membrane	27
2.2 Chitosan	36
2.3 Polyvinyl alcohol	39
Chapter 3 Experimental	41
3.1 Materials	41
3.1.1 Pretreatment of as-received materials	41
3.1.1.1 Pretreatment of nickel foam	41
3.1.1.2 Pretreatment of Nafion [®] membrane	41
3.2 Preparation of electrode binder solution	41
3.2.1 Preparation of PVA binder solution	41
3.2.2 Preparation of chitosan binder solution	42
3.3 Preparation of electrode	42
3.3.1 Electrode prepared by ink paste method	42
3.3.1.1 General procedure of ink paste method	43
3.3.1.2 Preparation of PVA or chitosan binder based electrode	43
3.3.2 Palladium electrode prepared by electrodeposition	43
3.3.3 Gold electrode prepared by sputtering deposition	44
3.3.4 Electron beam physical vapor deposition	44
3.4 Preparation of polymer membrane electrolyte	45
3.4.1 Preparation of PVA membrane	45
3.4.1.1 Preparation of PVA solution	45
3.4.1.2 Preparation of PVA and glutaraldehyde solution mixture	45
3.4.1.3 Preparation of PVA hydrogel membrane	45

3.4.2 Preparation of chitosan membrane.....	46
3.4.2.1 Preparation of pristine chitosan membrane.....	46
3.4.2.2 Preparation of chitosan hydrogel membrane	47
3.4.2.3 Preparation of homogenously cross-linked chitosan membrane	47
3.5 Characterization of polymer membrane electrolyte and electrode.....	47
3.5.1 Scanning electron microscopy (SEM)	47
3.5.2 Fourier transform infrared spectroscopy (FTIR)	48
3.5.3 Thermal analysis	48
3.5.4 Mechanical test	49
3.5.5 Water uptake measurement	49
3.5.6 Ionic conductivity measurement.....	50
3.5.7 Borohydride crossover measurement.....	51
3.6 Fuel cell assembly	52
3.7 Fuel cell performance measurement.....	53
Chapter 4 Results and Discussion.....	64
4.1 A parametric study of Ni-based anode in a direct borohydride fuel cell.....	64
4.1.1 Influence of operation condition on DBFC performance	65
4.1.2 Performance stability of DBFC using Ni-based anode.....	72
4.1.3 Effect of anodic catalyst loading.....	74
4.1.4 Effect of co-catalyst	76
4.1.5 Use of hydrogen peroxide as the oxidant.....	78

4.1.6 Use of Ni foam as anode substrate.....	81
4.2 Polymer chemical hydrogel as electrode binder.....	84
4.2.1 Reactions leading to polymer chemical hydrogel.....	84
4.2.2 Polymer chemical hydrogel binder based electrode	88
4.2.3 Power performance of DBFCs using polymer chemical hydrogel binder	92
4.3 PVA hydrogel membrane	99
4.3.1 Power performance of NaBH ₄ -H ₂ O ₂ fuel cells using PVA hydrogel membrane.....	99
4.3.2 Performance of PVA hydrogel membrane based DBFCs using oxygen or air as the oxidant.....	105
4.4 Chitosan hydrogel membrane.....	112
4.4.1 Glutaraldehyde cross-linked chitosan membrane	112
4.4.2 Sulfuric acid/sulfate modified chitosan membrane.....	117
4.4.2.1 Membrane characterization.....	119
4.4.2.2 Power performance of DBFCs using chitosan hydrogel membrane.....	130
4.4.2.3 Ionic transport through chitosan hydrogel membrane	136
4.4.3 Multivalent phosphate modified chitosan membrane	138
4.4.3.1 Membrane characterization.....	140
4.4.3.2 Performance of DBFCs.....	156
Chapter 5 Summary and Future Work.....	164

References..... 170

List of Figures

Figure 1.1 A schematic diagram of a direct borohydride fuel cell employing alkaline borohydride as fuel, cation exchange membrane as electrolyte and oxygen, air or hydrogen peroxide as oxidant.	5
Figure 2.1 (a) Nafion [®] perfluorinated ionomer; (b) Model of Nafion [®] clusters.....	31
Figure 2.2 Description of chitosan structure and production.....	38
Figure 3.1 Typical setup for electrodeposition.....	55
Figure 3.2 A schematic diagram of the sputtering apparatus.....	55
Figure 3.3 A schematic diagram of a two-probe conductivity measurement cell.....	56
Figure 3.4 A schematic diagram of a set-up for crossover measurement of borohydride fuel.	56
Figure 3.5 A picture of an assembled fuel cell.....	57
Figure 3.6 A schematic diagram of a DBFC test system.	57
Figure 4.1 Curves of cell polarization and power density of DBFC using humidified oxygen and air at 28 and 60 °C.	70
Figure 4.2 Curves of cell polarization and power density of DBFC using dry and humidified oxygen at 28 °C.	71
Figure 4.3 Performance stability of the DBFC using Ni-based composite anode catalyst,	

operating at current density of 50 mA cm ⁻² at room temperature.	73
Figure 4.4 Curves of cell polarization and power density of DBFC at different anode loadings at 60 °C.	75
Figure 4.5 Curves of cell polarization and power density of DBFC using Ni+Pt/C or Ni+Pd/C as anode electrocatalyst at 60 °C.	77
Figure 4.6 SEM of electrodeposited palladium-coating on carbon cloth.	79
Figure 4.7 Curves of cell polarization and power density of DBFC using hydrogen peroxide as oxidant.	80
Figure 4.8 Curves of cell polarization and power density of DBFC using Ni foam as anode substrate.	82
Figure 4.9 Performance stability of the DBFC using Ni foam as anode substrate, operating at current density of 50 mA cm ⁻² at room temperature.	83
Figure 4.10 A schematic diagram of two-phase transport in anode diffusion layer in DBFC.	83
Figure 4.11 Reaction between glutaraldehyde and PVA leading to the formation of PVA chemical hydrogel.	85
Figure 4.12 Reaction between glutaraldehyde and chitosan leading to the formation of chitosan chemical hydrogel.	86
Figure 4.13 A picture of PVA or chitosan chemical hydrogel along with a Teflon-coated magnetic stirring bar in an inverted glass beaker.	87
Figure 4.14 Scanning electron micrographs of (a) PVA binder-based anode, (b) chitosan	

binder-based anode, (c) Nafion [®] binder-based anode, (d) PVA binder-based cathode, (e) chitosan binder-based cathode, and (f) Nafion [®] binder-cathode.....	91
Figure 4.15 Plots of cell voltage and power density versus current density for DBFCs with PVA chemical hydrogel binder-based electrodes at different operating cell temperatures.....	96
Figure 4.16 Plots of cell voltage and power density versus current density for DBFCs with chitosan chemical hydrogel binder-based electrodes at different operating cell temperatures.....	97
Figure 4.17 Plots of cell voltage and power density versus current density for DBFCs with Nafion [®] binder-based electrodes at different operating cell temperatures.	98
Figure 4.18 A SEM picture of sputtered gold on carbon cloth.	102
Figure 4.19 Curves of cell polarization and power density of DBFCs using PVA hydrogel membrane and hydrogen peroxide as the oxidant at different temperatures.	103
Figure 4.20 Curves of cell polarization and power density of a NaBH ₄ -H ₂ O ₂ fuel cell using a PVA hydrogel membrane electrolyte (PHME) or a Nafion [®] membrane electrolyte (NME) at 60 °C.....	104
Figure 4.21 Cell polarization and power density curves of DBFCs which employ PVA hydrogel membrane at different temperatures with oxygen as the oxidant.	106
Figure 4.22 Cell polarization and power density curves of DBFCs which employ PVA hydrogel membrane at different temperatures with air as the oxidant.....	107
Figure 4.23 Curves of cell polarization and power density of a DBFC using a PVA hydrogel membrane electrolyte (PHME) or a Nafion [®] membrane electrolyte (NME) with oxygen as	

the oxidant at 60 °C.....	108
Figure 4.24 Curves of cell polarization and power density of a DBFC using a PVA hydrogel membrane electrolyte (PHME) or a Nafion [®] membrane electrolyte (NME) with air as the oxidant at 60 °C.....	109
Figure 4.25 Chronopotentiometric data for determination of fuel efficiency in a DBFC based on PVA hydrogel membrane.	110
Figure 4.26 Performance stability of a PVA hydrogel membrane-based DBFC operating at current density of 50 mA cm ⁻² at ambient temperature.	111
Figure 4.27 A picture of a glutaraldehyde cross-linked chitosan membrane and an electrode prepared by electron beam evaporation on Ni foam substrate.....	114
Figure 4.28 Plots of cell polarization and power density versus current density for DBFCs using chitosan membrane cross-linked by glutaraldehyde, and electron beam deposited Ni-based composite anode at 60 °C.	115
Figure 4.29 A picture of sulfuric acid modified chitosan membrane.....	117
Figure 4.30 Chemical structures of chitosan and sulfate ion cross-linked chitosan.	118
Figure 4.31 Thermogravimetric analysis curve for sulfate modified chitosan membrane. ..	120
Figure 4.32 Nyquist plots of (a) Nafion [®] 212, and (b) sulfuric acid modified chitosan hydrogel membrane recorded by electrochemical impedance spectroscopy.	126
Figure 4.33 Grötthus-type mechanism of proton conduction.	127
Figure 4.34 Segmental-motion mechanism of ionic conduction in alkaline membrane electrolytes.	127

Figure 4.35 (a) Dependence of peak anodic current at gold electrode on borohydride concentration; a typical linear sweep voltammogram (LSV) recorded during estimation of borohydride crossover through (b)Nafion [®] 212 membrane, and (c) sulfuric acid modified chitosan hydrogel membrane.	128
Figure 4.36 Plots of cell polarization and power density versus current density for DBFCs using sulfuric acid chitosan (CCS) hydrogel membrane and Nafion [®] 212 (N212) membrane, chitosan chemical hydrogel (CCH) binder and Nafion [®] binder at 30 and 60 °C.	132
Figure 4.37 Cell polarization and power density plots for DBFC employing sulfate modified chitosan membrane and chitosan anode binder at 70 °C.	133
Figure 4.38 Fuel cell performance stability data for a DBFC, which employs chitosan anode binder and chitosan hydrogel membrane, recorded by operating it at a current density of 120 mA cm ⁻² at 30 °C.	135
Figure 4.39 (a) Scanning electron micrograph of cathode surface, and (b) Na-mapping EDS image of cathode surface after used in a DBFC at a current density of 50 mA cm ⁻² for 2 h.	137
Figure 4.40 Chemical structures of chitosan and phosphate and triphosphate cross-linked chitosan.	139
Figure 4.41 The FTIR spectra for uncross-linked chitosan membrane and chitosan membrane modified with TPP.	142
Figure 4.42 SEM pictures of (a) surface and (b) cross-sectional morphology of chitosan	

membrane modified by TPP.....	144
Figure 4.43 EDX spectra of (a) surface and (b) cross section of chitosan membrane modified by TPP.....	145
Figure 4.44 TGA thermograms of (a) Nafion [®] , (b) pristine chitosan, (c) CsP, and (d) CsTP membranes.....	149
Figure 4.45 DSC thermograms of CsP and CsTP membranes.....	150
Figure 4.46 Stress–strain curves of (a) Nafion [®] , (b) CsP, and (c) CsTP membranes.....	153
Figure 4.47 Plots of cell polarization and power density versus current density for DBFCs using Nafion [®] , CsP, and CsTP membranes at 30 and 60 °C.....	157
Figure 4.48 Performance stability of a DBFC using CsP membrane at 30 °C.....	159
Figure 4.49 Performance stability of a DBFC using CsTP membrane at 30 °C.....	159
Figure 4.50 Comparative performance stability of chitosan-based DBFC and Nafion [®] -based DBFC at 60 °C.....	160
Figure 4.51 Fuel efficiency of a DBFC using Nafion [®] membrane and Nafion [®] binder at 30 °C.....	162
Figure 4.52 Fuel efficiency of a DBFC using CsP membrane and chitosan hydrogel binder at 30 °C.....	163
Figure 4.53 Fuel efficiency of a DBFC using CsTP membrane and chitosan hydrogel binder at 30 °C.....	163

List of Tables

Table 1.1 Comparisons of different types of fuel cells.	6
Table 1.2 Thermodynamic characteristics of DBFCs, DMFCs and H ₂ -PEFCs.....	9
Table 2.1 Physical and chemical properties of sodium borohydride.	10
Table 2.2 A list of anode material properties.	22
Table 2.3 DBFC performance data obtained with various electrode catalysts and membranes.	32
Table 2.4 General chemical identity and physical properties of polyvinyl alcohol.....	40
Table 3.1 A list of materials, their properties and vendors.....	58
Table 3.2 Description of electrode prepared by ink paste method.....	61
Table 4.1 Electrochemical performance durability data for a DBFC using chitosan membrane cross-linked by glutaraldehyde, and electron beam deposited Ni-based anode at 60 °C.....	116
Table 4.2 Summary of properties of chitosan membrane modified by sulfate salt of sodium.	120
Table 4.3 Comparison between properties of chitosan hydrogel membrane and Nafion [®] 212 membrane.....	129
Table 4.4 Infrared band assignments for chitosan membrane.....	141

Table 4.5 Water uptake values of Nafion [®] , CsP, and CsTP membranes.....	150
Table 4.6 Ionic conductivity and borohydride crossover values of CsP and CsTP membranes.....	155

Chapter 1 Introduction

Fuel cells constitute an attractive class of renewable and sustainable energy sources alternative to conventional energy sources such as petroleum that has finite reserves. Energy generation from petroleum oil and natural gas through combustion in a heat engine being subject to Carnot Cycle limitation is inherently inefficient and is accompanied with environmental pollution. In contrast, a fuel cell is intrinsically energy efficient, non-polluting, silent, and reliable. In some embodiments, it is a low temperature device that provides electricity instantly upon demand, and exhibits a long operating life. Fuel cells combine the advantages of both combustion engines and batteries, at the same time eliminating the major drawbacks of both. Similar to a battery, a fuel cell is an electrochemical energy device that converts chemical energy into electricity, and akin to a heat engine, a fuel cell supplies electricity as long as fuel and oxidant are supplied to it.

Table 1.1 gives a list of common fuel cell types and their characteristics. Among them, the polymer electrolyte fuel cell (PEFC) employs polymer membrane as the electrolyte. Compared to other types of fuel cells, it is capable of achieving reasonably high power performance at relatively low working temperatures (≤ 100 °C), and thus is considered a promising power supply for transport, stationary and also portable applications. Research and development on PEFCs using hydrogen as the fuel have progressed enormously but their successful commercialization is restricted because of poisoning of platinum anode by

carbon monoxide while using a reformer in conjunction with the PEFC and the safety and storage efficiency of the flammable hydrogen gas. In order to overcome these difficulties, liquid methanol is used instead to fuel PEFCs. Direct use of liquid fuel in a PEFC simplifies the engineering issues, thereby driving down the system complexity and hence cost. PEFCs that are fed with methanol as fuel are referred to as direct methanol fuel cells (DMFCs). However, DMFCs have limitations of inefficient methanol electro-oxidation, low open circuit potential, and methanol cross-over from anode to cathode compartment.

The problems arising from the use of methanol in DMFCs can be overcome by using other hydrogen carrying materials such as various borohydride compounds as fuel. Sodium borohydride (NaBH_4), which has a capacity value of 5.67 Ah g^{-1} and a hydrogen content of 10.6 wt. % [1, 2], is a good alternative to methanol as a fuel. The direct borohydride fuel cell (DBFC) uses sodium borohydride (NaBH_4) or potassium borohydride (KBH_4) in aqueous alkaline solution directly as the fuel. The oxidant used in a DBFC is oxygen, air or hydrogen peroxide (H_2O_2). Although the concept of DBFC was first demonstrated by Indig and Snyder [3] in the early 1960s, Amendola et al. were the first to report a direct borohydride-air fuel cell that employed an anion exchange membrane (AEM) as electrolyte and exhibited a maximum power density of 60 mW cm^{-2} at 70°C [1].

Figure 1.1 depicts a schematic diagram of a direct borohydride fuel cell which employs a polymer electrolyte membrane separating anode from cathode. Fluid flow field plates are placed in contact with the rear of the electrodes. Graphite and stainless steel are two common materials of flow plates. The channels on the flow field plates give path to fuel

and oxidant to the anode and cathode respectively. A single fuel cell can be operated in two modes: active or passive. In an active fuel cell system, the fuel solution is fed into the anode chamber and the oxidant into the cathode chamber through a peristaltic pump or a mass flow controller.

Compared to other types of polymer electrolyte fuel cells such as H₂-PEFCs and DMFCs, DBFCs have several advantageous thermodynamic characteristics including highest theoretical cell potential, highest number of electron transferred etc., as shown in Table 1.2. Other advantages of DBFC systems include:

- (a) DBFCs use liquid fuel which needs no modifying and processing of the fuel.
- (b) Alkaline medium opens up the possibility of using non-noble anode electrocatalysts.
- (b) Cooling plates are not necessary in DBFC stacks, since the liquid fuel solution can serve as heat exchange medium to cool the stacks.
- (c) Cathode gas humidifier can be eliminated, since water could be electroosmotically dragged to the cathode.

DBFCs share similarities in terms of fuel cell components and materials, fuel cell system design, electrode and membrane electrolyte preparation methods etc. with H₂-PEFCs and DMFCs which have been developed intensely for decades. However, the DBFC has its unique issues and its development is still in the infant stage.

The major component of a single DBFC is the membrane-electrode-assembly (MEA) that consists of either an anion exchange membrane (AEM) or a cation exchange membrane (CEM) sandwiched between an anode and a cathode. The anode and cathode

are separated by a solid polymer electrolyte membrane which should have good ionic conductivity and no electronic conductivity. An electrode generally consists of a catalyst layer (CL) and a diffusion layer (DL). The CL must have facile transport of reactants and products as well as good ionic and electronic conductivity. Therefore, the CL has high porosity and large electrochemically active surface. The DL consists of a macroporous layer and possibly a microporous layer. It serves the following functions: (1) conduct electrons to and from the CL; (2) transport reactants and remove products from the CL; (3) support the CL mechanically and prevent the catalysts tenting into flow plate channels; (4) transport heat to and from the CL.

Cost and power performance are two important factors which affect the commercialization of fuel cells. MEA accounts for over 50% of a fuel cell stack cost [4]. The development of high performance and cost-effective materials for MEA will promote the successful commercialization of fuel cells. This research attempts to develop a high performance MEA of DBFC using cost-effective materials. Ways to achieve this goal include: (1) use of Ni-based composite anode electrocatalysts loaded on Ni foam substrate, (2) use of chitosan or polyvinyl alcohol (PVA) chemical hydrogel as electrode binder (3) use of PVA or chitosan hydrogel membrane as polymer electrolyte.

Chapter 2 gives a comprehensive and critical review of direct borohydride fuel cells as well as materials employed as binder and membrane in this research. Experimental section is presented in chapter 3 followed by results and discussion in chapter 4. Finally conclusion of this research and suggested future work are written in chapter 5.

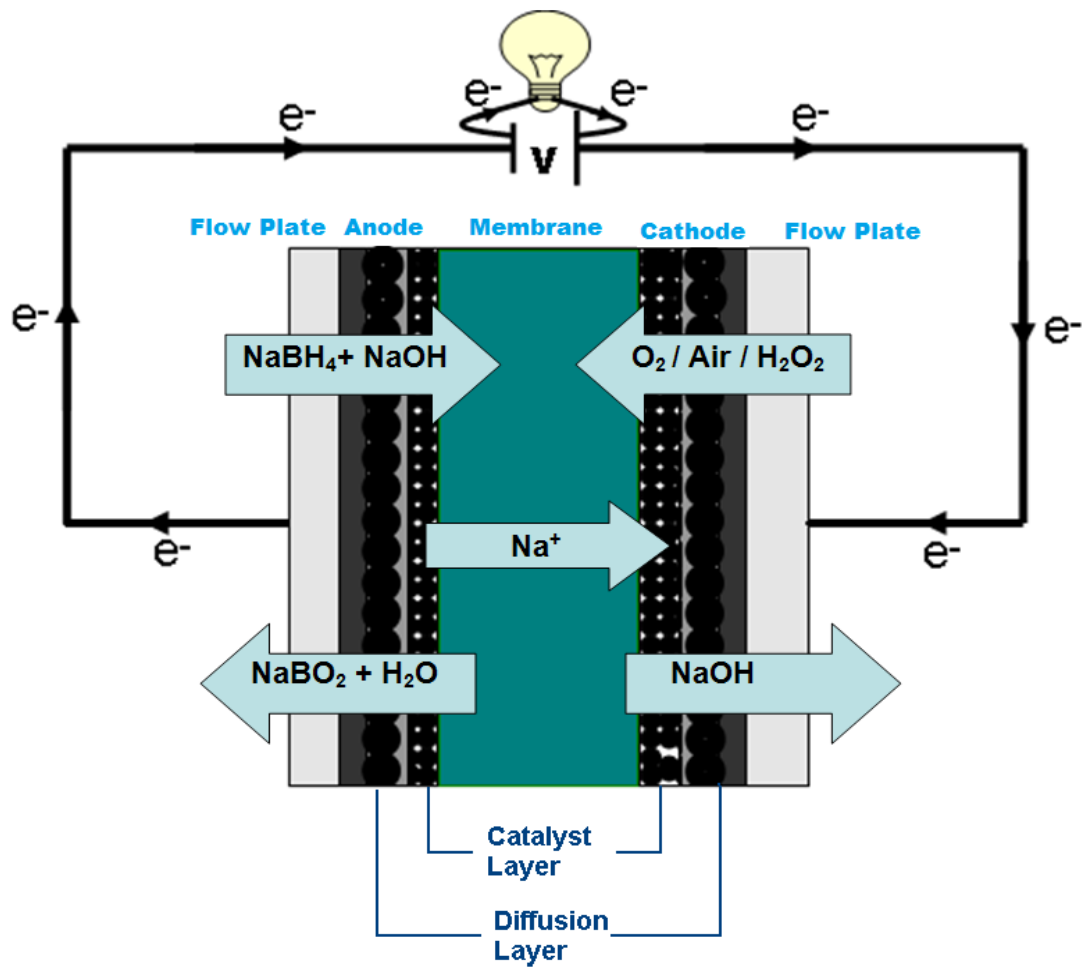


Figure 1.1 A schematic diagram of a direct borohydride fuel cell employing alkaline borohydride as fuel, cation exchange membrane as electrolyte and oxygen, air or hydrogen peroxide as oxidant.

Table 1.1 Comparisons of different types of fuel cells [5].

Fuel cell name	Electrolyte	Electrode reaction	Working temperature (°C)	Efficiency	Cell output
Alkaline	Potassium hydroxide aqueous solution	Anode reaction $H_2 + 2OH^- \rightarrow 2H_2O + 2e^-$ Cathode reaction $1/2O_2 + H_2O + 2e^- \rightarrow 2OH^-$	150-200	70%	300W-5kW
Molten carbonate	Molten salts, like sodium or magnesium carbonate	Anode reaction $H_2 + CO_3^{2-} \rightarrow H_2O + CO_2 + 2e^-$ $CO + CO_3^{2-} \rightarrow 2CO_2 + 2e^-$ Cathode reaction $1/2O_2 + CO_2 + 2e^- \rightarrow CO_3^{2-}$	650	60-80%	2MW-100MW

(Continued)

Table 1.1: *Continued*

Phosphoric acid	Molten phosphoric acid	<p>Anode reaction</p> $\text{H}_2 \rightarrow 2\text{H}^+ + 2\text{e}^-$ <p>Cathode reaction</p> $\frac{1}{2}\text{O}_2 + 2\text{H}^+ + 2\text{e}^- \rightarrow \text{H}_2\text{O}$	150-200	40-80%	200kW-11MW
Solid oxide	Ceramic compounds of metal oxides, such as YSZ	<p>Anode reaction</p> $\text{H}_2 + \text{O}^{2-} \rightarrow \text{H}_2\text{O} + 2\text{e}^-$ $\text{CO} + \text{O}^{2-} \rightarrow \text{CO}_2 + 2\text{e}^-$ $\text{CH}_4 + 4\text{O}^{2-} \rightarrow 2\text{H}_2\text{O} + \text{CO}_2 + 2\text{e}^-$ <p>Cathode reaction</p> $\frac{1}{2}\text{O}_2 + 2\text{e}^- \rightarrow \text{O}^{2-}$	1000	60%	100kW

7

(Continued)

Table 1.1: *Continued*

Direct methanol	Proton exchange membrane	Anode reaction $\text{CH}_3\text{OH} + \text{H}_2\text{O} \rightarrow \text{CO}_2 + 6\text{H}^+ + 6\text{e}^-$ Cathode reaction $3\text{O}_2 + 6\text{H}^+ + 6\text{e}^- \rightarrow 3\text{H}_2\text{O}$	<85	20–30%	100 mW – 1 kW
∞ Polymer electrolyte membrane	Proton exchange membrane	Anode reaction $\text{H}_2 \rightarrow 2\text{H}^+ + 2\text{e}^-$ Cathode reaction $1/2\text{O}_2 + 2\text{H}^+ + 2\text{e}^- \rightarrow \text{H}_2\text{O}$	50–120 (Nafion®) 125–220 (PBI)	40-50%	50 kW - 250 kW

Table 1.2 Thermodynamic characteristics of DBFCs, DMFCs and H₂-PEFCs [6].

	DBFC (NaBH ₄ /O ₂)	DMFC (CH ₃ OH/O ₂)	PEFC (H ₂ /O ₂)	DBFC (NaBH ₄ /H ₂ O ₂)	DBFC (NaBH ₄ / H ₂ O ₂ (H ⁺))
Number of electrons transferred	8	6	2	8	8
Theoretical cell voltage (V)	1.64	1.21	1.23	2.11	3.01
Theoretical specific energy (Wh kg ⁻¹)	9295	6073	32707	11959	17060
Pure compound capacity (Ah kg ⁻¹)	5668	5019	26591	5668	5668
Energy efficiency (%)	0.91	0.92	0.83	0.97	0.97

Chapter 2 Literature Review

2.1 Direct borohydride fuel cells

2.1.1 Properties of sodium borohydride

Sodium borohydride, also known as sodium tetrahydroborate or tetrahydridoborate, has the chemical formula NaBH_4 . It is a versatile reducing agent with wide application in chemical productions. Table 2.1 summarizes some physical and chemical properties of NaBH_4 .

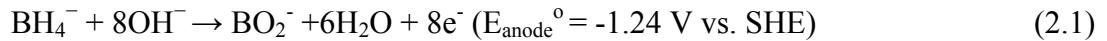
Table 2.1 Physical and chemical properties of sodium borohydride [7].

CAS No.	CAS 16940-66-2
Appearance	White to grey-white microcrystalline powder or lumps
Odor	Odorless
Solubility	Soluble in water; reacts with hot water
Specific gravity	1.074
% Volatiles by volume at 294 K	0
Melting point	778 K (10 atm H_2)
Vapor density(air = 1)	1.3
Stability	Hygroscopic; stable in dry air up to 573 K; decomposes slowly in moist air or vacuum above 673 K
Structure at ambient condition	NaCl-type

2.1.2 Reactions occurring in DBFC

2.1.2.1 Reactions occurring at anode

Borohydride ion, in aqueous alkaline medium, can be oxidized directly on a large variety of electrode materials liberating a maximum of eight electrons. The reaction for the electro-oxidation of BH_4^- is shown in Equation 2.1 as follows:



A big problem associated with the anodic reaction in DBFC is that BH_4^- hydrolyzes quasi-spontaneously to generate hydroxyl borohydride intermediate and hydrogen on various electrode materials [8]. Hydrolysis of BH_4^- takes place through the formation of trihydroxy borate ion intermediate to generate hydrogen [9] as shown in Equations 2.2 and 2.3:



The presence of atomic hydrogen on DBFC anode makes the anode potential a mixed potential of reactions shown in Equations 2.1 and 2.4, and the observed anode potential is between -1.24 and -0.828V vs. SHE [10].



Since hydrogen molecules are formed on the surface of electrodes, it is possible to get them immediately oxidized with the state of the art porous electrodes giving eight electrons provided that BH_4^- hydrolysis does not take place too fast [11].

The detailed mechanism of BH_4^- electro-oxidation is not yet fully understood. However, a possible reaction pathway for electro-oxidation of BH_4^- on platinum electrode is reported in literature [12]. Gyenge [13] studied the electrochemical oxidation of BH_4^- on platinum electrode and concluded that BH_4^- undergoes hydrolysis to yield H_2 which is further oxidized at the potential between -0.7 and -0.9 V versus Ag/AgCl, and the direct electro-oxidation of BH_4^- occurs in the potential range from -0.15 to -0.05 V vs. Ag/AgCl. Mirkin et al. [14] reported that BH_4^- electro-oxidation on gold electrode took place by an electrochemical-chemical-electrochemical reaction mechanism involving unstable intermediates as shown in Equations 2.5-2.7:



The monoborane (BH_3) intermediate then undergoes further reaction to produce a total of eight electrons.

Cheng and Scott [15] studied the kinetics of borohydride electro-oxidation on rotating gold disk electrode. The authors reported that the number of electrons transferred in the borohydride electro-oxidation was around 8 at 0.45 V; the rate constant was between 0.016 and 6.13 cm s⁻¹; the orders of the electro-oxidation reaction with respect to tetrahydroborate and hydroxide ions were 1.0 and 1.1, respectively; the activation energy for borohydride electro-oxidation was 27.0 kJ mol⁻¹. A rotating ring disk electrode study by Krishnan et al. [16] reveals that the electro-oxidation of BH₄⁻ occurs over a wide potential range of -0.500 to 0.400 V vs. NHE on gold electrode under hydrodynamic conditions and also the extent of BH₃(OH)⁻ generated increases with increase in anodic polarization of the disc electrode. The authors opined that the increase in the amount of BH₃(OH)⁻ with increased electrode polarization is a concern with respect to fuel utilization efficiency in DBFC.

The direct oxidation of NaBH₄ in concentrated NaOH solution has been studied by Chatenet et al. [17] on silver and gold electrocatalysts. The authors opined that the BH₄⁻ electro-oxidation mechanism on silver and gold electrodes varies at different [OH⁻]/[BH₄⁻] ratios. When BH₄⁻ concentration is low, a negligible amount of BH₃OH⁻ is produced and the oxidation reaction proceeds without the chemical hydrolysis of BH₄⁻. The authors found that the reaction intermediates are all adsorbed at the electrode surface and BH₄⁻ oxidation mechanism start following the adsorption step shown in Equation 2.8 and electrochemical step shown in Equation 2.9:



At low $[\text{OH}^-]/[\text{BH}_4^-]$ ratio, BH_4^- undergoes spontaneous hydrolysis into non-negligible amounts of BH_3OH^- which is further oxidized at very low potential ($<-1\text{V}$ versus NHE). BH_4^- is oxidized at much higher potential (above -0.6V versus NHE for Au/C and -0.3V versus NHE for Ag/C). The initial steps of BH_4^- direct oxidation might be much slower than the BH_3OH^- oxidation. In addition, there seems to be a particle size effect for carbon-supported metals since the onset for the oxidation wave is at least 0.1V lower for the nanoparticles than that for the bulk metals. The state of the electrode surface also plays a role in the tetrahydroborate oxidation reaction. For silver electrodes, surface oxides need to be present to enable the reaction that is not observed for gold electrodes. Nanoparticles have at least 0.1V lower onset oxidation wave than bulk metals.

Lee et al. [18] studied the mechanism of electro-oxidation of BH_4^- on hydrogen storage alloy and stated that hydrogen releasing agent such as BH_4^- first releases hydrogen and electrons in the aqueous electrolyte solution through electrochemical decomposition and oxidation by the hydrogen storage alloy catalyst according to Equation 2.10.



The released hydrogen (H) is stored in a hydrogen storage alloy (M) as metal hydride (MH_x); the reaction can be expressed by Equation 2.11.



Hydrogen stored as metal hydride (MH_x) in the hydrogen storage alloy produces electrons by dehydrogenation of the latter as shown by Equation 2.12:

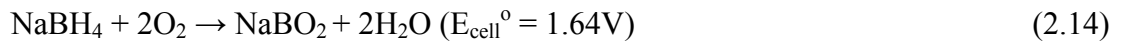


2.1.2.2 Reactions occurring at cathode

The cathodic reaction with oxygen as the oxidant is written as Equation 2.13:



The mechanism of oxygen reduction reaction is complicated and it involves generation of hydrogen peroxide and metal oxide byproduct intermediates that decrease the activity of the electrocatalysts. The net cell reaction for DBFC with oxygen as oxidant is written in Equation 2.14:



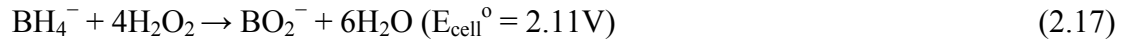
The cathodic reaction with H₂O₂ as oxidant is represented by Equation 2.15:



In DBFC, H₂O₂ is prone to decomposition at cathode catalyst surface producing oxygen and water as expressed by Equation 2.16:



The liberated oxygen is further electrochemically reduced at the cathode according to Equation 2.13. The net cell reaction for DBFC using H₂O₂ as oxidant is expressed as Equation 2.17.

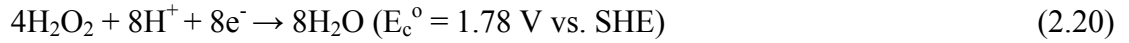


Cathode potential varies with pH of the oxidant according to Equations 2.18 and 2.19 as shown below.

$$E(\text{O}_2) = 1.23 - 0.059 \text{ pH} \quad (2.18)$$

$$E(\text{H}_2\text{O}_2) = 1.78 - 0.059 \text{ pH} \quad (2.19)$$

As the pH decreases, the rate of H₂O₂ decomposition at the cathode catalyst surface decreases. At lower pH values, the probability of direct electro-reduction of H₂O₂ increases, whereas at higher pH values the possibility of decomposition of H₂O₂ to O₂ followed by the reduction of the latter increases. Direct electro-reduction of H₂O₂ and chemical decomposition of H₂O₂ to O₂ followed by the electro-reduction of the latter in DBFC are expressed as Equations 2.20, 2.21, and 2.22, respectively.



Depending on the pH of H₂O₂ solution, the theoretical OCV varies between 1.64 and 3.02 V [19].

2.1.3. Electrode

2.1.3.1 Anode catalyst materials

Anode catalysts examined in DBFCs are primary metallic materials including platinum (Pt), gold (Au) palladium (Pd), silver (Ag), ruthenium (Ru), nickel (Ni) etc. The transition metals have unfilled d-orbitals and unpaired d-orbital electrons to bond with the adsorbed species. Therefore these metals typically have good electrochemical activity as catalysts. The activities of transition metals vary due to the difference in the free energy of adsorption

which depends on the number of unpaired d-electrons and their energy levels [20]. Some anode catalyst material properties are summarized in Table 2.2.

Electrocatalysts such as Ni, Pt, and Pd have good catalytic activity towards both the electrochemical oxidation reaction and the hydrolysis reaction [13,21]. Therefore, DBFCs using these metals as anode give high power density but low faradic efficiencies, e.g., 50% for nickel [21]. Higher fuel efficiencies can be achieved on Pd and Pt electrodes at low BH_4^- concentrations and high anode currents [21]. Electrocatalysts such as Ag and Au, has little or no catalytic activity towards borohydride hydrolysis and therefore high coulombic efficiencies towards borohydride electro-oxidation. Chatenet et al. [17] have reported that electro-oxidation of BH_4^- yields about 7.5 electrons on gold and silver electrodes in contrast to about 4 electrons on platinum. The high utilization efficiencies of gold and silver towards BH_4^- electro-oxidation are due to their low activity towards hydrolysis of BH_4^- . Nevertheless, gold and silver exhibit slow kinetics towards electro-oxidation of BH_4^- , the former being better than the latter. Cheng et al. [22] used cyclic voltammetry to compare the activity of various metallic catalysts towards the electro-oxidation of borohydride, and observed the following order for the reaction rate of borohydride electro-oxidation: $\text{Au} > \text{Pt} > \text{Ag} > \text{Ni}$. Further cell performance tests with DBFCs using these anode catalysts demonstrated the same order in terms of peak power density at 85 °C. However, in another study, DBFC with Ni as anode catalyst gave higher power performance than that with Pt under similar conditions [23], probably due to the different

catalyst preparation methods used. Table 2.3 summarizes DBFC performance data obtained with various electrode catalysts.

Various research groups have employed Ni-based electrocatalyst and achieved good performance as given in Table 2.3. In alkaline environment, BH_4^- ions undergo electro-oxidation readily on non-precious nickel. In fact, Ni has been employed as a catalyst in Sabatier and Senderens reaction [24], which is the oldest method for hydrogenation of unsaturated hydrocarbons probably due to its unique affinity towards adsorption of hydrogen and hydrogen containing unsaturated organic compounds. Moreover, Ni is a major component of hydrogen storage materials such as AB_2 and AB_5 -type alloys. A problem with Ni electrode is that it might gradually form stable oxide or hydroxide, and so porous Ni electrode gradually increases its polarizations as shown by the stability tests [25].

Bimetallic and multimetallic catalysts could have superior activity and stability to the monometallic catalysts. An interesting alloying strategy might be to combine the metal of high coulombic efficiency with that having high catalytic effect for dehydrogenation. Gyenge et al. [26] prepared colloidal Pt, Pt-alloys, and Atwan et al. prepared colloidal Os, Os-alloys [27], Au, Au-alloys [28], Ag, and Ag-alloys [29] by modified Bönnerman method and investigated them as electrocatalysts for BH_4^- oxidation. Alloying Au with Pd or Pt was shown to improve the kinetics of borohydride oxidation, and higher cell voltage was obtained using Au-Pt than colloidal Au. The particle size of colloidal Au is larger than that of Pt and Pd, and therefore by alloying colloidal Au with Pt or Pd, the mean particle size of

catalyst is reduced. Yet, further studies are needed to determine whether the particle size effect contributes to the improvement in electrode kinetics of borohydride oxidation in addition to the mechanistic and kinetic effects.

Some researchers investigated bimetallic Ni–Pt catalyst and showed that they can be superior to the monometallic Ni or Pt catalyst towards borohydride electrooxidation [23,30]. Geng et al. [23] prepared carbon-supported Ni and Ni-Pt alloy catalysts by chemical reduction of $\text{Ni}(\text{NO}_3)_2$ and a mixture of $\text{Ni}(\text{NO}_3)_2$ and H_2PtCl_6 with hydrazine respectively and employed them as anode catalysts in DBFCs. Electrochemical measurements showed that Ni–Pt/C had improved electro-catalytic activity and stability than Ni/C catalyst.

Another alloying strategy is to combine metals such as Ru which mainly completes the hydrolysis of borohydride and a second metal such as Pt which oxidizes the hydrogen and also borohydride, so as to achieve indirect oxidation of BH_4^- . A complete eight electron borohydride electro-oxidation on Pt–Ru nanoparticles was observed in 0.01 mol dm^{-3} NaBH_4 and 2 mol dm^{-3} NaOH solution [31].

Although Ag has worse characteristics in terms of kinetics for borohydride electro-oxidation in comparison to Au, it exhibits better activity than gold towards the BH_3OH^- direct oxidation and therefore can serve as co-catalyst to efficiently oxidize the by-product of BH_4^- hydrolysis [17]. Feng et al. [32] studied Ag and Ag-Ni alloy anode for DBFCs and found that Ag- and AgNi-based anode could realize direct electro-oxidation of BH_4^- , giving more than 7 electrons per BH_4^- . Ag-Ni alloy based-borohydride fuel cells

exhibited a higher discharge voltage and capacity than Ag, possibly because of the electro-catalytic activity of Ni towards BH_4^- electro-oxidation and the inhibition effect of Ag towards BH_4^- hydrolysis.

Hydrogen storage alloys (HSAs) are metallic materials capable of reversibly absorbing and releasing significant quantities of hydrogen through electrochemical hydrogenation or gas phase hydrogenization. Two types of HSAs, AB_5 and AB_2 alloys are of interest in DBFCs. AB_5 alloys consists of A= a rare earth metal (Lanthanum (La), Cerium (Ce), Neodymium (Nd), Praseodymium (Pr), Yttrium (Y)) or mischmetal (alloys of rare earth metals) and B= Ni or other transition metals. AB_2 alloys, also known as Laves phase alloy, combine A= Titanium (Ti), Zirconium (Zr) or Hafnium (Hf) with B= transition metals (Manganese (Mn), Chromium (Cr), Vanadium (V), Ni etc.). Because hydrogen storage alloys can absorb large quantities of hydrogen, they are expected to reduce hydrogen evolution in DBFCs. Because hydrogen storage alloys can absorb a large amount of hydrogen, they are expected to reduce hydrogen evolution and improve coulombic efficiency in DBFCs. However, hydrogen evolution is not completely eliminated by the amount of the hydrogen storage alloy typically used in the anode, due to the limited storage ability of the alloys (less than 200 mL H_2 /g alloy) [2]. As in case of Pd and Pt, the coulombic efficiency of HSAs is strongly dependent on borohydride concentrations. In a concentrated borohydride solution (2.4 M NaBH_4 +6 M NaOH), borohydride electro-oxidation was shown to be a four electron process, while a higher coulombic number was obtained in a lower borohydride concentration. It was proposed that only at

relatively low borohydride concentrations, the electro-oxidation of the absorbed atomic hydrogen was kinetically favorable and subsequently contributed to a high coulombic efficiency [33]. Anode polarization was shown to be improved by reducing the particle size of HSAs and decreasing operating temperatures. However, this improvement was accompanied with a lower coulombic efficiency.

Table 2.2 A list of anode material properties [34].

Anode material	Number of electrons	Open circuit potential vs. SHE (V)
Ni	4	-1.03
Au	7-8	-0.99
Pt	2-4	-1.0
Dispersed Pd on Ni	6	-1.00,-0.91
Dispersed Pt on Ni	5-6	-0.91
Dispersed Au on Ni	NA	-0.99
Hydrogen storage alloys	4	-1.15

2.1.3.2 Cathode catalyst materials

Precious-metal catalysts, predominantly carbon supported Pt, are used for oxygen reduction reaction (ORR) in H₂-PEFCs. A major concern for using Pt as the cathode catalyst is its high cost. Intensive studies have been going on to find low cost alternative materials to replace Pt-based catalysts while maintain the same level of effectiveness for oxygen reduction reaction. A class of low cost substitutes is metal (e.g. Co, Fe) complex with macrocycles (tetraphenylporphyrin (TPP), tetramethoxyphenylporphyrin (TMPP), tetraazaannulene (TAA) and phthalocyanine (Pc)). It was revealed that the expensive macrocyclic compounds could be substituted by individual nitrogen containing precursors [35]. The M-N_x (M = Co, Fe) was proposed to be the active sites for ORR [36]. However, such catalysts gave good initial performance for ORR but insufficient stability in H₂-PEFCs. A major progress has been made by Rajesh Bashyam and Piotr Zelenay [37] in the development of “(non-precious metal)/(heteroatomic polymer)” catalysts for ORR. In particular, cobalt-polypyrrole-carbon (Co-PPY-C) was synthesized by a chemical method. Polypyrrole serves to incorporate cobalt and the active Co-N sites for ORR are generated as a result. Co-PPY-C catalyst (0.06 mg cm⁻² Co loading) showed not only high activity for ORR but also remarkable performance durability (stable operation for more than 100 hours) in a H₂-PEFC.

In DBFCs, Pt is also widely used and its effectiveness toward ORR has been confirmed. In the study of Cheng et al. [22], cyclic voltammetry showed that various cathode catalysts exhibited the following order for ORR activity in NaOH solution: Pt > Pd > Ag > Ni.

Among these electrocatalysts investigated, Pt also demonstrated the best power performance and stability at both room temperature and elevated temperatures. The high ORR activity of Pt was also demonstrated in the study of Chatenet, in which linear sweep voltammogram revealed that the following sequence for oxygen reduction activity of various electrocatalysts in the presence of NaOH solution [38]: Pt > MnO_x > Ag ≥ Au.

In DBFCs the crossover borohydride might cause performance loss to cathode catalyst. Therefore beside cost borohydride tolerance is another important concern for cathode catalyst selection. Borohydride has been found to deteriorate Pt performance. Chatenet et al. [38] found that the onset potential for oxygen reduction and the open circuit potential significantly reduced in the solution containing 10⁻² M NaBH₄, which rendered Pt unusable in this condition. Compared to Pt, the negative effect of NaBH₄ is less pronounced for Ag and Au possibly due to their less effectiveness as catalysts for borohydride hydrolysis. On the other hand, manganese oxide-based electrocatalyst, a non-precious material, seems to be much less affected by the borohydride. The open circuit potential of MnO_x was found to shift negatively by only 0.075 V when NaBH₄ was added to the electrolyte. Even in presence of NaBH₄, MnO_x-based electrocatalyst still demonstrated higher ORR activity than that of Ag and Au in pure NaOH solution. The borohydride tolerance of the manganese oxide-based electrocatalyst was also observed by Ma et al. [39].

As given in Table 2.3, other non-precious cathode catalysts such as cobalt phthalocyanine (CoPc) [40], iron phthalocyanine (FePc) [41] were investigated for the

activity towards ORR and borohydride tolerance. Cyclic voltammogram showed that the cathodic reduction current of CoPc or FePc dramatically increased in air-saturated solution compared to in Ar-saturated KOH solution, which led the authors concluded that CoPc or FePc had a good activity for ORR in alkaline solution. However, it might be more informative to compare the intrinsic ORR activity of these catalysts with that of the Pt catalyst. The polarization curves of the CoPc or FePc electrocatalyst with BH_4^- present were found to be almost identical to that obtained from the alkaline solution, indicating that the existence of BH_4^- has almost no negative effect on this cathode.

Iron tetramethoxyphenyl porphyrin (FeTMPP) was another cost effective electrocatalyst investigated in DBFCs [42]. Cyclic voltammetry and steady-state potentiostatic polarization measurements showed FeTMPP had lower ORR activity than Pt but higher activity than Ag and Ni. Besides, FeTMPP demonstrated the best borohydride tolerance among the catalysts. The stability FeTMPP cathode was studied by applying a constant load and measuring the cell voltage. Although FeTMPP was shown to have insufficient stability in acidic medium, it gave acceptable stability in alkaline media.

Qin et al. investigated the effectiveness of cobalt-polypyrrole-carbon (Co-PPY-C) as cathode catalysts in DBFCs. The DBFC based on Co-PPY-C cathode achieved a peak power density of 65 mW cm^{-2} comparable to the result of Pt/C and a short term stability of 50 hours [43]. However, no paper so far investigated the effectiveness of borohydride tolerance of this kind of catalyst.

Ma et al. [44] prepared carbon-supported LaNiO_3 perovskite catalysts by the citrate based sol-gel method and employed them as cathode catalyst for DBFC. A DBFC with LaNiO_3/C -catalysed cathode and hydrogen storage alloy-catalyzed anode and no membrane separator exhibited a peak power density of 127 mW cm^{-2} at $65 \text{ }^\circ\text{C}$ under atmospheric pressure and good performance stability for 500 h.

Candidate metallic cathode catalyst materials for H_2O_2 reduction include Pt, Au, Pd, Pd-Ir, Pd-Ru etc. Since H_2O_2 decomposes easily on various metals, acid is usually added to increase its stability. However, the addition of acid also increases the corrosivity of the oxidant solution. Thus, it is beneficial to select catalysts which can minimize H_2O_2 decomposition and also resist corrosion. Gu et al.[45] used Pourbaix diagram of H_2O_2 aqueous system and those of various noble metals for cathode catalyst selection, and identified Au as an effective catalyst. Further fuel cell performance tests with various transition metals were carried out. Au showed a relatively good power density. Although slightly higher peak power densities were obtained using Pd or Os cathode catalyst, a large amount of gas evolution was observed.

Non-precious materials, including Co_3O_4 [46], carbon supported lead sulphate (PbSO_4/C), carbon supported iron tetramethoxy phenyl porphyrin (FeTMPP/C) [47] and Prussian Blue (PB) or Iron (III) hexacyanoferrate ($\text{Fe}_4[\text{Fe}(\text{CN})_6]_3$) [48], have also been investigated as cathode catalysts for $\text{NaBH}_4\text{-H}_2\text{O}_2$ fuel cells. While these materials demonstrated activity for H_2O_2 reduction, they generally gave relatively low power performance.

2.1.3.3 Catalyst supporting materials

Catalyst supporting material has a very important role in obtaining high performance of an electrode and hence the fuel cell. It was shown by Kim et al. [49] that the performance of a DBFC employing 1.5 mg cm^{-2} carbon-supported platinum anode was comparable to that of a DBFC employing an unsupported platinum anode with 6 mg cm^{-2} platinum loading. Further, coulombic efficiencies of DBFCs using carbon-supported and unsupported platinum anodes have been found to be 62.3 and 68.1 %, respectively. The carbon-supported platinum anode possesses higher catalytic activity and hence, is more cost-effective as compared to unsupported platinum anode.

Titanium mesh was adopted by Cheng and Scott [50] as catalyst support. DBFCs with the Ti mesh-supported Ag or Au anode showed superior performance as compared to the DBFCs employing same anodes supported on carbon for all catalyst loadings. Cell voltages of DBFCs with Ti mesh-supported anodes are higher than those of DBFCs with carbon-supported anodes for the entire duration of the stability test. Ponce de Le'on et al. [51] used titanate nanotubes supported gold as catalyst for electro-oxidation of BH_4^- and it was found that Au nanoparticles deposited on the nanotubular titanate support carried approximately twice the electrical charge compared to carbon supported Au during the electro-oxidation of BH_4^- .

2.1.4 Membrane

Since cathode electrocatalysts such as Pt are active toward borohydride electro-oxidation and hence, it is necessary to keep the fuel from crossing over to the cathode while allowing the transport of ions. Both anion exchange membrane (AEM) and cation exchange membrane (CEM) serve this purpose to a great extent. AEMs allow efficient transport of OH^- from cathode to anode compartment, but suffer from the problem of BH_4^- crossover. Compared to AEM, use of CEM greatly alleviates the effect of borohydride crossover. Besides, CEMs are commercially available and among them the perfluorinated membranes specially show good ion conductivity, chemical and mechanical stability [52]. Nafion[®] membranes are a kind of CEMs that was first employed in DBFC by Li et al. [2] and is still employed in a majority of DBFCs. Figure 2.1 shows the model of Nafion[®] clusters and the structure of Nafion[®] perfluorinated ionomer. Nafion[®] has tetrafluoroethylene (Teflon) backbone with perfluorovinyl ether groups ended with sulfonate groups. The nano-scale region of Nafion[®] has three parts: A – hydrophobic and stable polymer backbone which is not ionic conductive; B – interfacial region; C – hydrophilic region which has ionic conductivity related to sulfonate groups after hydration. In DBFC, the sodium ion is transported through the Nafion[®] membrane instead of the hydrogen ion in case of hydrogen PEFC. Prior to assembly, Nafion[®] membranes are pretreated by boiling in H_2O_2 solution to remove the remaining contaminants. Without the pretreatment, the membrane induced lower and less stable voltage compared to the pretreated membrane [25].

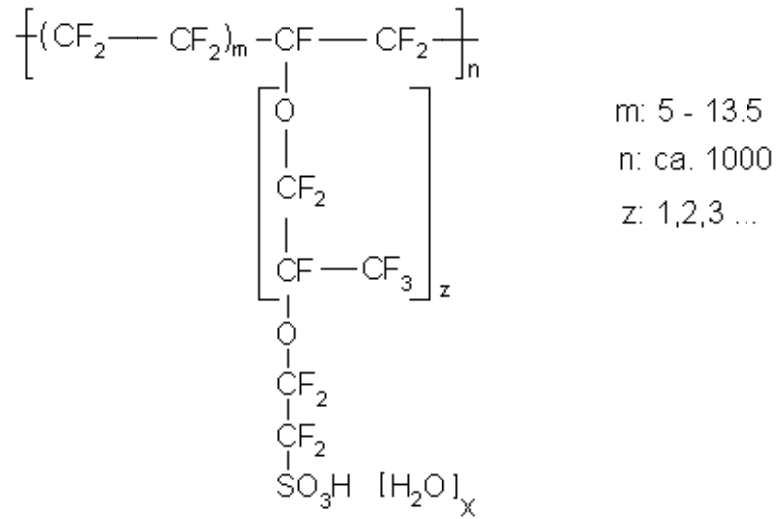
The problem with the usage of CEMs in DBFC is that it would reduce alkali concentration in the anolyte, which causes instability and inefficient use of the borohydride. Moreover, the build up of alkali in the cathode associated with the use of CEMs as well as ORR results in the formation of carbonates in the presence of CO₂ in air, which deactivates the cathode as well as membrane and restricts flow of oxygen / air to the cathode. The problem becomes more severe in a longer operation and therefore a way to remove CO₂ and to return the NaOH from catholyte to anolyte is needed.

Besides commonly used Nafion[®] membranes, various alternative membranes (as given in Table 2.3) are employed and examined as electrolyte in DBFCs. Cheng et al. [53] prepared several ion exchange membranes (CU1, CU2, CU3) by radiation grafting technique and evaluated them in DBFCs. CU1 membrane fabricated by grafting styrene onto polyethylenetetrafluoroethylene followed by a subsequent sulphonation reaction gave the highest power performance in DBFC among all the new membranes investigated in the research presented in this paper. The said membrane also yielded better performance than Nafion[®] 117 membrane in DBFC due to its high ionic conductivity and high ion exchange capacity. However, this membrane did not show good stability in terms of peak power density.

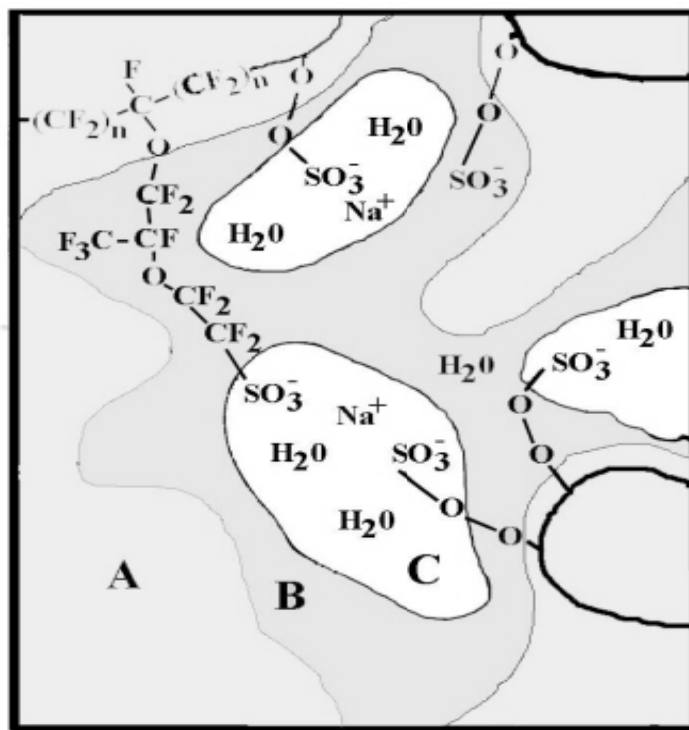
Cheng et al. [22] made a comparison between Nafion[®] 117 and laboratory-made 3541P membrane, which consists of ethylene-tetrafluoroethylene (65%) backbone and polysulphonic acid (35%) grafting polymers. The 3541P ionomer membrane had higher ion exchange capacity, equilibrium water capacity, and ionic conductivity and therefore,

gave better performance than Nafion[®]117 membrane. However, the 3541P ionomer membrane was unsuitable for application at elevated temperatures (e.g. 70 °C), despite its good stability at ambient temperature

Finally, it should be noted that operating a DBFC without a membrane or any other separator will simplify the engineering aspects. In order to achieve this, some researchers used cathodes that are inactive towards electro-oxidation and chemical hydrolysis of BH_4^- . With the usage of these organo-metallic compounds and perovskite-based oxides as cathode materials, which have high selectivity towards ORR and excellent tolerance towards BH_4^- electro-oxidation, probability of developing mixed-reactant DBFCs that employ no membrane separators and hence cost-effective, is increased.



(a)



(b)

Figure 2.1 (a) Nafion[®] perfluorinated ionomer; (b) Model of Nafion[®] clusters [54].

Table 2.3 DBFC performance data obtained with various electrode catalysts and membranes.

Anode electrocatalyst	Cathode electrocatalyst	Membrane	Oxidant	Temperature (°C)	Peak Power density (mW cm ⁻²)	Ref
Ni	Pt/C	Nafion [®] 211	Air	25	40	52
Ni/C	Pt/C	Nafion [®] 212	O ₂	60	150	23
Ni/C	Pt/C	Nafion [®] 117	O ₂	85	40.5	22
Pd/C	Pt/C	Nafion [®] 117	Air	25	19.4	55
Pd/C	Pt/C	Nafion [®] 117	O ₂	85	89.6	22
Pt/C	Pt/C	Nafion [®] 212	O ₂	60	100	23
Pt/C	Pt/C	Nafion [®] 117	O ₂	85	51.3	22
Pt/C	Non-platinum catalyst/Ni mesh	Morgane [®] ADP	Air	RT	200	56

(Continued)

Table 2.3: *Continued*

Ni+Pd/C	Pt/C	Nafion [®] 112	Air	60	250	57
Ni+ Pd/C+ Zr–Ni alloy	Co-PPY-C	Nafion [®] 117	Air	Ambient	65	43
Ni ₃₇ –Pt ₃ /C	Pt/C	Nafion [®] 212	O ₂	60	221	23
Pt–Ni/C	Non-platinum catalyst/Ni mesh	Morgane [®] ADP	Air	RT	115	56
Pt–Ru	Pt/C	Morgane [®] ADP	O ₂	60	149.33	58
Ag/C	Pt/C	Nafion [®] 117	O ₂	85	43.6	22
Ag/Ti	Pt/C	Nafion [®] 117	O ₂	85	50	50
Au/C	Pd/C	Nafion [®] 117	O ₂	85	65.6	22
Au/C	Ag/C	Nafion [®] 117	O ₂	85	32.8	22
Au/C	Ni/C	Nafion [®] 117	O ₂	85	35.4	22

(Continued)

Table 2.3: *Continued*

Au/C	Pt/C	Nafion [®] 117	O ₂	85	72.2	59
Au/C	FeTMPP	Nafion [®] 117	O ₂	85	65.3	42
Au/Ti	Pt/C	Nafion [®] 117	O ₂	85	81.4	50
Au	silver nitrate	AEM	Air	RT	12	60
Au	MnO ₂	AEM	Air	RT	28	60
Au-Pt	MnO ₂	AEM	Air	RT	20	60
Au	Pt/C	Nafion [®] 117	Acidified H ₂ O ₂	20	37.5	61
Pd	Au	Nafion [®]	Acidified H ₂ O ₂	60	680	45
MmNi _{3.6} Al _{0.4} Mn _{0.3} Co _{0.7}	PbSO ₄ /C	Nafion [®] 961	H ₂ O ₂ + H ₂ SO ₄	25	10	62
MmNi _{3.55} Al _{0.3} Mn _{0.4} Co _{0.75}	Prussian blue	Nafion [®] 117	H ₂ O ₂ + H ₂ SO ₄ + KCl	30	68	48
MmNi _{3.55} Co _{0.75} Mn _{0.4} Al _{0.3}	Cobalt Phthalocyanine	None	Air	RT	90	40

(Continued)

Table 2.3: *Continued*

$\text{MmNi}_{3.55}\text{Co}_{0.75}\text{Mn}_{0.4}\text{Al}_{0.3}$	Iron Phthalocyanine	None	Air	RT	92	41
$\text{MmNi}_{3.55}\text{Al}_{0.3}\text{Mn}_{0.4}\text{Co}_{0.75}$	FeTMPP/C	Nafion [®] 117	$\text{H}_2\text{O}_2 + \text{H}_2\text{SO}_4$	70	82	47
$\text{MmNi}_{3.55}\text{Al}_{0.3}\text{Mn}_{0.4}\text{Co}_{0.75}$	PbSO_4/C	Nafion [®] 117	$\text{H}_2\text{O}_2 + \text{H}_2\text{SO}_4$	70	120	47
$\text{MmNi}_{3.6}\text{Al}_{0.4}\text{Mn}_{0.3}\text{Co}_{0.7}$	Au/SS mesh	Nafion [®] 961	$\text{H}_2\text{O}_2 + \text{H}_2\text{SO}_4$	25	50	63
$\text{MmNi}_{3.35}\text{Co}_{0.75}\text{Mn}_{0.4}\text{Al}_{0.3}$	MnO_2/C	None	O_2	25	70	39
$\text{MmNi}_{4.5}\text{Al}_{0.5}$	Pt/C	Nafion [®] 117	H_2O_2	70	130	64
$\text{MmNi}_{3.2}\text{Al}_{0.2}\text{Mn}_{0.6}\text{Co}_{1.0}$	Pt/C	Nafion [®] 117	H_2O_2	70	100	64
$\text{MmNi}_{3.55}\text{Al}_{0.3}\text{Mn}_{0.4}\text{Co}_{0.75}$	Pt/C	Nafion [®] 117	H_2O_2	70	150	64
$\text{MmNi}_{3.2}\text{Al}_{0.2}\text{Mn}_{0.6}\text{B}_{0.03}\text{Co}_{1.0}$	Pt/C	Nafion [®] 117	H_2O_2	70	125	64
$\text{Zr}_{0.9}\text{Ti}_{0.1}\text{Mn}_{0.6}\text{V}_{0.2}\text{Co}_{0.1}\text{Ni}_{1.1}$	Pt/C	Nafion [®] 117	O_2	85	190	2
$\text{Zr}_{0.9}\text{Ti}_{0.1}\text{V}_{0.2}\text{Mn}_{0.6}\text{Cr}_{0.05}\text{Co}_{0.05}\text{Ni}_{1.2}$	Pt/C	Nafion [®] 117	H_2O_2	70	70	64

2.2 Chitosan

Chitosan [β -(1,4)-2-amino-2-deoxy-D-glucopyranose] shown in Figure 2.2, is a hydrophilic, inexpensive, biodegradable, and non-toxic natural polymer that is derived by deacetylation of chitin [poly(N-acetyl-d-glucosamine)]. Chitin, which is present in the exoskeleton of arthropods, is the second most abundant natural biopolymer next to cellulose [65]. Chitosan is insoluble in water and most organic solvents. It is, however, soluble in dilute aqueous solution of a weak acid such as acetic acid, which converts glucosamine unit (R-NH₂) of chitosan into its protonated form (R-NH₃⁺). Because of the presence of cationic moiety (-NH₃⁺) on its polymer backbone, chitosan dissolved in aqueous medium behaves as a polycation [66]. Chitosan dissolved in dilute aqueous solution of acetic acid reacts dialdehydes, and in particular glutaraldehyde, to form chitosan chemical hydrogel [67]. The aldehyde groups form covalent imine bonds with the amino groups of chitosan, due to the resonance established with adjacent double ethylenic bonds [68] via a Schiff mechanism.

As an abundant bioresource, chitosan has been attracting interest in a number of different fields. In the biomedical field, it has been used in tissue engineering, wound healing, burn treatment, artificial skin, ophthalmology, drug delivery etc. Chitosan and its derivatives also have industrial applications, including cosmetics, water engineering, paper industry, textile industry, food processing, agriculture, photography, separation, solid state batteries etc. Chitosan can be prepared in various forms including fibers, gels, beads, microcapsules, microspheres and membranes. Among them, chitosan membranes are

widely used as candidate materials for biological, chemical, energy and environmental applications. Recently chitosan has been used as a polymer host for solid polymer electrolytes (SPE) for batteries [69,70] and proton exchange membranes for fuel cells [71,72,73]. To enhance the conductivity of chitosan as SPE in a solid-state protonic battery, several approaches have been suggested, including the use of blend polymers, the addition of a ceramic filler, plasticizer etc. For application in fuel cells, cross-linked chitosan membranes have been synthesized as ion exchange membranes. Cross-linking is used as chemical modification to ensure good mechanical and chemical stability. Typical cross-linking agents include glutaraldehyde, sulfuric acid, and tannic acid etc. The cost-effectiveness and simple fabrication technique involved in the synthesis of cross-linked chitosan membranes make their applicability in fuel cell quite attractive.

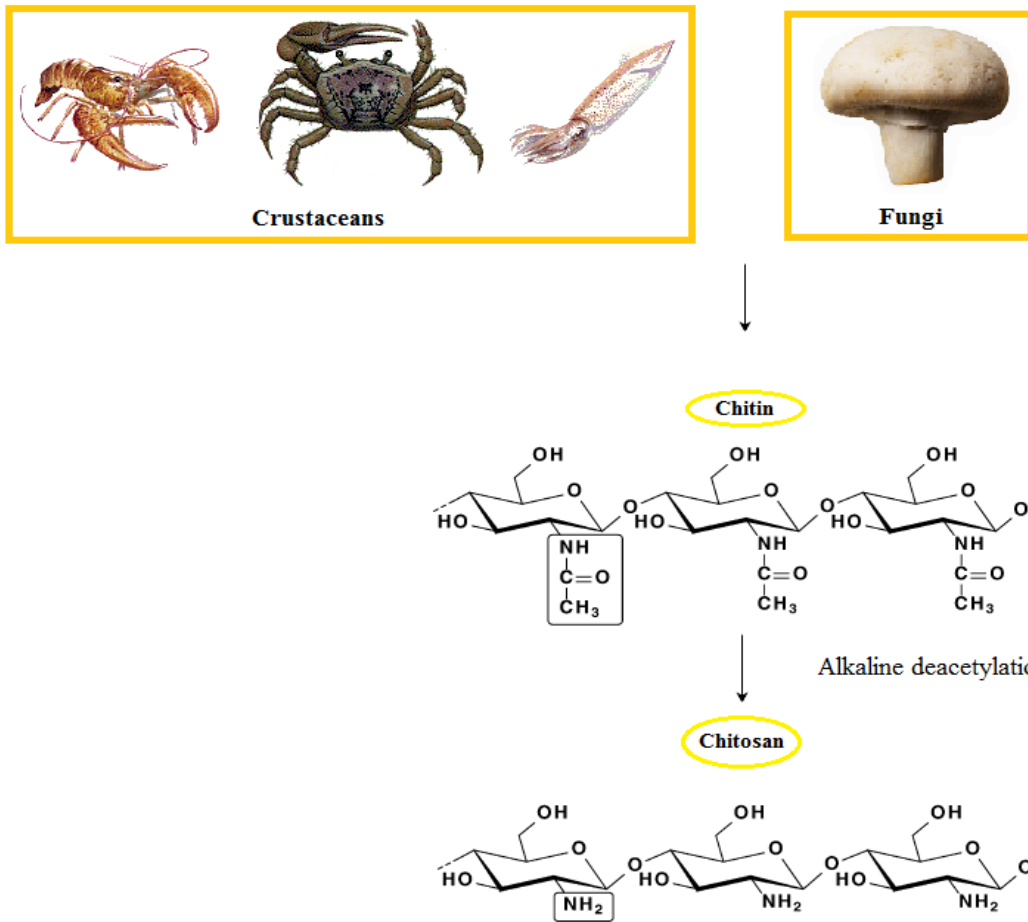


Figure 2.2 Description of chitosan structure and production.

2.3 Polyvinyl alcohol

Polyvinyl alcohol (PVA) is a cheap, non-toxic, and chemically stable synthetic polymer used since the early 1930s in a wide range of industrial, commercial, medical and food applications [74]. General chemical and physical properties of PVA are summarized in Table 2.4. PVA is prepared by hydrolysis or partial hydrolysis of polyvinyl acetate. Different length of the initial vinyl acetate polymer and the degree of hydrolysis under alkaline or acidic conditions yield PVA of differing physical properties. Under acidic conditions, the –OH groups of PVA react with –CHO groups of certain aldehydes to form acetal or hemiacetal linkages [75]. The result entity is gel like in nature and can be cast into membranes.

Sahu et al. characterized the PVA membrane using different techniques [76]. The scanning electron micrograph reveals a smooth surface of the PVA membrane with no defects. The X-ray diffraction pattern of PVA membrane exhibits broad peaks at 2θ values of 11° , 20° and 41° respectively. The broad peaks in the XRD pattern indicate a partially amorphous nature of the PVA membrane. The thermogravimetric analysis of acidic PVA membrane shows a weight loss of about 10 % in the temperature range between 30 and 150 $^\circ\text{C}$ due to evaporation of surface and moderately bound water. The PVA membrane undergoes total thermal oxidation at temperature between 150 and 470 $^\circ\text{C}$ due to the decomposition of its polymer chain. The midpoint ASTM glass transition temperature for PVA membrane is 108.26 $^\circ\text{C}$. The Young's modulus and proportional limit stress values for PVA membrane are 3.24 and 0.977 MPa, respectively. The water uptake value for PVA

membrane is about 1.3 g H₂O/g PVA hydrogel membrane. FTIR spectra of uncross-linked and cross-linked PVA membranes have been studied by Guo et al. [77]. Intensity of the peak in the wave number region 3000-3400 cm⁻¹ of the FTIR spectrum, which is due to –OH group of PVA, has been found to be lesser in the cross-linked PVA membrane as compared to uncross-linked PVA membrane. The decrease in the peak intensity is attributed to the gradual disappearance of –OH group of PVA because of its reaction with aldehyde group of glutaraldehyde. It has also been observed that two new peaks at 997 and 1240 cm⁻¹, attributed respectively to acetal (-C-O-C-O-) and ether (-C-O-C) groups that result from the reaction between –OH group of PVA and -CHO group of glutaraldehyde, appeared in the spectrum of cross-linked PVA membrane.

Table 2.4 General chemical identity and physical properties of polyvinyl alcohol.

Molecular weight	30,000-200,000
Structural formula	$(-\text{CH}_2\text{CHOH}-)_n(-\text{CH}_2\text{CHOCOCH}_3)_m$
Physical appearance	Odorless, white to cream colored granular powder
Specific gravity	1.19-1.31
Solubility	Insoluble in aliphatic and aromatic hydrocarbons, esters, ketones, and oils, water soluble

Chapter 3 Experimental

3.1 Materials

A list of materials, their properties and vendors is given in Table 3.1

3.1.1 Pretreatment of as-received materials

3.1.1.1 Pretreatment of nickel foam

As-received nickel foam was roller pressed to a thickness of 0.5 mm. To remove grease from the surface, nickel foam was immersed in acetone with ultrasonication, and then dried in ambient environment. After this process, Ni foams were immersed in 1.5 M H₂SO₄ for 10 min at ambient temperature to remove any oxide layer and etch the surface. Finally, degreased and etched foam was rinsed with deionised water to remove chemicals prior to further use.

3.1.1.2 Pretreatment of Nafion[®] membrane

The as-received Nafion[®] membrane was boiled in aqueous solution of 3 wt.% H₂O₂ and 3 wt.% H₂SO₄ for 1 h and then boiled in deionized water for 1 h.

3.2 Preparation of electrode binder solution

3.2.1 Preparation of PVA binder solution

An aqueous solution of PVA (0.05 g mL^{-1}) was prepared by adding the required amount of PVA in a certain volume of DI water in a glass beaker and magnetically stirring the contents in a boiling water bath for 12 h. A certain volume of a 0.05 g mL^{-1} aqueous solution of PVA was mixed with an optimized volume of 25% aqueous solution of glutaraldehyde and the contents were stirred magnetically at ambient conditions of temperature and pressure for 12 h. In a typical preparation, 20 mL of 0.05 g mL^{-1} aqueous solution of PVA was mixed thoroughly with 0.2 mL of 25% aqueous glutaraldehyde by stirring magnetically for 12 h at ambient temperature. The mixture was allowed to remain still for 12 h in order to allow the air bubbles to disappear from the viscous solution.

3.2.2 Preparation of chitosan binder solution

An aqueous solution of 0.25 % (w/v) chitosan was prepared by adding the required amount of chitosan powder in 1 % (v/v) aqueous solution of acetic acid or L(+)-Lactic acid in a glass beaker and stirring the contents magnetically at ambient temperature until a homogenous solution was formed.

3.3 Preparation of electrode

3.3.1 Electrode prepared by ink paste method

Table 3.2 gives a list of various electrodes prepared by ink paste method.

3.3.1.1 General procedure of ink paste method

The required amount of catalyst powder was mixed with the desired amount of solvent to form a suspension which was agitated in an ultrasonic water bath. Then the required amount of binder solution was added dropwise to the suspension of catalyst powders with continued ultrasonication. The catalyst slurry was then coated on one side of an electrode substrate with an appropriate sized camel hair brush. Finally, the electrode was dried at an appropriate temperature until its weight was constant. For Nafion[®] binder based catalyst ink, isopropyl alcohol was used as solvent. The solvent for PVA or chitosan binder based catalyst ink was DI water.

3.3.1.2 Preparation of PVA or chitosan binder based electrode

The dried PVA binder-based catalyst ink-coated electrode substrate was dipped in 90 % (v/v) aqueous solution of glacial acetic acid for ~ 5 h to cause the cross-linking reaction between PVA and glutaraldehyde to occur. The dried chitosan binder-based catalyst ink-coated electrode substrate was dipped in 6.25 % (v/v) aqueous solution of glutaraldehyde for ~ 5 h for cross-linking reaction between chitosan and glutaraldehyde to occur. After the treatment, the electrode was washed thoroughly with DI water to remove excess of impurities.

3.3.2 Palladium electrode prepared by electrodeposition

Typical set up for electrodeposition is shown in Figure 3.1. The working electrode was Zorflex[®] activated carbon cloth (FM 10) with a thickness of 0.5 mm. A piece of platinum wire was used as the counter electrode. The electrodeposition process was performed in a palladium electroplating bath by applying constant voltage with a Keithley sourcemeter at ambient conditions of temperature and pressure. After deposition, the carbon cloth was rinsed thoroughly with deionized (DI) water and dried in ambient environment until it reached a constant weight. Then a desired amount of Nafion[®] solution was applied to the surface of the electroplated carbon cloth before it was further dried in oven at 80 °C.

3.3.3 Gold electrode prepared by sputtering deposition

A schematic diagram of set up for sputtering deposition is shown in Figure 3.2. Gold was sputtering deposited on Zorflex[®] activated carbon cloth using a plasma current of 15 mA for 60 s.

3.3.4 Electron beam physical vapor deposition

Electron beam physical vapor deposition was done using an in-house instrument at ITN Energy Systems of Littleton Colorado. An e-beam with a multi-pocket hearth (Temescal type) was employed and it allowed sequential deposition of up to four different materials. Evaporation rates were determined by depositing several thicknesses of each material, in the thickness range that can be measured by Dektak profilometer. Once the rate curves are established, fairly precise thicknesses can be produced by using a slow deposition rate

(low emission current, ~ 0.02 A) and a shutter above the evaporation source. Deposition rates were about 0.1 \AA s^{-1} for total thicknesses of less than 100 \AA , and rate of about 0.5 \AA s^{-1} for thicker films. All deposition runs were made after establishing a chamber base pressure of 2.0×10^{-6} Torr or less.

3.4 Preparation of polymer membrane electrolyte

3.4.1 Preparation of PVA membrane

3.4.1.1 Preparation of PVA solution

An aqueous solution of PVA (0.1 g mL^{-1}) was prepared by adding the required amount of PVA in a certain volume of de-ionized (DI) water in a glass beaker covered with a Petri dish and magnetically stirring the contents in a boiling water bath for 12 h.

3.4.1.2 Preparation of PVA and glutaraldehyde solution mixture

A certain volume of a 0.1 g mL^{-1} aqueous solution of PVA was mixed with an optimized volume of 25 % aqueous solution of glutaraldehyde and the contents were stirred magnetically at ambient conditions of temperature and pressure for 12 h.

3.4.1.3 Preparation of PVA hydrogel membrane

PVA hydrogel membrane was prepared by a modified solution casting method in which a mixture of an aqueous solution of PVA and an optimized quantity of glutaraldehyde (25 % aqueous solution) was cast on a glass Petri dish and left at ambient

conditions of temperature and pressure for ~ 48 h to allow the water to evaporate. In a typical preparation, 10 mL of 0.1 g mL⁻¹ aqueous solution of PVA was mixed with 0.2 mL of 25 % aqueous glutaraldehyde by stirring magnetically for 12 h and cast on a glass Petri dish. After the evaporation of water, a dry film comprising of a homogeneous mixture of PVA and glutaraldehyde was left at the bottom of the Petri dish. A sufficient volume of 1 M sulphuric acid was then added to the Petri dish so as to completely dip the dried composite film inside the acid solution. The film was then left at room temperature for about 12 h to allow the cross-linking reaction to occur. Due to the cross-linking reaction, the membrane was easily peeled off the surface of the Petri dish. The membrane was then taken out of the acid bath, washed thoroughly with DI water and stored in DI water bath.

3.4.2 Preparation of chitosan membrane

3.4.2.1 Preparation of pristine chitosan membrane

2 g chitosan powder was dissolved in 100 mL of 1 % (v/v) aqueous solution of L(+)-Lactic acid or acetic acid and vigorously stirred to form a solution. The solution was cast in a Petri-dish and left in ambient conditions for about 12 h for degassing. After that, the Petri-dish with the viscous chitosan solution was transferred to an oven where it was heated at 55-60 °C for 24 h.

3.4.2.2 Preparation of chitosan hydrogel membrane

To prepare chitosan hydrogel membrane, a sufficient volume of reagent was added to the pristine chitosan membrane for cross-linking in ambient conditions. The cross-linking reagent used included 0.5 M sulfuric acid or sodium sulfate, 0.0136 M sodium triphosphate or sodium phosphate tribasic dodecahydrate aqueous solution. Finally, the membrane formed was thoroughly washed by DI water and stored in DI water. Due to the absorption of salt solution and subsequent ionic cross-linking reaction, the chitosan mass turned into a solid hydrogel membrane which was then washed with DI water and stored in DI water bath.

3.4.2.3 Preparation of homogenously cross-linked chitosan membrane

In 50 mL, 2 % chitosan in 1% acetic acid aqueous solution, 80 μ L of 25% glutaraldehyde was added dropwise while the solution was stirred intensely for 1 h. Then 7 mL the solution was poured in a polystyrene dish and dried in ambient environment until it can be peeled off.

3.5 Characterization of polymer membrane electrolyte and electrode

3.5.1 Scanning electron microscopy (SEM)

Scanning electron micrographs of PVA, chitosan, and Nafion[®] binders-based anodes as well as cathodes were recorded on a Jeol JSM-IC 848 scanning electron microscope.

A Pt electrode of a chitosan-based DBFC surface was examined by SEM (Quanta200) and energy-dispersive X-ray spectroscopy (EDS) after the fuel cell was operated at a current density of 50 mA cm^{-2} for 2 h.

Morphology of sputtered gold electrode, electrodeposited palladium electrode was investigated by SEM (XL-30 ESEM).

Surface and cross-sectional area of chitosan membrane was examined under SEM with EDS analyzing system (XL-30 ESEM).

3.5.2 Fourier transform infrared spectroscopy (FTIR)

FTIR spectra were recorded on a Renishaw - Smiths Detection Combined Raman - IR Microprobe. Membrane samples were put in appropriate physical contact with the sampling plate of the spectrometer accessory, yielding high quality and reproducible spectra.

3.5.3 Thermal analysis

Membrane samples were dried at $25 \text{ }^{\circ}\text{C}$ for 24 h before thermal analysis measurement. Thermogravimetric analysis (TGA) studies on chitosan membrane were carried out under nitrogen atmosphere by employing a Perkin Elmer Thermal Analysis Controller (TAC 7/DX) in the temperature range of $20\text{-}800^{\circ}\text{C}$ at a temperature scan rate of $10 \text{ }^{\circ}\text{C min}^{-1}$. The flow rate of N_2 during purging as well as during heating was maintained at 60 mL min^{-1} .

Differential scanning calorimetry (DSC) spectra of membranes were obtained on TA instrument DSC model 2920. DSC Measurements were performed in nitrogen atmosphere from room temperature to 200 °C at a heating rate of 10 °C min⁻¹ in hermetically sealed aluminum pans.

3.5.4 Mechanical test

The mechanical strength of chitosan membrane in its swollen state was characterized by Instron table mounted testing machine with a transducer capacity of 50 lb. The membrane sample size was 30 mm (length) × 20 mm (width) and the stretching speed was 10 mm min⁻¹ at ambient temperature.

3.5.5 Water uptake measurement

Membrane samples were stored in DI water at room temperature for several days to ensure sufficient water uptake. To determine the water uptake at hydration, the membranes were removed from water, blotted dry with filter paper to remove surface water, and quickly weighed to give the initial wet weight. After that, the sulfate ion modified chitosan membrane pieces were dried at 110 °C in an oven for 48 h to evaporate all the absorbed water. Multivalent phosphate modified chitosan membranes were dried at atmospheric conditions for 24 h (step I), and then further dried in an air convection oven (Carbolite) at 100 °C for 3 h (step II) until the weight of membranes were constant. The percentage water

uptake values of the membranes were then calculated from their wet and dry weights using the Equation 3.1:

$$\text{Water uptake (\%)} = \frac{W_h - W_d}{W_d} \times 100 \quad (3.1)$$

Where W_h is the weight of hydrated membrane, and W_d is the weight of dry membrane.

3.5.6 Ionic conductivity measurement

Ionic conductivity measurement was carried out in a two-point-probe conductivity cell (Figure 3.3) at room temperature. The cell frame was machined from Teflon material and two copper electrodes were used to contact the membrane on both sides. The electrode diameter was 1 cm. Potentiostatic EIS measurement was carried out in the frequency range of 10^{-1} - 10^5 Hz at open circuit potential with an AC voltage of 5 mV, by means of Gamry electrochemical system (model number: PCI4). Membrane thickness was measured by a digital micrometer (Mitutoyo). Before conductivity measurement, membranes were equilibrated for 24 h in DI water or 10 wt.% aqueous NaOH solution at room temperature. Prior to the assembly of cell, the membrane was surface dried by wiping it with tissue paper, and then the swollen membrane was placed quickly between the copper electrodes in the measurement cell. To ensure good membrane electrode contact, two cell frames were held tightly with bolts. The water content of the membrane was assumed to remain constant

during the short period of time required for the measurement. Membrane conductivity σ (S cm^{-1}) was calculated using Equation 3.2:

$$\sigma = \frac{L}{R \times A} \quad (3.2)$$

Where σ (S cm^{-1}) is membrane conductivity, L (cm) is the thickness of membrane inside the conductivity cell, A (cm^2) is geometric area of the membrane, and R (Ω) is bulk resistance calculated from high-frequency intercept on the real axis of the complex impedance plot.

3.5.7 Borohydride crossover measurement

Ex-situ studies were carried out to determine the extent of borohydride crossover by using passive fuel cell hardware as shown in Figure 3.4. The chambers of the hardware are two high-density graphite blocks, each of which had a number of holes of 1 mm diameter. Chamber A contained an aqueous solution of 30 wt.% NaBH_4 in 6 M NaOH and chamber B was filled with 6 M NaOH aqueous solution. The two chambers were separated by a piece of membrane and were held in tight contact with bolts. The membrane samples were equilibrated in 6 M NaOH for 24 h prior to employing in the experiments. The set-up was kept at room temperature to allow the chemical species to crossover through the membrane. After a certain amount of time, crossovered borohydride was analyzed quantitatively.

A number of methods have been used to determine the concentration of borohydride, including titrimetric [78], polarographic [79], spectrophotometric [80], and voltammetric methods [81]. Among them, voltammetric method is a simple, rapid, and accurate analytical method that can be used directly in a reaction system. In this study the concentration of borohydride was measured according to reported voltammetric method [82]. The detection limit of borohydride using voltammetric method is 10^{-5} M [83]. This method links the maximum oxidation current of BH_4^- , under linear sweep voltammetry, to the concentration of borohydride solution, using a three-electrode electrochemical cell. The working electrode was a 0.1 mm diameter high purity gold wire (Aldrich) of 3 cm length. The counter electrode was a piece of nickel mesh with an area of $1.1 \text{ cm} \times 3.3 \text{ cm}$. The reference electrode was a mercury / mercury oxide (MMO) reference electrode (Radiometer Analytical). As supplied, the reference electrode was filled with a 1 M KOH solution, and its potential is 0.115 V vs. SHE. The linear sweep voltammogram was recorded using a Gamry electrochemical system. The potentiostat was set to scan between -0.8 and 0.2 V (vs. MMO) at 100 mV s^{-1} .

3.6 Fuel cell assembly

Single fuel cell hardware was purchased from Fuelcelltechnologies, Inc. Gaskets were Teflon coated fiberglass tape (Saint Gobian). The thickness of the gasket was 100-150 micron less than electrode thickness. The flow plates of both anodes and cathodes were two 76.2×76.2 mm graphite blocks. Each graphite block had 5 cm^2 square flow area with

rectangular channels of 0.8 mm width and 1 mm depth. The channels in the blocks supply alkaline sodium borohydride solution to the anode and oxidants to the cathode. The graphite blocks were provided with tiny holes to accommodate thermocouples. A constant temperature was maintained by a temperature controller. The channels supply alkaline sodium borohydride solution to the anode and oxygen, air, or hydrogen peroxide to the cathode. Electrical heaters are placed behind in the endplates to heat the cell to a desired temperature.

To prepare the MEAs, a piece of membrane was held together between two electrodes. The MEAs were placed between anode and cathode flow-field graphite plates and tightened together by applying a torque of 100-110 inch pound. The anode and cathode of the MEA were contacted on their rear with gas/fluid flow field plates machined from high-density graphite blocks. The ridges between the channels make electrical contact to the rear of the electrode and conduct current to the external circuit. A picture of an assembled DBFC single cell is shown in Figure 3.5.

3.7 Fuel cell performance measurement

The fuel was recirculated through the anode chamber with a peristaltic pump. The anode flow rate was 5 mL min^{-1} . The oxidants used were oxygen, air, or acidified hydrogen peroxide. Dry oxygen was supplied from a high-pressure oxygen cylinder and its pressure was reduced by a pressure regulator to 3 psi. The flow rate of oxygen was controlled by a mass controller. The dry oxygen was humidified while it passed through a bubbler with a

spiral heating tape at 25 °C. After passing through the bubbler, the wet oxygen reached the single cell and reacted in the cathode, and then was fed to ambient environment. Figure 3.6 shows a schematic diagram of the DBFC test system. The cathode gas flow rate was 0.15 L min⁻¹. The hydrogen peroxide was recirculated through the cathode chamber with a peristaltic pump at a flow rate of 5 mL min⁻¹.

The fuel cell performance was measured using Scribner Associates fuel cell test system (Series 890e, Scribner Associates Inc., USA). The performance stability of the fuel cell was evaluated by monitoring cell voltage as a function of time at a constant load current density. Coulombic efficiency was analyzed under a constant current discharge with a start from the cell to be fueled with a certain amount of fuel solution. Different current densities were applied to the fuel cell and the cell voltages were recorded. Coulombic efficiency, which indicates the ratio of the actual discharging capacity to the theoretical discharging capacity, is defined in Equation 3.3:

$$\eta = \frac{\text{Discharging capacity}}{\text{Theoretical discharging capacity}} = \frac{it}{8NVF} \quad (3.3)$$

where i (A) is the discharging current, t (s) the time of the discharging process, N (M) is the concentration of the fuel solution, V (L) is volume of the fuel solution, F (96485 C mol⁻¹) is Faraday constant.

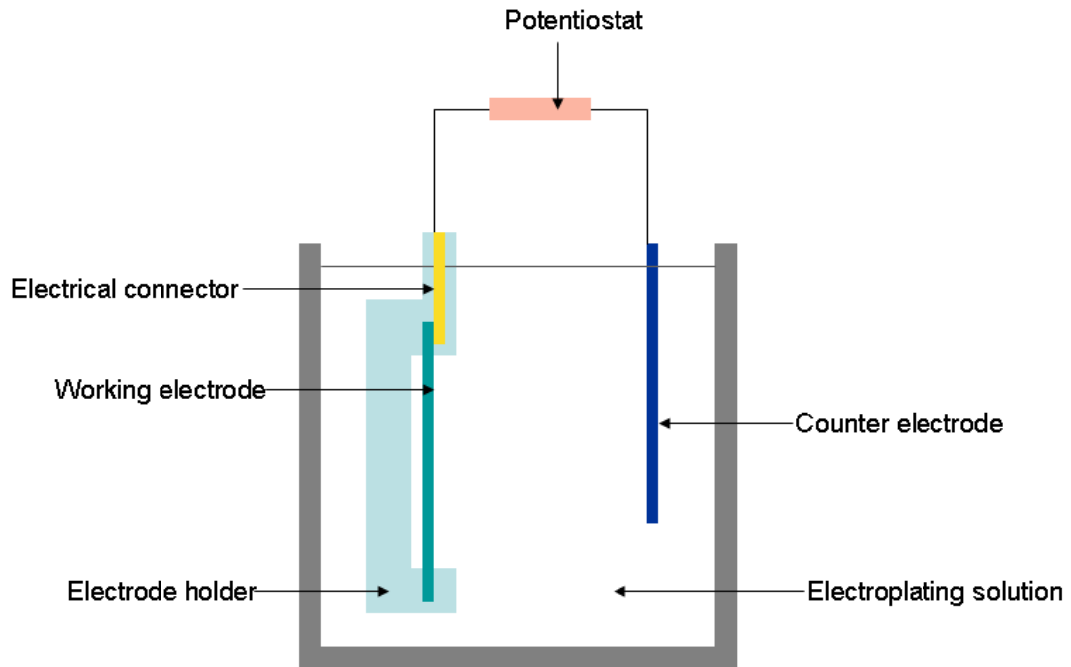


Figure 3.1 Typical setup for electrodeposition.

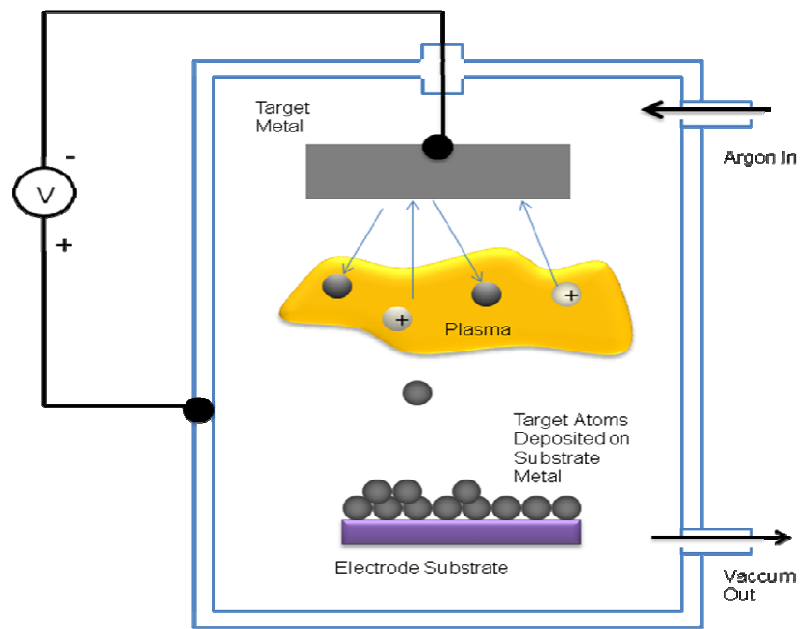


Figure 3.2 A schematic diagram of the sputtering apparatus.

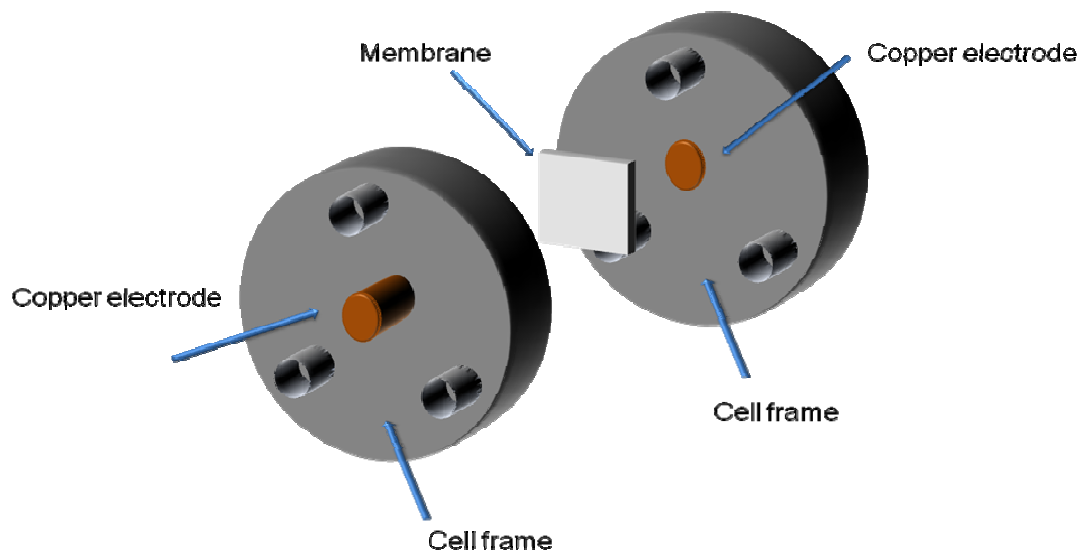


Figure 3.3 A schematic diagram of a two-probe conductivity measurement cell.

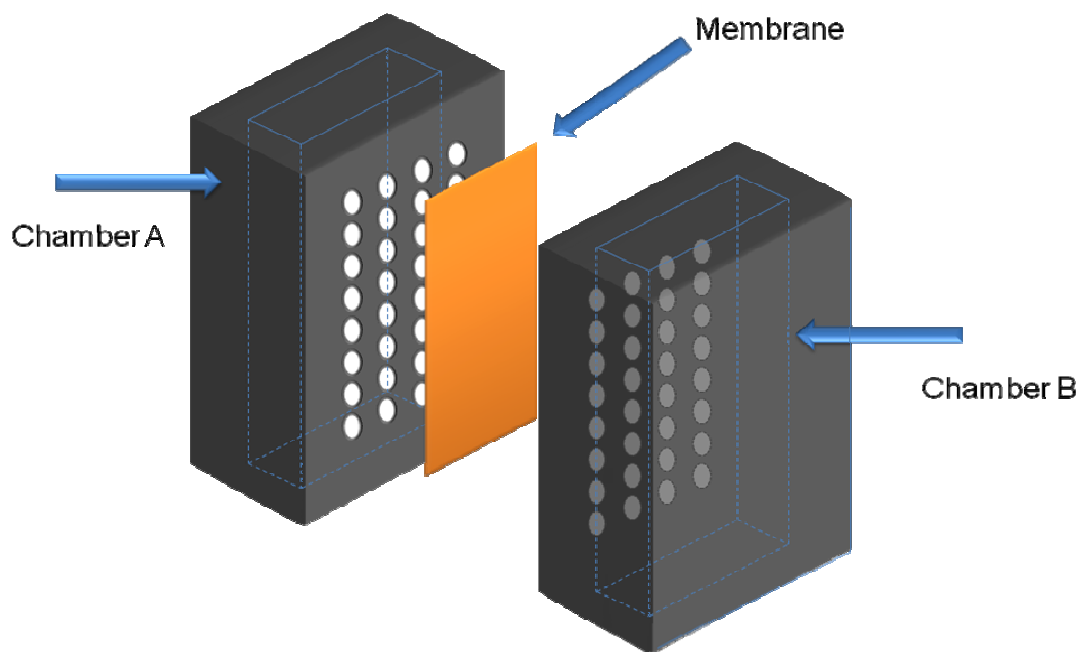


Figure 3.4 A schematic diagram of a set-up for crossover measurement of borohydride fuel.

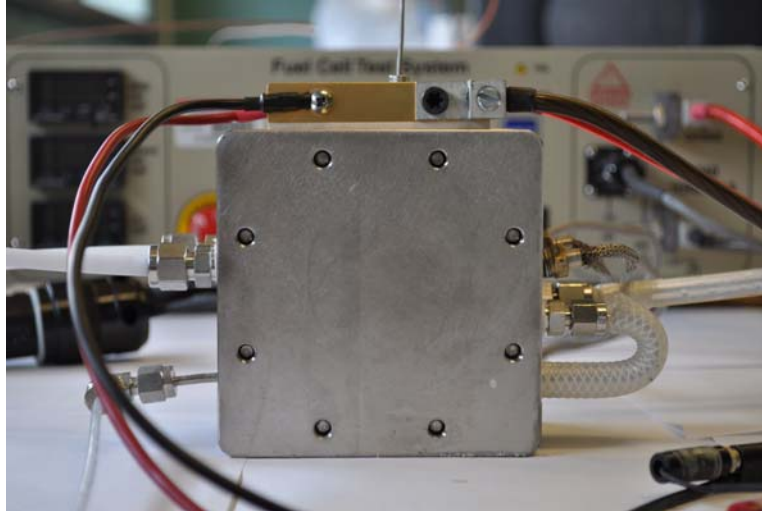


Figure 3.5 A picture of an assembled fuel cell.

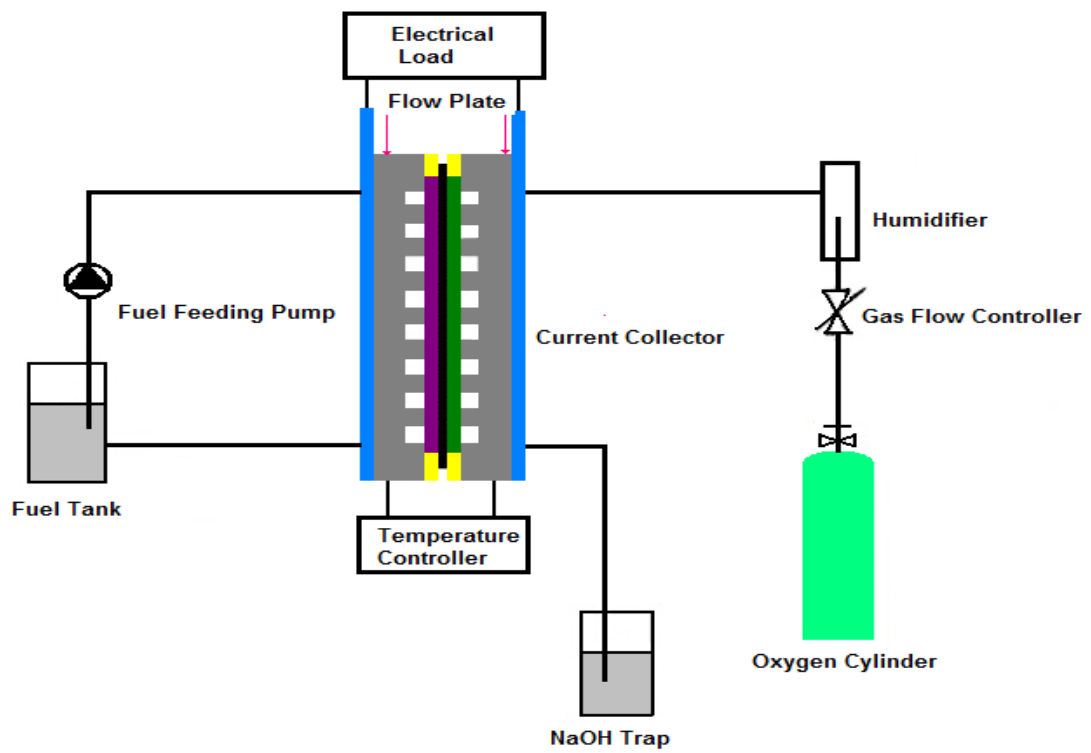


Figure 3.6 A schematic diagram of a DBFC test system.

Table 3.1 A list of materials, their properties and vendors.

Materials	Properties	Vendors
Acetone	Certificated ACS grade	Fisher Scientific
AB ₅ alloy powder	Weight percentage composition La _{10.5} Ce _{4.3} Pr _{0.5} Nd _{1.4} Ni _{60.0} Co _{12.7} Mn _{5.9} Al _{4.7}	Ovonic Battery Company
Chitosan powder	MW=100000-300000	Acros Organics
Glacial acetic acid	Certificated ACS grade	Fisher Scientific
Glutaraldehyde	25% aqueous solution	Alfa Aesar
Isopropyl alcohol	Certificated ACS grade	Fisher Scientific
L(+)-Lactic acid	90% solution in water	Acros Organics
Nafion [®] solution	Equivalent weights: 1000 EW, Composition: 4.95-5.05 wt.% Nafion [®] , 20 wt.% Water, 75 wt.% isopropanol, Density: 0.86 g/cm ³	Ion Power
Nafion [®] membrane	Type 212, Dry thickness: 0.002 inch Type 117, Dry thickness: 0.007 inch	Ion Power
Nickel foam	IPASO-0050679-0001, Density: 500 g/m ² , Pore size: 590 μm, Thickness: 1.7 mm	INCO

(Continued)

Table 3.1: *Continued*

Nickel powder	Type 210, Fisher sub-sieve size: 0.5-1.0 μm , Bulk density: $< 0.8 \text{ g cm}^{-3}$, Typical specific area: 1.5-2.5 $\text{m}^2 \text{ g}^{-1}$ (BET)	INCO
Palladium on carbon powder	10 wt.% Pd on Vulcan XC-72	BASF Fuel Cell
Palladium electroplating solution	Pallaspeed VHS solution with 30 gms/gallon	Technic
Palladium on activated carbon	10 wt. % Pd	Aldrich
Platinum electrode	1mg cm^{-2} Pt loading, 20 wt. % Pt/Vulcan XC-72, Thickness:10-11 mils, 30% Teflon treated	Electrochem
Platinum on carbon powder	10 % Pt on Vulcan XC-72	BASF Fuel Cell
Polyvinyl alcohol	95% hydrolyzed, average MW 95000	Acros Organics

(Continued)

Table 3.1: *Continued*

Sodium borohydride powder	≥98.0%	Acros Organics
Sodium hydroxide	Certificated ACS grade	Fisher Scientific
Sodium phosphate tribasic dodecahydrate	≥98.0%	Aldrich
Sodium triphosphate	purum p.a., ≥98.0%	Aldrich
Sulfuric acid	Certificated ACS grade	Acros Organics
Toray [®] Carbon paper	Thickness of EC-TP1-030 type: 0.11 mm, Thickness of EC-TP1-060 type: 0.19 mm	Electrochem
Vulcan Carbon XC-72		Carbot
Zorflex [®] activated carbon cloth	Type FM 10, Thickness: 0.55 mm	Chemviron Carbon/Calgon Carbon

Table 3.2 Description of electrode prepared by ink paste method.

Electrode	Catalyst		Binder		Electrode substrate
	Composition	Loading, mg cm ⁻²	Type	wt.% of catalyst	
Anode	Mixture of Ni powder and carbon-supported palladium powder, weight ratio of Ni:Pt=25:1	1, 2, or 5	Nafion [®] solution	15	Toray carbon paper EC-TP1-030 type
Anode	Mixture of Ni powder and carbon-supported platinum powder, weight ratio of Ni:Pt=25:1	1, 5	Nafion [®] solution	15	Toray carbon paper EC-TP1-030 type
Anode	Mixture of Ni powder and carbon-supported palladium powder, weight ratio of Ni:Pt=25:1	5	Nafion [®] solution	15	Ni foam as received

(Continued)

Table 3.2: *Continued*

Anode	Mixture of AB ₅ alloy powder (La _{10.5} Ce _{4.3} Pr _{0.5} Nd _{1.4} Ni _{60.0} Co _{12.7} Mn _{5.9} Al _{4.7}) and Vulcan XC 72 carbon powder, amount of carbon powder: 10 wt. % of AB ₅ alloy powder	30	Nafion [®] solution	5	Zorflex [®] Activated Carbon Cloth
Anode	Mixture of AB ₅ alloy powder (La _{10.5} Ce _{4.3} Pr _{0.5} Nd _{1.4} Ni _{60.0} Co _{12.7} Mn _{5.9} Al _{4.7}) and Vulcan XC 72 carbon powder, amount of carbon powder: 10 wt. % of AB ₅ alloy powder	30	PVA binder solution	5	Zorflex [®] Activated Carbon Cloth
Anode	Mixture of AB ₅ alloy powder (La _{10.5} Ce _{4.3} Pr _{0.5} Nd _{1.4} Ni _{60.0} Co _{12.7} Mn _{5.9} Al _{4.7}) and Vulcan XC 72 carbon powder, amount of carbon powder: 10 wt. % of AB ₅ alloy powder	30	Chitosan binder solution	0.5	Zorflex [®] Activated Carbon Cloth

(Continued)

Table 3.2: *Continued*

Cathode	Activate carbon supported palladium, 10 wt.% Pd	1	Nafion [®] solution	20	Zorflex [®] Activated Carbon Cloth
Cathode	Activate carbon supported palladium, 10 wt.% Pd	1	PVA binder solution	20	Zorflex [®] Activated Carbon Cloth
Cathode	Activate carbon supported palladium, 10 wt.% Pd	1	Chitosan binder solution	2	Zorflex [®] Activated Carbon Cloth
Anode	Mixture of Ni powder and carbon-supported palladium powder, the weight ratio of Ni:Pd: 25:1	5	Nafion [®] solution	12.5	Nickel foam 0.5 mm thickness
Anode	Mixture of Ni powder and carbon-supported palladium powder, the weight ratio of Ni:Pd: 25:1	5	Chitosan binder solution	2	Nickel foam 0.5 mm thickness

Chapter 4 Results and Discussion

4.1 A parametric study of Ni-based anode in a direct borohydride fuel cell

An active single fuel cell system was set up to examine the performance of membrane-electrode-assembly (MEA). A borohydride fuel cell, consisting of Nafion[®] 212 membrane electrolyte, Ni-based composite anode was assembled and tested. The anode was made by ink paste method. The anode catalysts were a composite of Ni with either carbon supported platinum (Pt/C) or carbon supported palladium (Pd/C). Ni electrode has more negative open circuit potential than that of Pt or Pd. Ni electrode also demonstrates smaller anode polarization than that of Pt or Pd. The borohydride electro-oxidation on Ni is generally a four electron process even with changing currents and borohydride concentration, while in case of Pd and Pt, the coulombic number is higher than four electrons at relatively low borohydride concentrations and high anode currents. The addition of electrode binder to catalyst layer tends to lower the borohydride concentration on the surface of catalyst particles [84]. Therefore composite of Ni and Pt or Pd can take the advantage of each component and thus hopefully enhance the electrode performance.

Both pure oxygen (or oxygen in air) and hydrogen peroxide were employed as the oxidant. For a DBFC using oxygen or air as the oxidant, a Pt electrode was employed as the cathode. This Pt cathode had 30% wet proof, which was 30% polytetrafluoroethylene (PTFE). Typically, porous carbon clothes or carbon papers with different thicknesses and

PTFE contents are employed as the cathode diffusion layer. A PTFE coating gives the electrode hydrophobic property which facilitates the transport of gaseous oxidants. On the other hand, the cathode should have hydrophilic property so as to be able to hold enough water for the use in the cathode reaction.

The MEA was made by sandwiching anode, membrane and cathode and pressing them together with mechanical force during the cell assembly. Hot pressing technique or membrane coating technique, which is commonly used for MEA fabrication in H₂-PEFCs, DMFCs, and also DBFCs, was not used. This is because proper space between the membrane and the anode is beneficial. Since, in this case hydrogen would be released more readily from the anode, and also fuel would be in a more complete contact with the anode [52]. However, large distance between the membrane and the anode results in increase in ohmic resistance. Therefore an optimal distance is needed to get the best cell performance. An optimum space in the MEA was achieved by applying optimal amount of torque during cell assembly.

4.1.1 Influence of operation condition on DBFC performance

The anolyte in DBFCs consisted of NaBH₄ in NaOH aqueous solution. Typically, the concentrations of NaBH₄ and NaOH lie in the range between 10 to 30 wt. % and between 10 to 40 wt.%, respectively. According to Nernst equation (Equation 4.1), a higher borohydride concentration yields a higher cell open circuit potential. However, this does not match experimental results. High borohydride concentration improves kinetics of

borohydride electro-oxidation and mass transport of the fuel. However, it also promotes borohydride crossover and hydrolysis. As depicted in half cell polarization, a concentrated borohydride solution enhances anode performance a little but deteriorates cathode performance to a larger extent due to borohydride crossover [85]. The overall DBFC performance was found to increase as borohydride concentration increased from 5 wt.% to 10 wt.%. However, a further increase of borohydride concentration to 20 wt.% decreased power performance [85].

$$E = E^0 - \frac{RT}{zF} \ln \frac{a[BO_2^-]a[H_2O]^2}{a[BH_4^-]a[O_2]^2} \quad (4.1)$$

Alkali concentration in the anolyte also affects the DBFC performance. According to Nernst equation, hydroxide concentration does not have an effect on the overall cell polarization, although it affects anode reaction positively and cathode reaction negatively. A high NaOH concentration reduces possible NaBH₄ hydrolysis. Yet, increased NaOH concentration leads to an increase in anolyte viscosity which decreases the mobility of sodium ions, a major charge carrier in DBFCs. As a result, ohmic resistance is increased especially at high current densities. In sum, both concentrations of NaBH₄ and NaOH need to be optimized to achieve good cell performance and fuel efficiency.

A high NaBH₄ concentration (10 wt.%) showed only slight power performance than low concentration (5 wt.%). Therefore, a borohydride concentration of 5 wt.% was employed in most of DBFC tests for the sake of fuel efficiency.

DBFC performance can be enhanced by increase in fuel flow rate, since a high flow rate improves mass transport of the fuel and also eliminates possible blocking of flow plate channels. However, this improvement due to flow rate increase is rather limited. Since the limiting transport resistance comes from the diffusion of borohydride ion in the catalyst layer, where the effect of convection is negligible. In addition, increase in fuel flow rate might give rise to a high pressure buildup in the anode compartment. This pressure buildup would force more anolyte and hence more BH_4^- to penetrate to the cathode compartment, thereby deteriorating the DBFC performance. Even though high fuel flow rate can affect the DBFC performance from both positive and negative aspects as aforementioned, its influence on its performance was experimentally proven to be small. Hence, from an economic point of view, using low fuel flow rate is more beneficial. An optimized flow rate of 5 mL min^{-1} was employed in DBFC tests.

Figure 4.1 shows curves of cell polarization and power density of DBFC using humidified oxygen and air at 28 and 60 °C. The membrane electrolyte was Nafion[®] 212 membrane. The anode consisted of Ni and Pd/C catalyst ($1 \text{ mg metal cm}^{-2}$) loaded on Toray[®] carbon paper. The anode binder was Nafion[®] ionomer which amounted 15 wt.% of the dry catalyst materials. The cathode was Pt cathode (1 mg Pt cm^{-2} on Toray[®] carbon paper). The fuel was 5 wt. % NaBH_4 and 10 wt. % NaOH aqueous solution, and its flow rate was 5 mL min^{-1} . The oxidant was oxygen or air with flow rate of 0.15 L min^{-1} . As seen, the power densities increased by increasing the temperature. Peak power densities of 77 mW cm^{-2} and 167 mW cm^{-2} were achieved using humidified air as the oxidant at 28 and 60

°C, respectively. Temperature increase has both positive and negative effects on the overall DBFC performance. Major advantages of temperature elevation include: (1) improvement of kinetics of both borohydride electro-oxidation and oxidation reduction reaction; (2) improvement of diffusion and mass transfer of the reactants; (3) enhancement of ionic conductivity of catholyte, anolyte and membrane electrolyte. Major disadvantages of elevated temperature include (1) increase in borohydride crossover, which might deteriorate the catalytic activity of the cathode electrocatalysts; (2) increase in borohydride hydrolysis, which results in reduction of fuel efficiency; (3) membrane dryness and poor water management inside the fuel cell, which leads to a larger cell resistance. Generally speaking, the beneficial effects on DBFC performance outweigh the detrimental effects of temperature increase, as demonstrated by more than two times power increase associated with a 30 °C temperature rise. It can also be seen that DBFCs can achieve reasonably good power performance at ambient temperatures, which makes DBFCs suitable for mobile applications.

Better performance was obtained by using oxygen compared to air under the same conditions. As shown in Figure 4.1, peak power densities of 95 mW cm⁻² and 237 mW cm⁻² were obtained using humidified oxygen at 28 and 60 °C, respectively. The enhancement in fuel cell performance using oxygen compared to air is due to the better cathode kinetics associated with using oxygen than air as the oxidant. Furthermore, due to the presence of CO₂ in air, carbonate is formed, which exerts a negative effect on electrode and electrolyte. It can be seen also from Figure 4.1, that the increase in cell performance over this

temperature range using oxygen was more than that using air. This is due to the reduction of activation loss and concentration loss by the higher oxygen concentration. Although DBFCs using air do not yield as good a performance as those using oxygen, it is desirable to develop a DBFC with air as oxidant, simply because it is freely available in nature and may avoid the use of extra equipment and gas supply.

To examine the effect of cathode humidification on cell performance, a DBFC was tested with both dry and humidified oxygen as the oxidant. The membrane electrolyte of this cell was Nafion[®] 212 membrane. The anode consisted of Ni and Pd/C catalyst (1 mg metal cm⁻²) with 15 wt.% Nafion[®] ionomer loaded on Toray[®] carbon paper. The cathode was Pt cathode (1 mg Pt cm⁻² on Toray[®] carbon paper). The fuel was 5 wt. % NaBH₄ and 10 wt. % NaOH aqueous solution, and its flow rate was 5 mL min⁻¹. The flow rate of oxidant was 0.15 L min⁻¹. Figure 4.2 shows curves of cell polarization and power density of DBFC using dry and humidified oxygen at 28 °C. A maximum power density of 89 mW cm⁻² was obtained at 215 mA cm⁻² by using dry oxygen as oxidant while a maximum power density of 95 mW cm⁻² was obtained at 235 mA cm⁻² by using humidified oxygen as oxidant. As seen, the electrochemical performance was not significantly different by the oxidant humidification and only a small increase of power density was observed. Humidification can be beneficial not only because water is a reactant in cathode reaction, but also because it reduces borohydride and carbonate accumulation on the cathode surface and prevents membrane dryness. However, the effect of moisture in oxidant is limited,

because water is electroosmotically dragged from the anode to the cathode which humidifies any coming dry gas, oxygen or air.

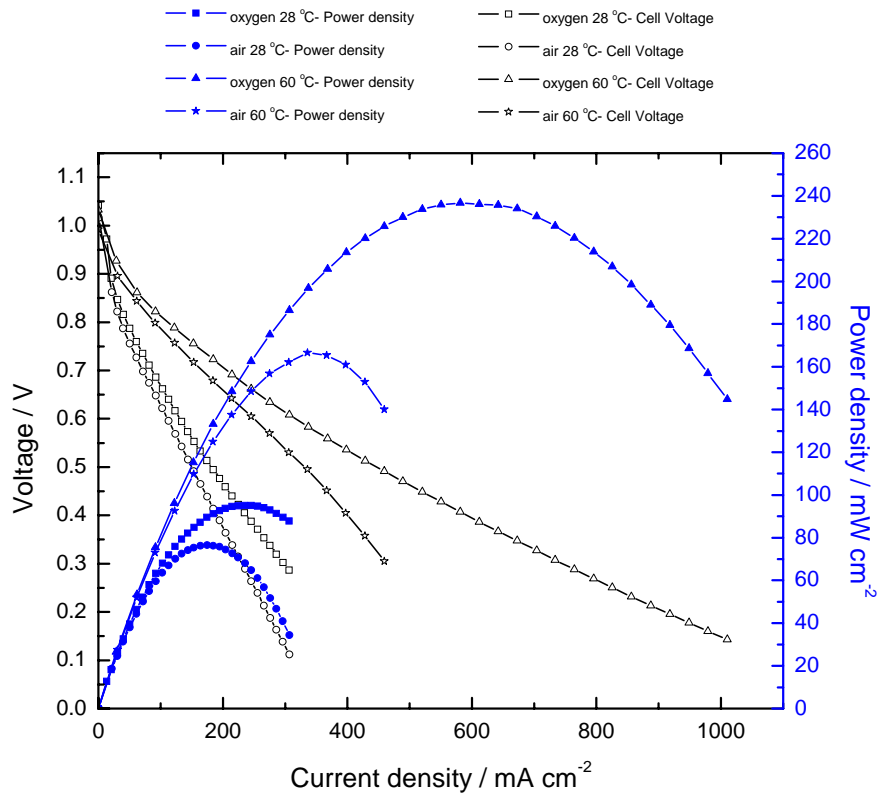


Figure 4.1 Curves of cell polarization and power density of DBFC using humidified oxygen and air at 28 and 60 °C.

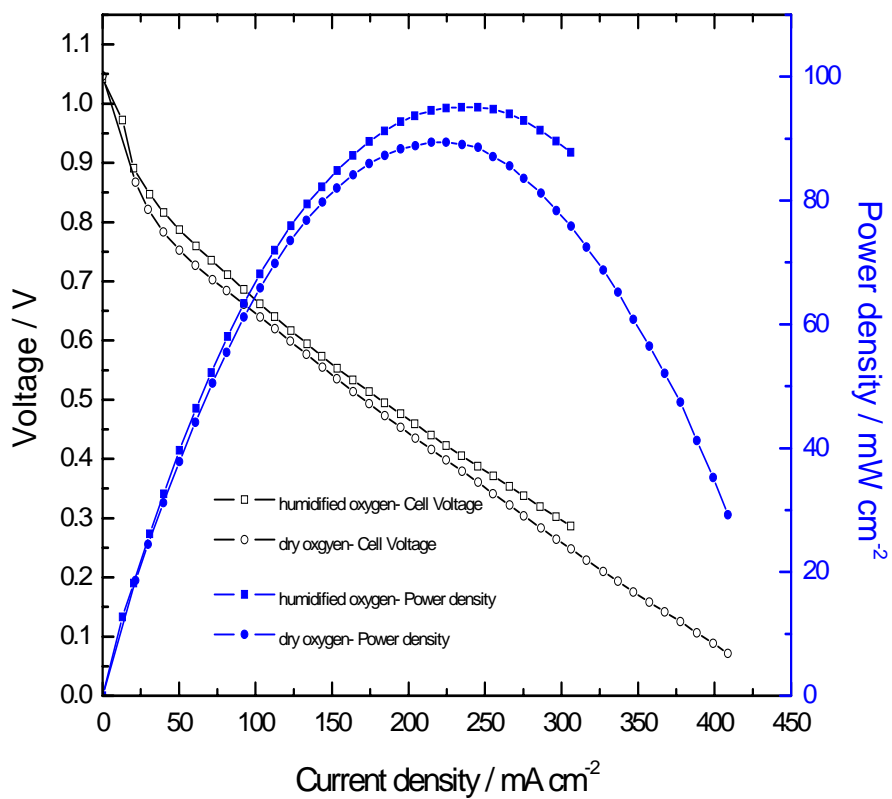


Figure 4.2 Curves of cell polarization and power density of DBFC using dry and humidified oxygen at 28 °C.

4.1.2 Performance stability of DBFC using Ni-based anode

In order to evaluate performance stability, a DBFC using Ni-based composite anode was assembled and tested. The membrane electrolyte of this cell was Nafion[®] 212 membrane. The anode consisted of Ni and Pd/C catalyst ($1 \text{ mg metal cm}^{-2}$) with 15 wt.% Nafion[®] ionomer loaded on Toray[®] carbon paper. The cathode was Pt cathode (1 mg Pt cm^{-2} on Toray[®] carbon paper). The fuel was 5 wt. % NaBH₄ and 10 wt. % NaOH aqueous solution, and its flow rate was 5 mL min^{-1} . The oxidant was oxygen with flow rate of 0.15 L min^{-1} . Short-term stability of DBFC was tested by monitoring the cell voltage change during the galvanostatic discharge of 50 mA cm^{-2} of the DBFC in a period of about 100 h at room temperature. As shown in Figure 4.3, the DBFC maintained a relatively stable performance with a little decay of cell voltage over the test period. The fluctuation in the cell voltage was due to addition of the new fuel solution, restarting the experiments, or small variation in cell temperature. The possible reasons for the gradual decline in cell performance with time may be due to dissolution or agglomeration of anode catalyst, poisoning of catalyst surface, deactivation of cathode and membrane by NaOH and Na₂CO₃. In addition, passivation occurs on Ni electrodes at potentials above $-0.6 \text{ V vs. Hg/HgO}$, leading to the formation of nickel oxide or nickel hydroxide which is hard to be reduced despite that NaBH₄ is a strong reducing agent [25].

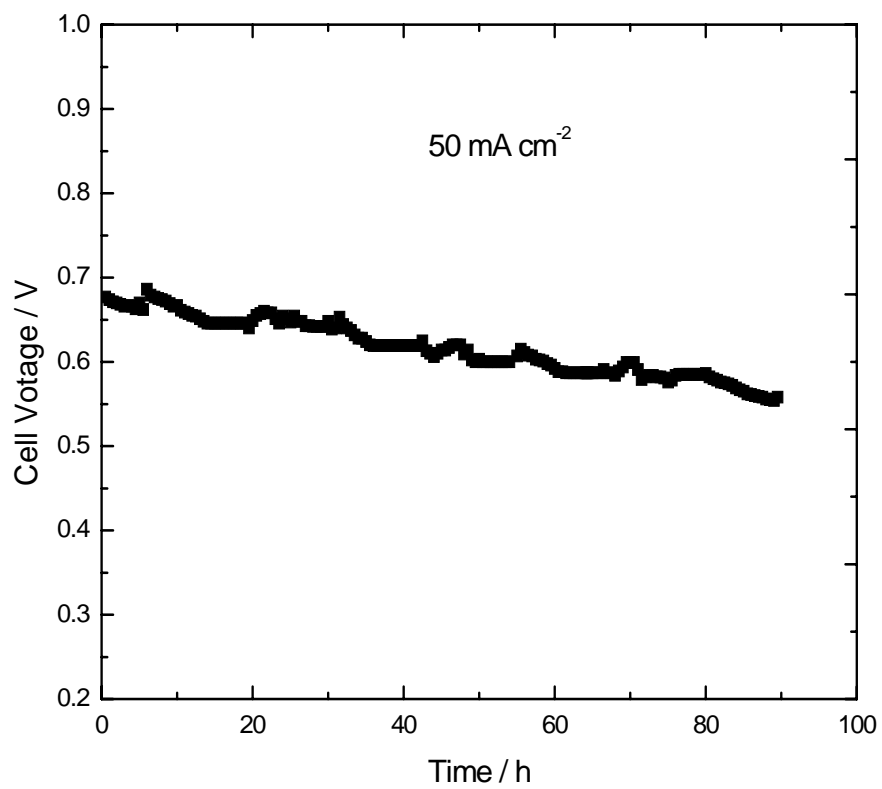


Figure 4.3 Performance stability of the DBFC using Ni-based composite anode catalyst, operating at current density of 50 mA cm^{-2} at room temperature.

4.1.3 Effect of anodic catalyst loading

In order to examine the effect of electrocatalyst loading on the fuel cell performance, Ni-based anode with different catalyst loading was prepared and tested in a DBFC. Nafion[®] 212 membrane was employed as membrane electrolyte. The anode was Ni+Pd/C on Toray[®] carbon paper with 1-5 mg metal cm⁻² and 15 wt.% Nafion[®] binder. The fuel was 5 wt.% NaBH₄ and 10 wt.% NaOH. Flow rate of the fuel was 5 mL min⁻¹. The cathode was Pt cathode (1 mg Pt cm⁻² on Toray[®] carbon paper). The oxidant was humidified oxygen. Flow rate of the oxidant was 0.15 L min⁻¹. Figure 4.4 shows cell polarization and power density of DBFC at different anode catalyst loading at 60 °C. An enhanced power density was found by increasing the loading of anodic catalyst. Peak power densities of 237 mW cm⁻², 243 mW cm⁻², and 261 mW cm⁻² were achieved by using catalyst loading of 1, 2, and 5 mg cm⁻², respectively. However, the increase in cell performance with the increase in anodic loading was not significant, possibly due to the negative effect of the thick catalyst layer on resistance and reduced mass transport of liquid and gaseous species. So the extra catalyst loading of 5 mg cm⁻² was not much advantageous for a small performance gain over 1 mg cm⁻² of anodic catalyst. Thus, it is economical to use relative low catalyst loading to achieve reasonably good power performance.

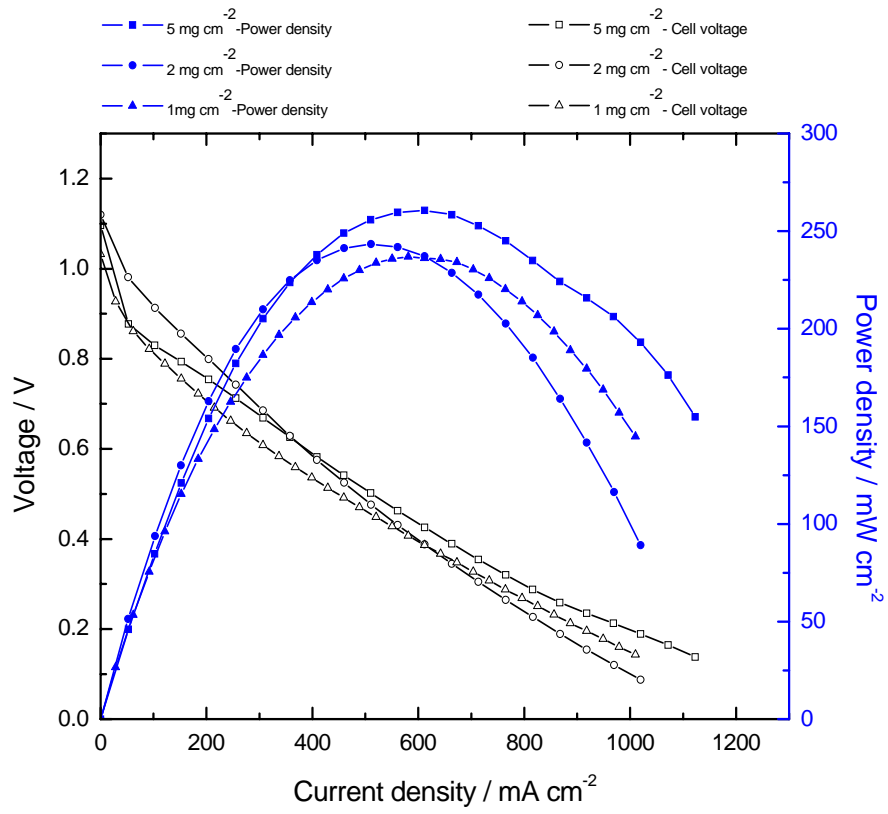


Figure 4.4 Curves of cell polarization and power density of DBFC at different anode loadings at 60 °C.

4.1.4 Effect of co-catalyst

Both Pd/C and Pt/C were employed as co-catalyst in the Ni-based anode and their performance in a DBFC was compared. The membrane electrolyte of this cell was Nafion[®] 212 membrane. The anode was Ni and Pt/C or Ni and Pd/C on Toray[®] carbon paper with 1 mg metal cm⁻² and 15 wt.% Nafion[®] binder. The cathode was Pt cathode (1 mg Pt cm⁻² on Toray[®] carbon paper). Fuel was 5 wt.% NaBH₄ and 10 wt.% NaOH. Flow rate of the fuel was 5 mL min⁻¹. Oxidant was humidified oxygen. Flow rate of the oxidant was 0.15 L min⁻¹. As depicted in Figure 4.5, a DBFC using Ni and Pt/C composite anode achieved a peak power density of 270 mW cm⁻² at 60 °C, which is approximately 33 mWcm⁻² higher power density than using Ni+Pd/C under similar conditions. It has been demonstrated that Pt is an effective catalyst for borohydride oxidation [13]. Electrochemical studies have shown that alloying Au with Pt improves borohydride oxidation activity more than alloying of Au with Pd (both Au-Pt and Au-Pd had 1:1 atomic ratio) [28,29]. It has been suggested [26] that Ni-Pt alloy had even higher activity than Au-Pt alloy (Pt-Au and Pt-Ni had 1:1 atomic ratio). In the present research, Nafion[®] ionomer was added to the Ni composite material in making the anode catalyst. The addition of Nafion[®] was found to reduce BH₄⁻ concentration on the catalyst surface. At low borohydride concentration (<1 M), the columbic number of Pd anode is between 6e and 8e while a quasi-8e-reaction occurs at Pt anode as the result of extra catalytic sites for H₂ electrooxidation [21]. Given that Pt is the best catalyst for hydrogen reduction, it is possible that Ni-Pt catalyst may be able to achieve a good balance between borohydride

oxidation and hydrolysis reactions, as H₂ released by hydrolysis may be oxidized effectively.

Geng et al. [23] reported a maximum power density of 221 mW cm⁻² achieved by a DBFC employing carbon supported platinum nickel alloy (Ni₃₇-Pt₃/C) as anode catalyst at 60 °C. The present research suggests that the DBFC performance can be improved simply by mixing Ni and Pt metals to get a composite catalyst and it may not be necessary to alloy them.

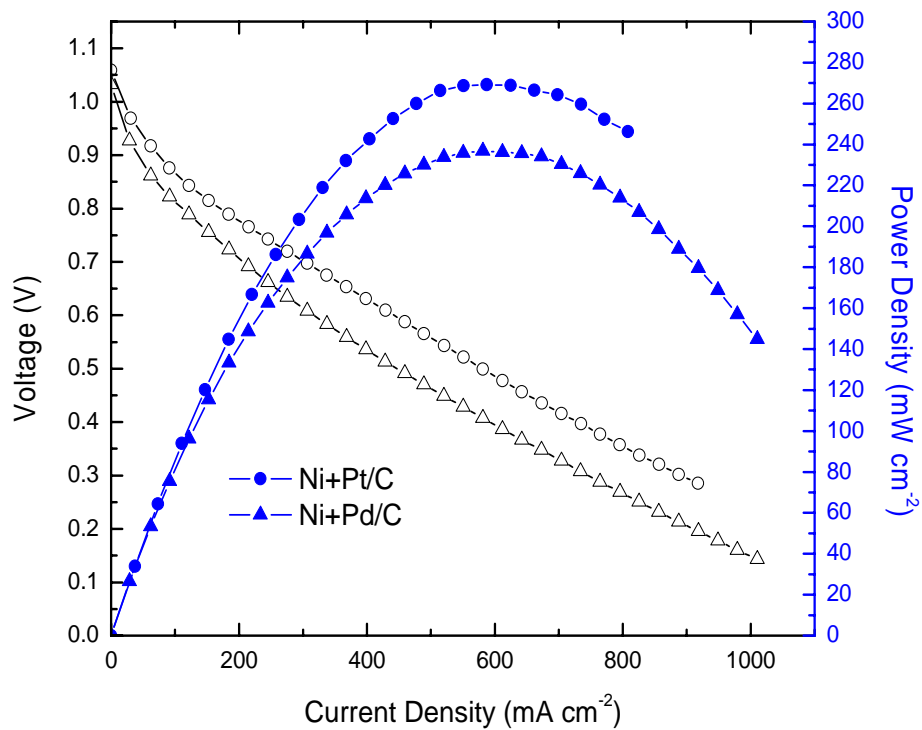


Figure 4.5 Curves of cell polarization and power density of DBFC using Ni+Pt/C or Ni+Pd/C as anode electrocatalyst at 60 °C.

4.1.5 Use of hydrogen peroxide as the oxidant

Besides oxygen and air, H_2O_2 was also used as the oxidant. $\text{NaBH}_4\text{-H}_2\text{O}_2$ fuel cells have some superior characteristics to $\text{NaBH}_4\text{-O}_2$ fuel cells. Besides some thermodynamic and energy advantages, the use of H_2O_2 enables DBFCs to work in anaerobic areas, such as outer space and underwater. A critical problem with using H_2O_2 is its decomposition on various transition metals [86]. To moderate this problem, sulfuric acid was added to H_2O_2 to increase its stability.

The cathode for hydrogen peroxide reduction was prepared by electrodeposition. Palladium was electrodeposited on the Zorflex[®] activated carbon cloth. Among noble metals, palladium-based catalysts show both good activity and selectivity to electro-reduction of hydrogen peroxide. Electro-deposition is able to deposit small particles where electronic and ionic conductions coexist, and therefore catalyst loading is reduced. This method has the advantage of ease of preparation and low cost requirement. As shown in Figure 4.6, Pd particles were deposited uniformly on carbon cloth and the particle size was around 100 nm.

A borohydride- H_2O_2 fuel cell with Ni-based composite anode and Pd cathode was assembled and tested. The membrane electrolyte of this cell was Nafion[®] 212 membrane. The anode was Ni+Pt/C on Toray[®] carbon paper with 5 mg metal cm^{-2} and 15 wt.% Nafion[®] binder. Fuel was 5 wt.% NaBH_4 and 10 wt.% NaOH. Flow rate of the fuel was 5 mL min^{-1} . Oxidant was 2.0 M H_2O_2 in 1.5 M H_2SO_4 . The flow rate of hydrogen peroxide was 5 mL min^{-1} . As can be seen in Figure 4.7, this fuel cell achieved peak power densities

of 327 mW cm^{-2} and 665 mW cm^{-2} at 28 and 60 °C, respectively. The peak power densities were also much higher compared to the use of oxygen or air. With H_2O_2 , the OCV of the cell was about 1.7 V compared to about 1.05 V with oxygen.

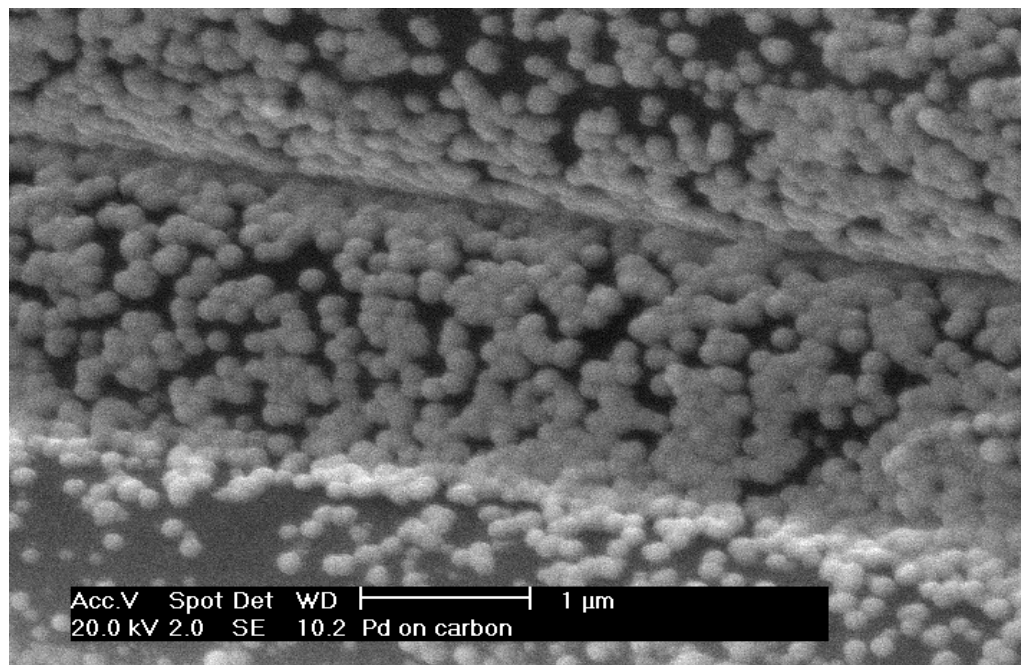


Figure 4.6 SEM of electrodeposited palladium-coating on carbon cloth.

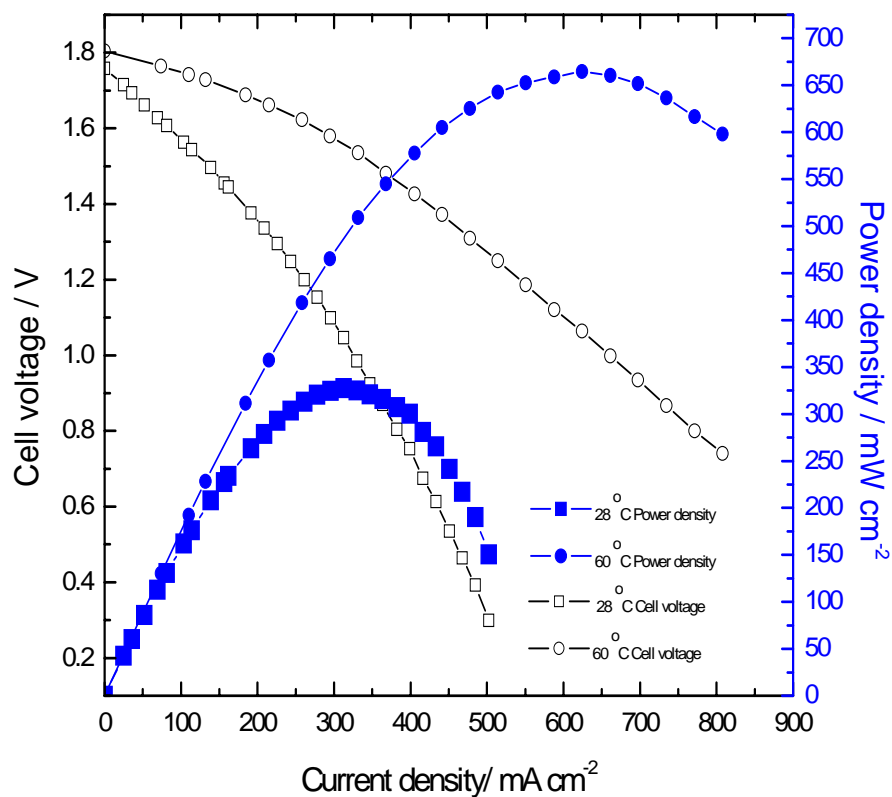


Figure 4.7 Curves of cell polarization and power density of DBFC using hydrogen peroxide as oxidant.

4.1.6 Use of Ni foam as anode substrate

A DBFC was assembled with Ni foam as anode substrate and its power performance and stability were recorded. The membrane electrolyte of this cell was Nafion[®] 212 membrane. The anode was Ni+Pd/C on Ni foam (as-received) with 5 mg metal cm⁻² and 15 wt.% Nafion[®] binder. The cathode was Pt cathode (1 mg Pt cm⁻² on Toray[®] carbon paper). Fuel was 5 wt.% NaBH₄ and 10 wt.% NaOH. Flow rate of the fuel was 5 mL min⁻¹. The oxidant was humidified oxygen. Flow rate of the oxidant was 0.15 L min⁻¹. As shown in Figure 4.8, peak power densities of 118 and 283 mW cm⁻² were achieved at 28 and 60 °C, respectively. Comparing these values with results shown in Figure 4.4, the DBFC with Ni foam obtained higher power density than that using carbon paper as anode substrate. This DBFC also demonstrated a good stability of 100 hours as shown in Figure 4.9.

At the anode, hydrogen is generated from hydrolysis reaction, which is a serious problem in DBFCs. When hydrogen is formed at a higher rate than its consumption at the anode, accumulation of hydrogen gas occurs in the anode compartment. As depicted in Figure 4.10, accumulated hydrogen gas hinders some of active sites of the catalysts and results in a two phase transport in the anode diffusion layer, and impedes the mass transport of liquid fuel. Despite the fact that hydrogen gas is formed in the anode, hydrophobic PTFE coating is not advantageous in DBFC anode diffusion layer [87,88], since although a large amount of hydrogen gas is generated, the transport of the liquid fuel is more important than that of the hydrogen gas. The use of Ni foam moderates this negative effective of hydrogen evolution on mass transport due to its high porosity and large pore size. Ni foam also

extends the electrochemical reaction zone, and therefore improves the catalyst utilization. In addition, the open structure of Ni foam enhances countercurrent gas–liquid flow, and facilitates the release of unreacted hydrogen so as to prevent the block of liquid flow path to the reaction sites by the hydrogen gas. As a result, an improvement in fuel cell performance and stability is achieved.

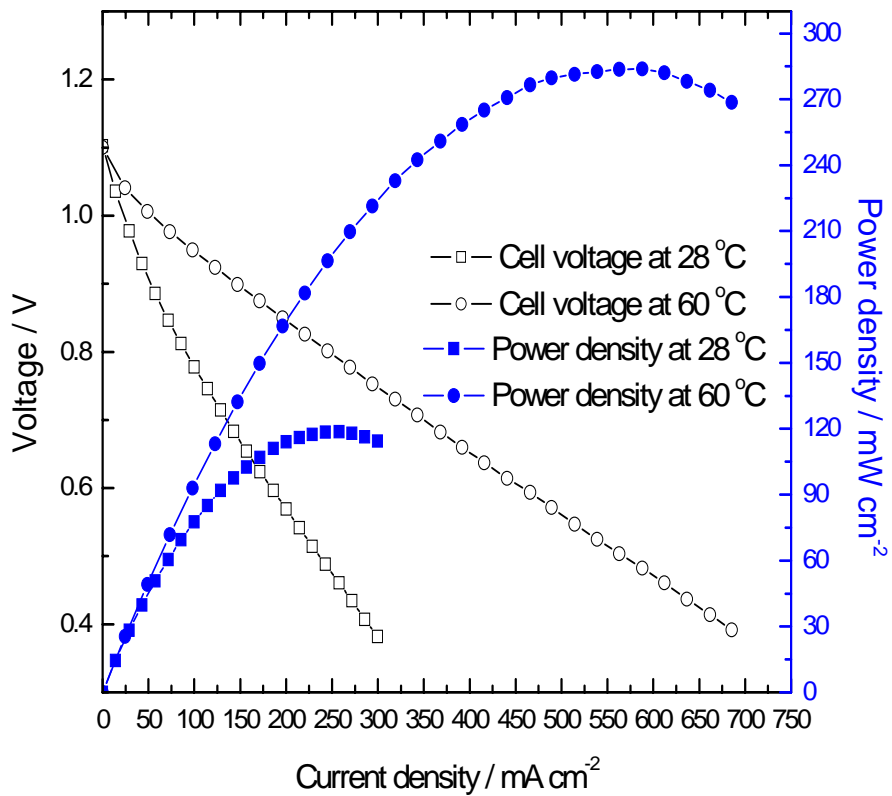


Figure 4.8 Curves of cell polarization and power density of DBFC using Ni foam as anode substrate.

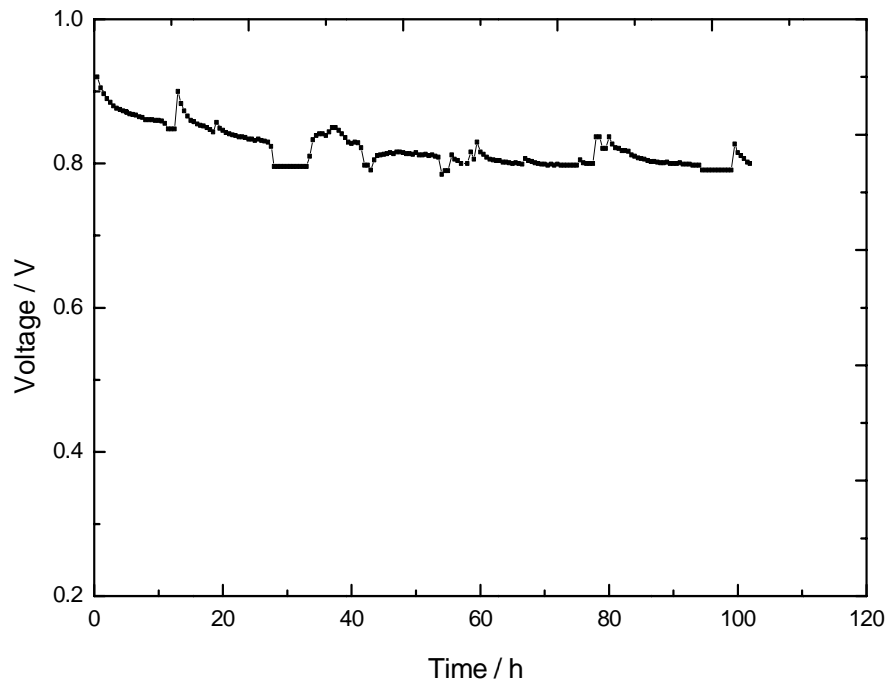


Figure 4.9 Performance stability of the DBFC using Ni foam as anode substrate, operating at current density of 50 mA cm^{-2} at room temperature.

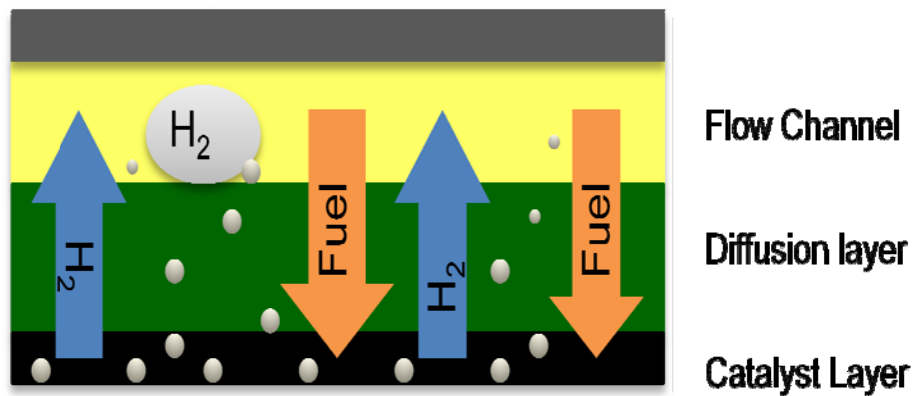


Figure 4.10 A schematic diagram of two-phase transport in anode diffusion layer in DBFC.

4.2 Polymer chemical hydrogel as electrode binder

4.2.1 Reactions leading to polymer chemical hydrogel

Efficient and cost-effective polymer chemical hydrogel was prepared and employed as electrode binders for DBFCs. The binder material was based on polyvinyl alcohol (PVA) or chitosan polymer. Hydrogel is macromolecular networks swollen in water or biological fluids [89]. Hydrogels can be classified as physical hydrogels or chemical hydrogels. Chemical hydrogels are formed by irreversible covalent links. Physical hydrogels are formed by reversible links, including ionic interactions and secondary interactions [90]. In cross-linked hydrogels, polymeric chains are interconnected by cross-linkers, leading to the formation of a 3D network. Cross-linkers have at least two reactive sites that allow the formation of bridges between polymer chains. The molecular weight of cross-linkers is much smaller than that of chains between two consecutive cross-links. Depending on the nature of the cross-linker, the main interactions forming the network are covalent or ionic bonds. The cross-linking reaction between PVA and glutaraldehyde leading to the formation of PVA chemical hydrogel is schematically depicted in Figure 4.11. The cross-linking reaction between chitosan and glutaraldehyde leading to the formation of chitosan chemical hydrogel is schematically depicted in Figure 4.12. Chitosan or PVA undergoes chemical cross-linking reaction with an aqueous solution of glutaraldehyde at ambient temperature and pressure. Due to the reaction, aqueous solution of chitosan or PVA turns into a solid mass with all water associated with the precursor solutions remaining absorbed in the polymer matrix of the solid entity. Such a solid entity is termed

as chitosan or PVA chemical hydrogel. During solidification process in the presence of electrode materials, the electrode materials get bonded to the electrode substrate. The PVA and chitosan chemical hydrogel in an inverted glass beaker are shown in Figure 4.13, where a Teflon-coated magnetic stirring bar that was used to mix solutions of chitosan or PVA and glutaraldehyde is seen stuck within the hydrogel at the bottom of the beaker. This figure clearly shows the solid nature of PVA and chitosan chemical hydrogel, and it also makes it easier to understand how the electrode materials are held within the hydrogel and bound to the carbon cloth substrate in the actual electrode while allowing transport of any water-soluble species such as ion, fuel or oxidant to the catalyst.

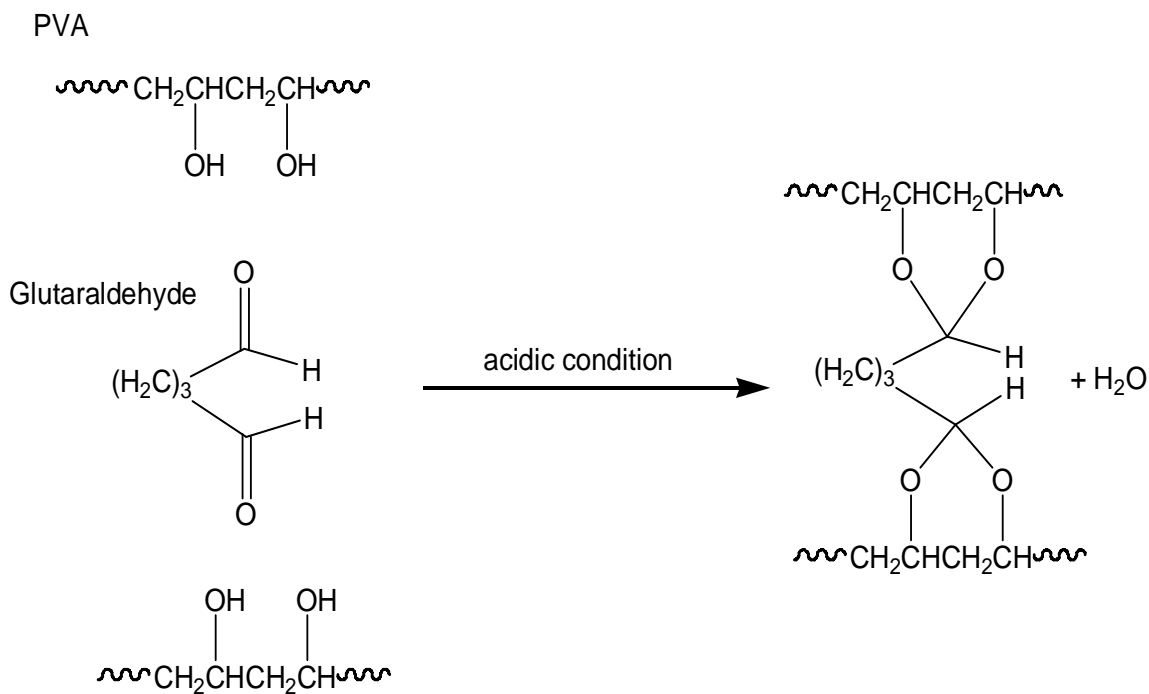


Figure 4.11 Reaction between glutaraldehyde and PVA leading to the formation of PVA chemical hydrogel.

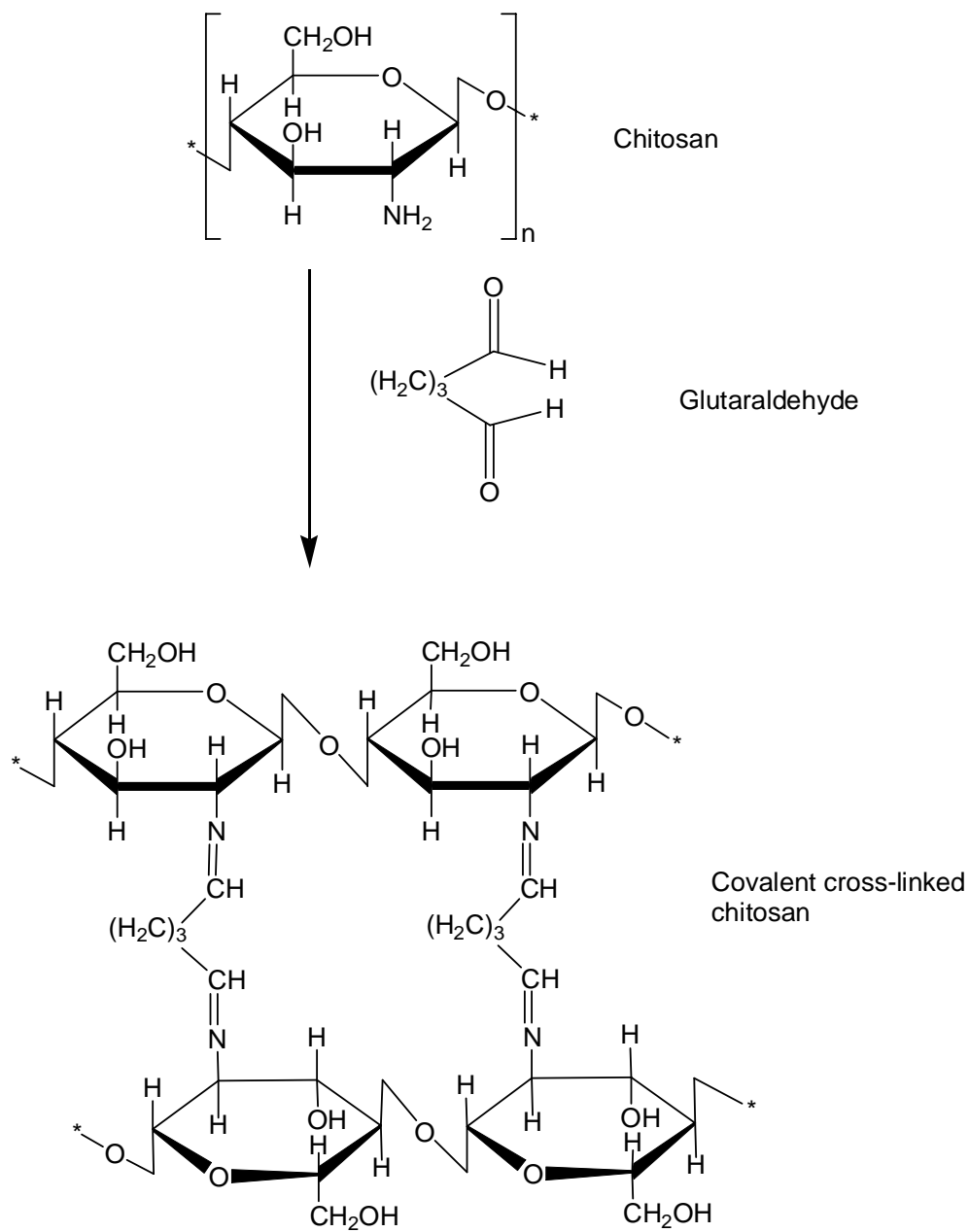


Figure 4.12 Reaction between glutaraldehyde and chitosan leading to the formation of chitosan chemical hydrogel.

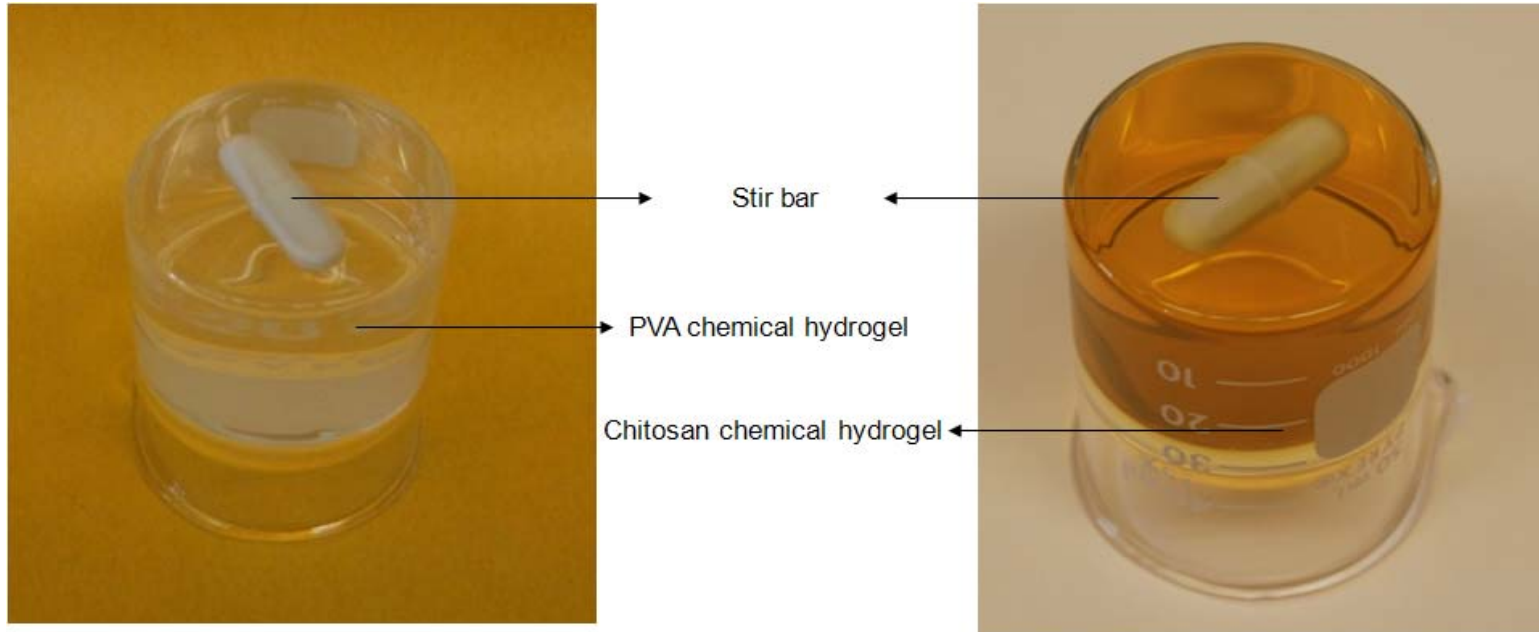


Figure 4.13 A picture of PVA or chitosan chemical hydrogel along with a Teflon-coated magnetic stirring bar in an inverted glass beaker.

4.2.2 Polymer chemical hydrogel binder based electrode

Both anode and cathode were prepared by ink paste method using Nafion[®], PVA and chitosan binder solution. The anode catalyst was AB₅ alloy powder of weight percentage composition La_{10.5}Ce_{4.3}Pr_{0.5}Nd_{1.4}Ni_{60.0}Co_{12.7}Mn_{5.9}Al_{4.7}, and Vulcan XC 72 carbon powder (10 wt. % of AB₅ alloy powder). The loadings of AB₅ alloy, PVA, chitosan, as well as Nafion[®] binders in anode were about 30 mg cm⁻², 5 wt. %, 0.5 wt. %, and 5 wt. %, respectively. The cathode catalyst was palladium on activated carbon (10 wt.% Pd). The loadings of Pd metal, PVA, chitosan, as well as Nafion[®] binders in cathode were about 1 mg cm⁻², 20 wt. %, 2 wt. %, and 20 wt. %, respectively. The electrode substrate for both anode and cathode was Zorflex[®] activated carbon cloth.

The loading of a polymer-based binder in the electrode of a fuel cell plays an important role in delivering high electrochemical performance. Optimum loadings of PVA binder in anode and cathode of DBFCs were found to be about 5 and 20 wt. %, respectively. A lower loading of PVA binder in the anode was sufficient because the anode comprised mostly of AB₅ metallic powder that has low surface area and only 10 wt % of Vulcan XC 72 carbon powder that has high surface area. A higher content of PVA binder in the cathode was needed because the cathode comprised of only 10 wt. % Pd metal that has low surface area and 90 wt. % Vulcan XC 72 carbon powder that has high surface area. In other words, the cathode material was fluffier than the anode material and hence needed more content of PVA binder for optimum performance in the DBFCs. It may be noted that for the same

electrode materials, the content of PVA binder needed was about ten times higher than that of chitosan binder.

Scanning electron micrographs of PVA binder-based anode, chitosan binder-based anode, Nafion[®] binder-based anode, PVA binder-based cathode, chitosan binder-based cathode, and Nafion[®] binder-cathode are presented as (a), (b), (c), (d), (e), and (f), respectively in Figure 4.14. A lower magnification was sufficient to observe morphological features of anode samples because of the relatively large particle size of AB₅ anode catalyst, whereas a higher magnification was necessary to observe morphological features of cathode samples because of the relatively small particle size of Pd/C cathode catalyst. Since these electrodes exhibited high electrochemical performance in DBFCs, the proportions of catalyst particles and polymer-based binders in these electrode samples are reasonably optimum. In other words, the contents of polymer-based binders in the electrode matrixes are high enough not only to keep the electrode materials intact and bound to the electrode substrate but also to facilitate efficient flux of fuel, oxidant as well as ions to the catalyst surface. Also, the contents of polymer-based binders in the electrode matrix are low enough to allow efficient flux of electrons among the catalyst particles in the electrode matrix as well as from catalyst particles to the electrode substrate and vice versa. The polymer-based binders appear as fluffy material whereas the catalyst material appears as solid particles. Both PVA binder and chitosan binder are able to bind catalyst particles nicely. The catalyst particles are quite uniformly dispersed. The small agglomerates seem to reduce the pore volume on the electrode surface. The degree of

coating of catalyst particles by polymer-based binders appears to be maximum in case of chitosan followed by PVA and Nafion[®] binders.

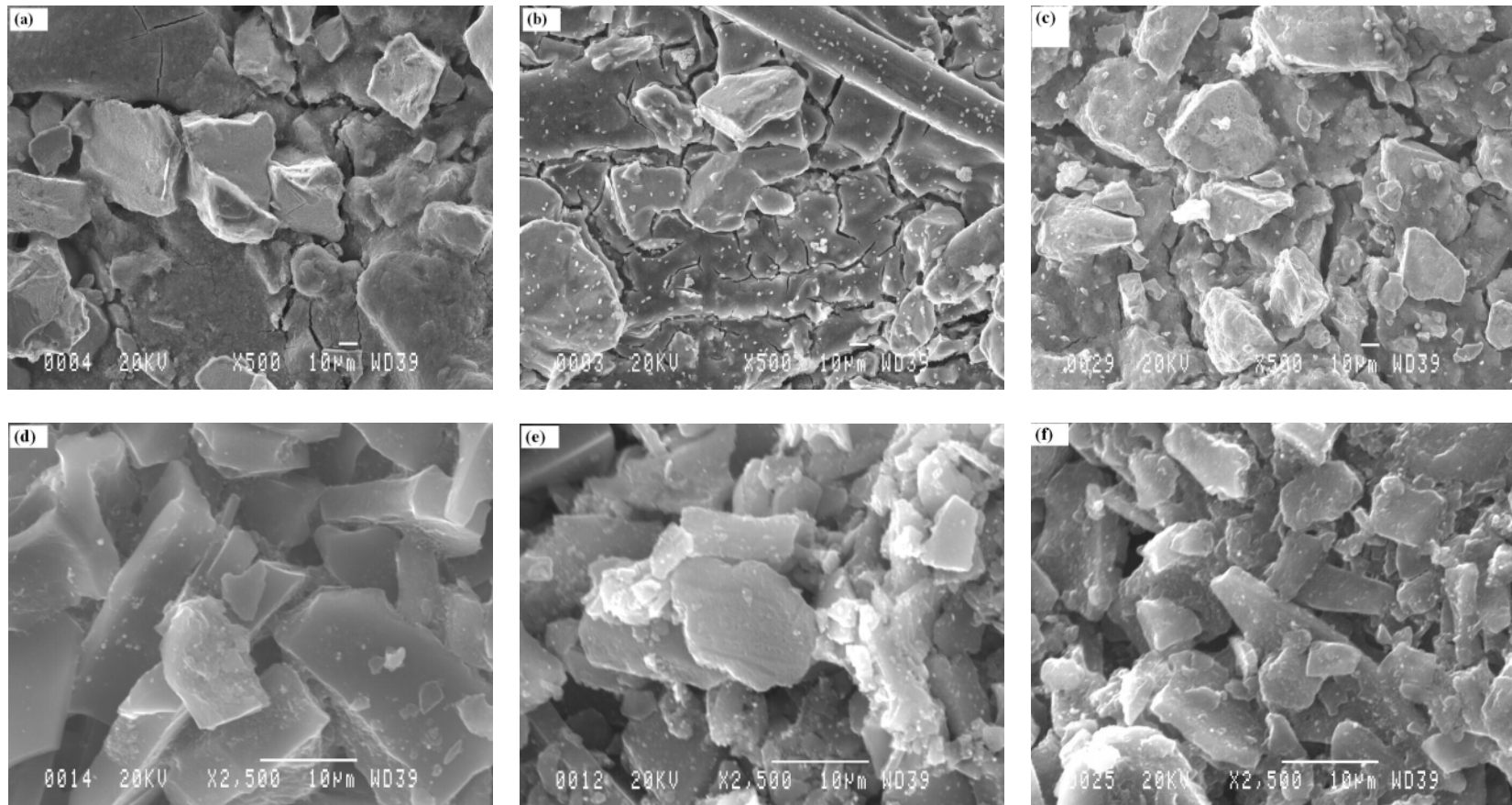


Figure 4.14 Scanning electron micrographs of (a) PVA binder-based anode, (b) chitosan binder-based anode, (c) Nafion[®] binder-based anode, (d) PVA binder-based cathode, (e) chitosan binder-based cathode, and (f) Nafion[®] binder-cathode.

4.2.3 Power performance of DBFCs using polymer chemical hydrogel binder

A $\text{NaBH}_4\text{-H}_2\text{O}_2$ fuel cell was assembled with the prepared electrodes and its power performance was recorded. The fuel comprised an aqueous solution of 1.7 M NaBH_4 in 7.0 M NaOH . The oxidant comprised an aqueous solution of 2.5 M H_2O_2 in 1.5 M H_2SO_4 . The flow rates for fuel and oxidant solutions were maintained constant at 5 and 10 mL min^{-1} , respectively, for all the electrochemical studies. The electrochemical performance data for DBFCs employing PVA, chitosan, and Nafion[®] binders-based electrodes and Nafion[®] 117 membrane at different operating cell temperatures are shown in Figure 4.15, Figure 4.16 and Figure 4.17, respectively. As seen, OCV values of DBFCs with all the three electrode binders are ~ 1.9 V. Moreover, the OCV values of DBFCs with all the three electrode binders increase with increase in cell temperature. As the cell temperature is increased from 30 to 70 $^\circ\text{C}$, the peak power density increases from 196 to 490 mW cm^{-2} for DBFC employing PVA as electrode binder, from 202 to 589 mW cm^{-2} for DBFC employing chitosan as electrode binder, and from 191 to 494 mW cm^{-2} for DBFC employing Nafion[®] as electrode binder, respectively. As the cell temperature is increased from 30 to 70 $^\circ\text{C}$, the current density corresponding to peak power increases from 173 to 449 mA cm^{-2} for DBFC employing PVA as electrode binder, from 204 to 551 mA cm^{-2} for DBFC employing chitosan as electrode binder, and from 183 to 448 mA cm^{-2} for DBFC employing Nafion[®] as electrode binder, respectively. Electrochemical performance data for DBFCs employing PVA and Nafion[®] electrode binders are comparable at all temperatures. Electrochemical performance data for DBFC employing chitosan as electrode binder are better as compared

to DBFCs employing PVA as well as Nafion[®] electrode binders at all temperatures. It is interesting to note that the improvement in electrochemical performance for DBFC employing chitosan as electrode binder becomes more prominent with increase in cell temperature.

The superior performance of chitosan chemical hydrogel binder to Nafion[®] or PVA binder can be understood by their difference in structure. Backbone of Nafion[®] contains C–F bonds that are well known as polar hydrophobic bonds [91]. Nafion[®] also possesses weakly polar C–O–C linkages and highly dissociable as well as hydrophilic sulfonic acid (–SO₃H) group in its structure. Because of the presence of the contrasting properties, Nafion[®] is understood to possess hydrophilic and hydrophobic zones separated by an intermediate region [92]. In PVA, polar functional groups present are mainly –C–O–C–O–, –C–O–C and possibly some unreacted polar hydroxyl group –OH. The –C–O–C–O– and –C–O–C groups in PVA form ring structures [93]. In PVA, water is not only bonded to electronegative oxygen atom by hydrogen bonding but also trapped inside the ring-structured –C–O–C–O– and –C–O–C groups. –OH group is a weakly ionizing group, and thus its hydrophilic nature and hence water-retaining capability is limited. Chitosan contains three different polar functional groups, namely, –OH, primary amine (–NH₂), and ether (C–O–C) groups in addition to six-member ring structures in its polymer backbone. Because of the presence of a variety of polar functional groups and six-member ring structures, chitosan is highly capable of forming hydrogen bond with water and trapping water in its ring structures. In other words, chitosan is a highly hydrophilic polymer. Due to

the cross-linking reaction between chitosan and glutaraldehyde, an extra chitosan chain gets hooked up to the first chitosan chain. Because of the increased number of chitosan chains getting chemically bonded together, the hydrophilicity of chitosan increases [94]. From the above discussion, it may be surmised that chitosan chemical hydrogel possesses higher hydrophilic characteristics as compared to both PVA chemical hydrogel and Nafion[®] ionomer. Higher water retaining capacity of chitosan implies that ionic conductivity and mobility of fuel/oxidant within chitosan binder-based electrode matrix are higher as compared to those within PVA as well as Nafion[®] binders-based electrode matrix. The higher ionic conductivity and mobility of fuel/oxidant within the chitosan binder-based electrode matrix leads to better improvement in electrochemical performance of the chitosan electrode binder-based DBFC as compared to that of DBFCs employing PVA and Nafion[®] binders-based electrodes at elevated temperatures. This result is significant in view of the fact that Nafion[®]-based electrode binder and PEM suffer from dehydration and hence loss in fuel cell performance at significantly high operating temperatures. Being a highly hydrophilic material, chitosan may prove to be a cost-effective and high performance material in high operating-temperature polymer electrolyte fuel cells.

When Nafion[®] or PTFE is employed as an electrode binder, the MEA is generally prepared by hot-compaction technique in which the mixture of electrode material and polymer binder is heated to a temperature that is in the range of glass transition temperature of the binding polymer. At the glass transition temperature, the polymer melts/softens and

while solidifying during cooling under pressure, it encompasses the electrode material with the electrode substrate and PEM. Unlike Nafion[®] or PTFE that acts as a binder due to a physical phenomenon such as heating/cooling, the binding actions of PVA and chitosan are due to chemical reactions in which PVA and chitosan undergo chemical reaction with a cross-linking reagent such as glutaraldehyde under ambient conditions of temperature and pressure. Binding actions of PVA and chitosan for the electrode mass are thus accompanied with breaking of some existing covalent bonds and formation of some new covalent bonds. Polymer-based electrode binders such as Nafion[®] are highly expensive whereas polymer hydrogel-based electrode binders are very inexpensive that can be prepared in-house. Catalyst inks with polymeric binders such as Nafion[®] are generally prepared in organic solvent, namely 2-propanol, because of the high hydrophobic nature of long carbon chain of polymers. Use of organic solvents not only adds to cost but also cause health and environmental hazards. Catalyst inks with hydrogel binders such as PVA and chitosan are generally prepared in water, thereby enhancing cost-effective and environmentally safe technologies.

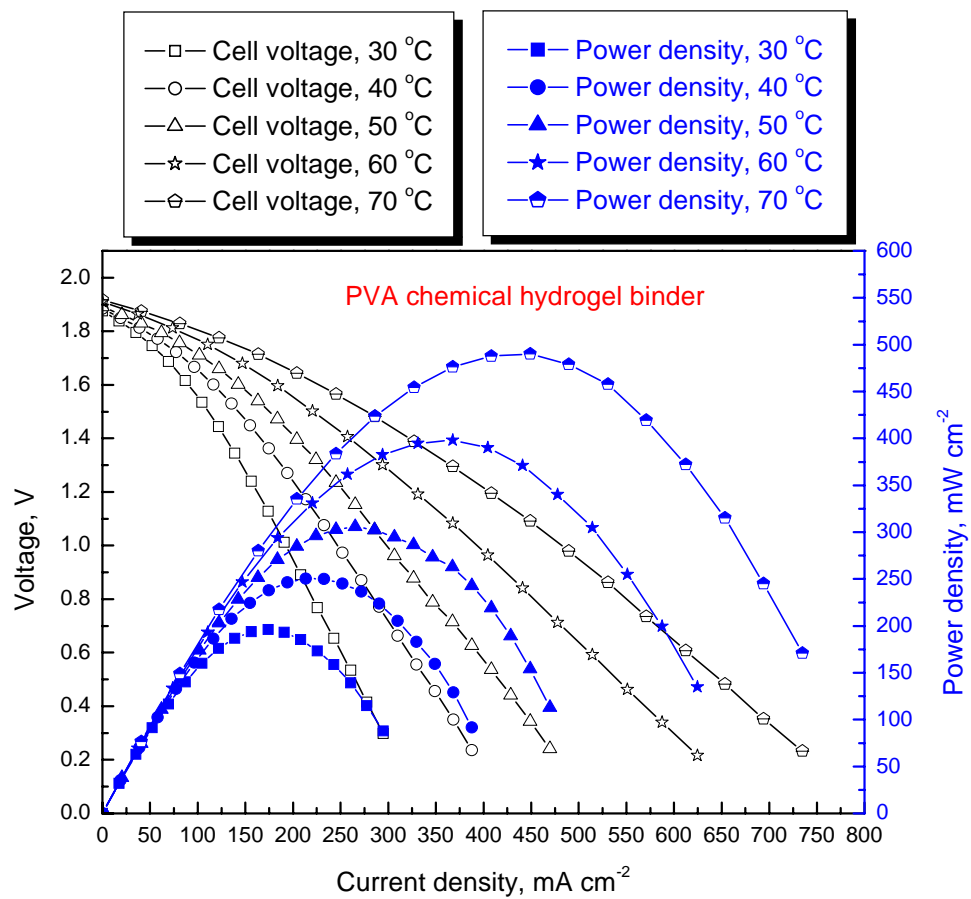


Figure 4.15 Plots of cell voltage and power density versus current density for DBFCs with PVA chemical hydrogel binder-based electrodes at different operating cell temperatures.

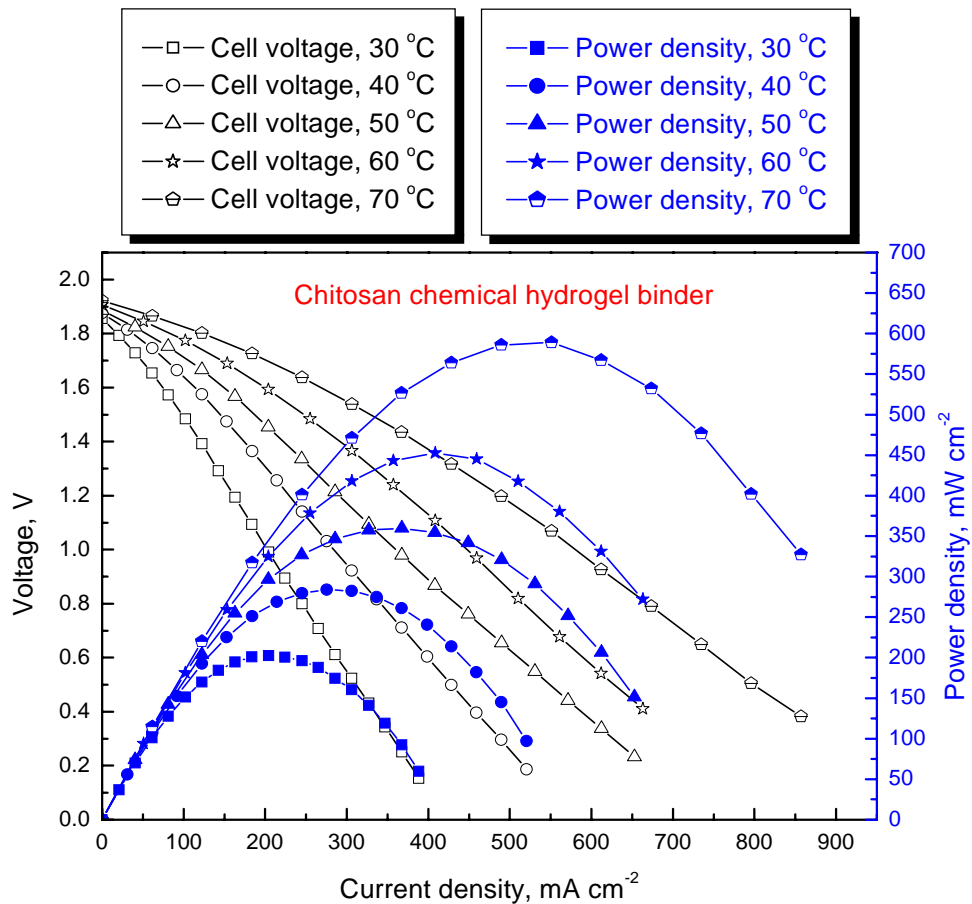


Figure 4.16 Plots of cell voltage and power density versus current density for DBFCs with chitosan chemical hydrogel binder-based electrodes at different operating cell temperatures.

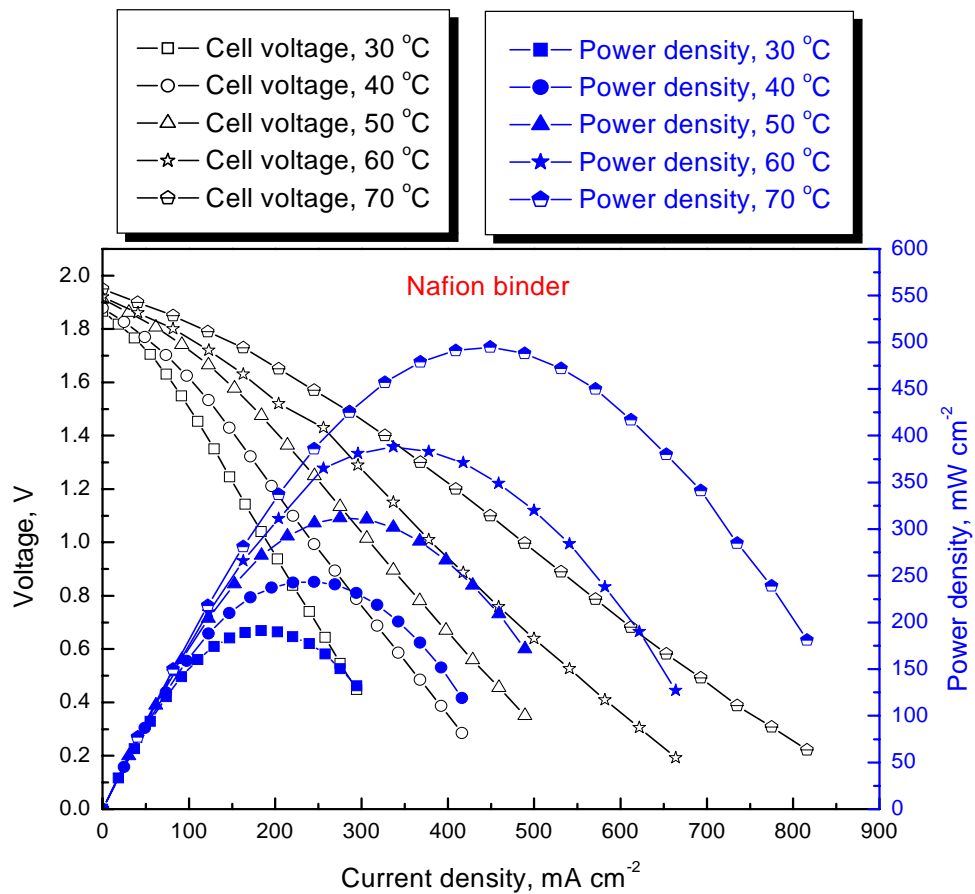


Figure 4.17 Plots of cell voltage and power density versus current density for DBFCs with Nafion[®] binder-based electrodes at different operating cell temperatures.

4.3 PVA hydrogel membrane

A PVA hydrogel membrane was prepared by a solution casting method and employed in a DBFC. The PVA hydrogel membrane was ca. 200 μm thick, transparent, colorless, and mechanically as well as chemically stable. The PVA hydrogel membrane was prepared by a chemical cross-linking reaction between PVA and glutaraldehyde in aqueous medium, which takes place at ambient conditions of temperature and pressure. Because of the cross-linking reaction, the PVA hydrogel membrane was insoluble in water. Protic acid, such as H_2SO_4 or HClO_4 , was used to catalyze the cross-linking reaction.

4.3.1 Power performance of $\text{NaBH}_4\text{-H}_2\text{O}_2$ fuel cells using PVA hydrogel membrane

A PVA hydrogel membrane was tested in a DBFC using hydrogen peroxide as the oxidant. Cathode was gold sputtered on Zorflex[®] activated carbon cloth. Au was identified as an effective catalyst which minimizes H_2O_2 decomposition and also resists corrosion. Figure 4.18 shows the SEM picture of sputtered Au on activated carbon cloth. Anode was Ni+Pd/C (5 mg metal cm^{-2}) with 15 wt.% Nafion[®] binder on Toray[®] carbon paper. Fuel was 10 wt.% NaBH_4 and 20 wt.% NaOH. Flow rate of fuel was 10 mL min^{-1} . Oxidant was 2 M H_2O_2 in 1.5 M H_2SO_4 . Flow rate of oxidant was 10 mL min^{-1} . Cell polarization and power performance data for the PVA hydrogel membrane-based DBFC employing hydrogen peroxide as the oxidant were obtained at four different temperatures. As shown in Figure 4.19, peak power densities of 81 mW cm^{-2} , 101 mW cm^{-2} , 130 mW cm^{-2} , and 176 mW cm^{-2} were obtained at 28, 40, 50, and 60 $^\circ\text{C}$, respectively.

The comparative cell performance data for NaBH₄-H₂O₂ fuel cells employing a PVA hydrogel membrane and a Nafion[®] 117 membrane at the elevated temperature are shown in Figure 4.20. The NaBH₄- H₂O₂ fuel cell with a Nafion[®] 117 membrane yielded a peak power density of 218 mW cm⁻² at 60 °C, while with a PVA hydrogel membrane a peak power density of 176 mW cm⁻² was obtained under the same conditions. The better cell performance of the Nafion[®] membrane-based DBFCs might be due to the structure difference between Nafion[®] membrane and PVA hydrogel membrane. During the preparation of PVA hydrogel membrane, protic acid was used as catalyst. It also acts as dopant which is responsible for ionic conductivity of the as-prepared PVA hydrogel membrane. Ionic conductivity of the as-prepared acidic PVA hydrogel membrane is of the order of 10⁻³ S cm⁻¹ at room temperature [95], increased almost linearly with increase in protic acid concentration in accordance with Nernst-Einstein equation. After thorough washing of the PVA hydrogel membrane with DI water, protic acid dopant is no more present in the polymer matrix of the PVA hydrogel membrane. Such a washed-membrane does not exhibit much ionic conductivity. The absence of ionic conductivity is because PVA hydrogel membrane is not an ionomer membrane like Nafion[®] membrane that possesses inherent ionic conductivity due to the presence of ionizable pendant -SO₃H group on their polymer backbone. PVA hydrogel membrane does not contain ionizable functional groups and hence lacks significant inherent ionic conductivity as a result. PVA hydrogel membrane is a 3-dimensional polymer matrix that absorbs and retains a large volume of water and serves as a medium for ion conduction as well as a separator between

anode and cathode compartments in DBFCs. The ionic conductivity of the PVA hydrogel membrane in DBFCs is contributed by a number of ions present in the anolyte and the catholyte.

The lower cell performance of the PVA hydrogel membrane-based DBFCs is also possibly due to the higher amount of crossover associated with PVA hydrogel membrane as compared to Nafion[®] membrane. The negative charge on the polymer backbone of Nafion[®] membranes resists the undesired crossover of anionic species, such as BH_4^- and SO_4^{2-} . When acidified H_2O_2 is used as the oxidant, the crossover of H^+ across the membrane neutralizes some of the alkaline fuel solution, and thereby reduces the power performance of the PVA hydrogel membrane-based DBFC. Both the crossover rates of H_2O_2 and H_2SO_4 across a PVA hydrogel membrane have been found to be higher than those through a Nafion[®] membrane [96].

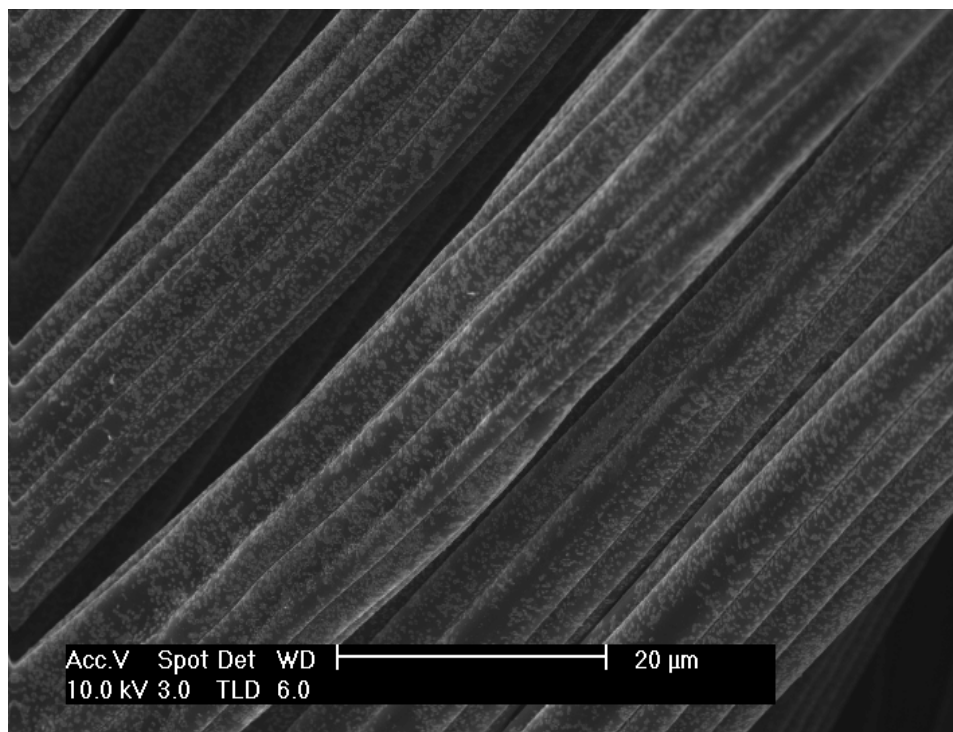


Figure 4.18 A SEM picture of sputtered gold on carbon cloth.

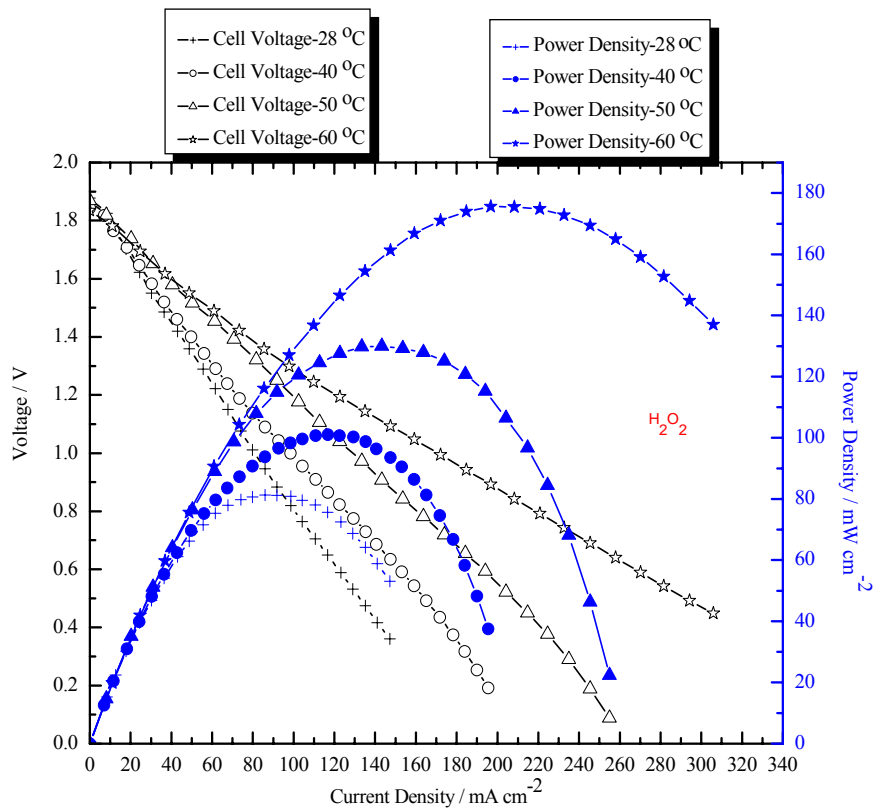


Figure 4.19 Curves of cell polarization and power density of DBFCs using PVA hydrogel membrane and hydrogen peroxide as the oxidant at different temperatures.

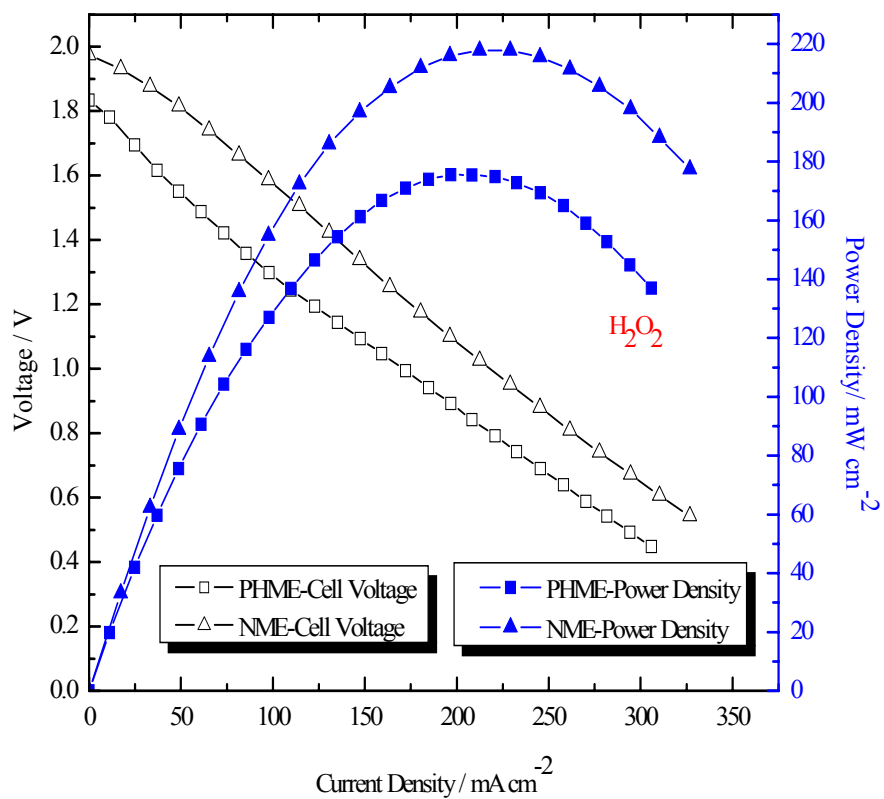


Figure 4.20 Curves of cell polarization and power density of a NaBH₄-H₂O₂ fuel cell using a PVA hydrogel membrane electrolyte (PHME) or a Nafion[®] membrane electrolyte (NME) at 60 °C.

4.3.2 Performance of PVA hydrogel membrane based DBFCs using oxygen or air as the oxidant

A PVA hydrogel membrane-based DBFC was assembled and tested with oxygen or air as the oxidant. Anode was Ni + Pd/C (1 mg metal cm⁻²) with 15 wt.% Nafion[®] binder on Toray[®] carbon paper. Cathode was Pt electrode (Pt/C, 1 mg Pt cm⁻² on Toray[®] carbon paper). Fuel was 5 wt.% NaBH₄ and 10 wt.% NaOH. Flow rate of fuel was 5 mL min⁻¹. Flow rate of gaseous oxidant was 0.15 L min⁻¹. Cell polarization and power performance data at four different temperatures for the PVA hydrogel membrane-based DBFC employing oxygen and air as oxidants are presented in Figure 4.21 and Figure 4.22, respectively. Peak power densities of 55.5 mW cm⁻², 103.4 mW cm⁻², 117.6 mW cm⁻² and 165.3 mW cm⁻² were obtained using oxygen in humidified air as the oxidant at 28, 40, 50 and 60 °C, respectively. Better power performance was obtained by using oxygen as compared to air under the same conditions. For instance, at 60 °C, the PVA hydrogel membrane- based NaBH₄-O₂ fuel cell yielded a maximum peak power density of 242 mW cm⁻², which is about 77 mW cm⁻² higher than that using air as the oxidant.

The comparative cell performance data for the DBFCs employing a PVA hydrogel membrane and a Nafion[®] 212 membrane at the elevated temperature are shown in Figure 4.23 and Figure 4.24, respectively. With Nafion[®] 212 membrane, peak power densities of 237 mW cm⁻² and 167 mW cm⁻² were achieved at 60 °C, using humidified oxygen and humidified air, respectively. In case of air or oxygen as oxidant, the peak power densities of the PVA hydrogel membrane-based DBFC are comparable to or even a little higher than

those of the Nafion[®] membrane-based DBFC at 60 °C. This result indicates that PVA hydrogel membrane is an effective membrane for NaBH₄-O₂ fuel cell. It should be noted that Nafion[®] 212 membrane has a dry thickness of 51 μm, whereas PVA hydrogel membrane is about 200 μm thick. It can be expected that by reducing the thickness of PVA hydrogel membrane, an even higher power performance can be achieved.

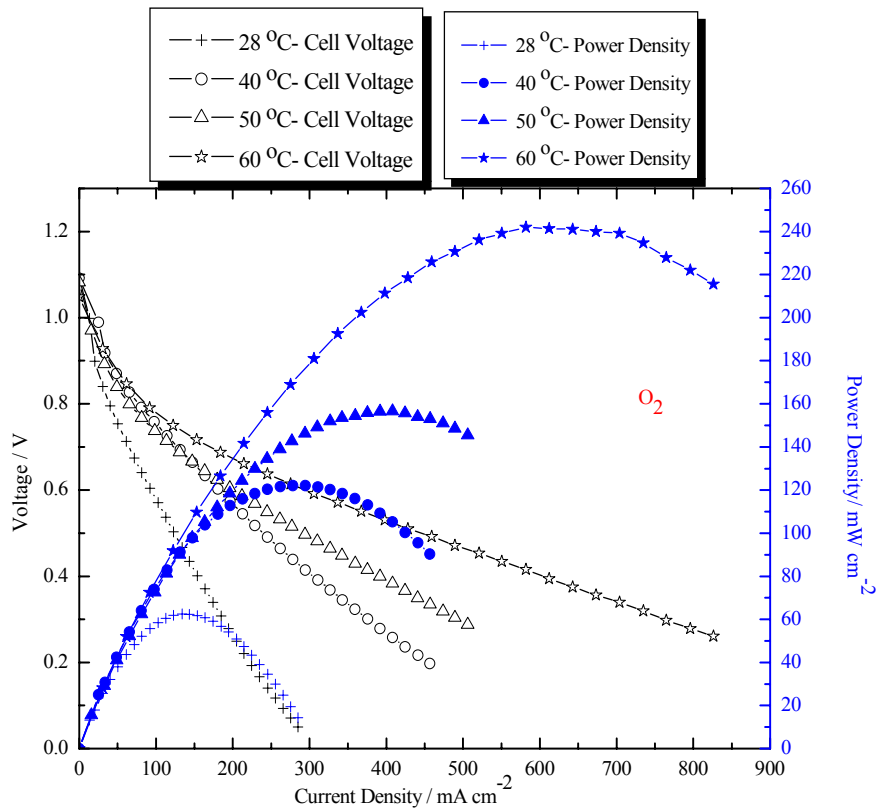


Figure 4.21 Cell polarization and power density curves of DBFCs which employ PVA hydrogel membrane at different temperatures with oxygen as the oxidant.

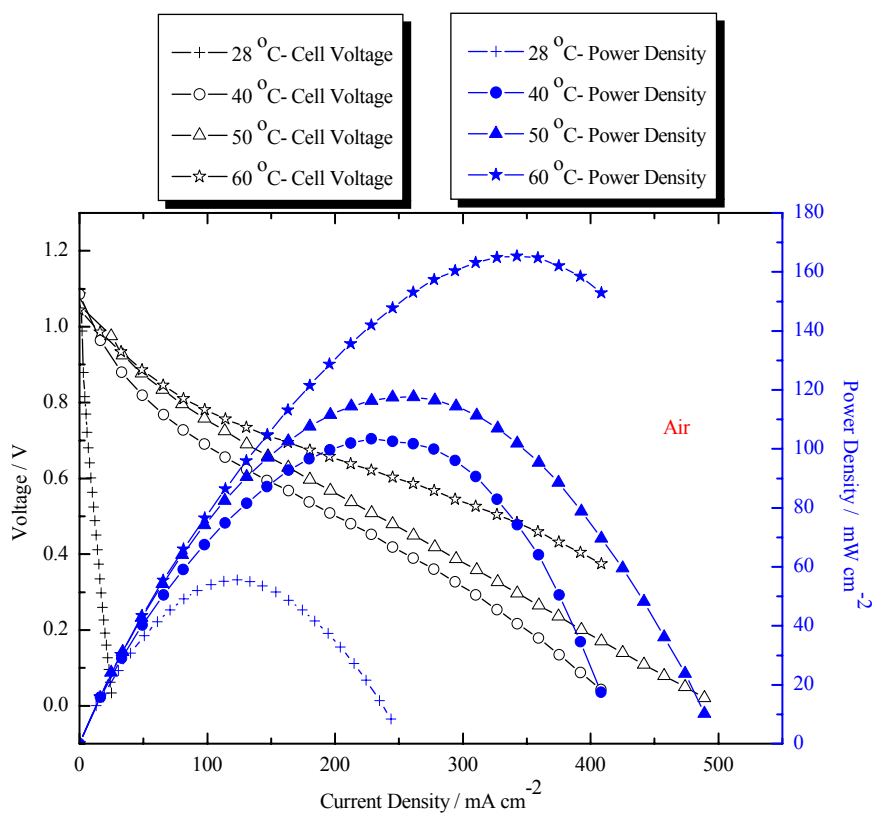


Figure 4.22 Cell polarization and power density curves of DBFCs which employ PVA hydrogel membrane at different temperatures with air as the oxidant.

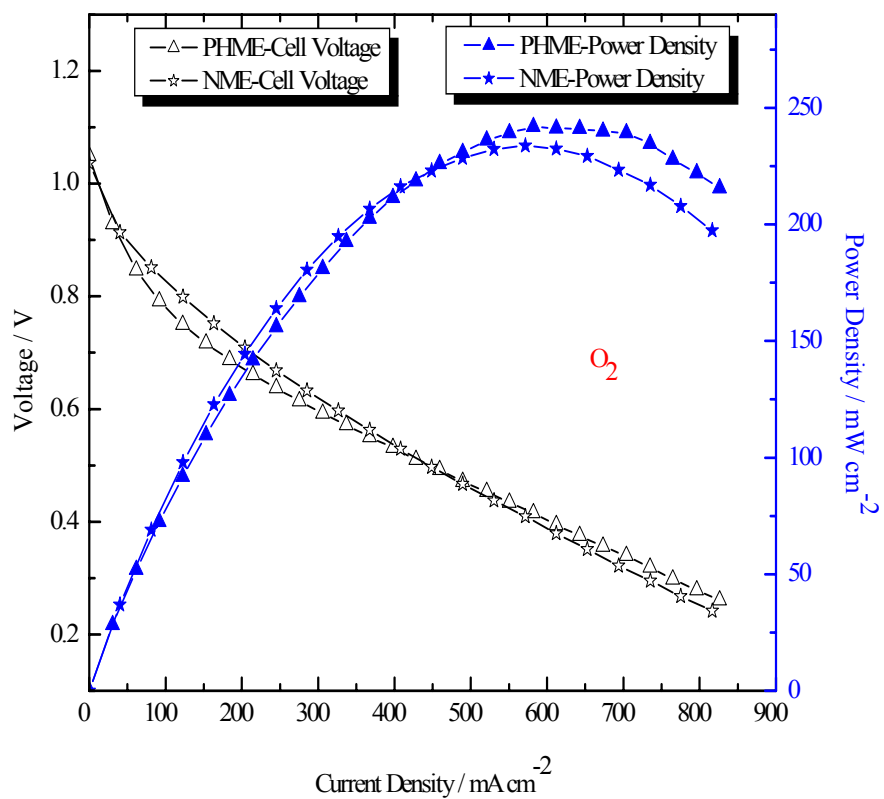


Figure 4.23 Curves of cell polarization and power density of a DBFC using a PVA hydrogel membrane electrolyte (PHME) or a Nafion[®] membrane electrolyte (NME) with oxygen as the oxidant at 60 °C.

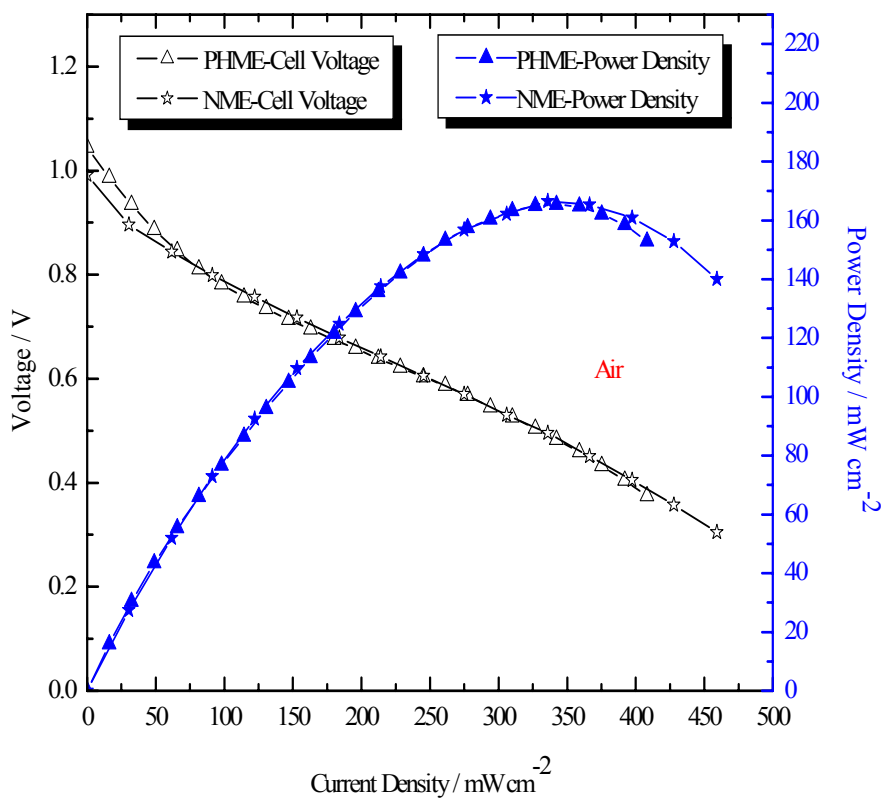


Figure 4.24 Curves of cell polarization and power density of a DBFC using a PVA hydrogel membrane electrolyte (PHME) or a Nafion[®] membrane electrolyte (NME) with air as the oxidant at 60 °C.

Faradic efficiency of the borohydride-oxygen fuel cell based on Ni-based anode and PVA hydrogel membrane was analyzed under a constant current discharge with a start from the cell to be fueled with 15 g fuel solutions comprising 5 wt.% NaBH₄ and 10wt.% NaOH at ambient temperature. Different current densities (25 mA cm⁻², 50 mA cm⁻², 75 mA cm⁻²) were applied to the fuel cell and the cell voltages were recorded. The final rapid drop of cell voltage was due to the exhaustion of sodium borohydride. Figure 4.25 shows the chronopotentiometric data for determination of fuel efficiency. Fuel efficiencies are calculated be in the range of 32%-41%.

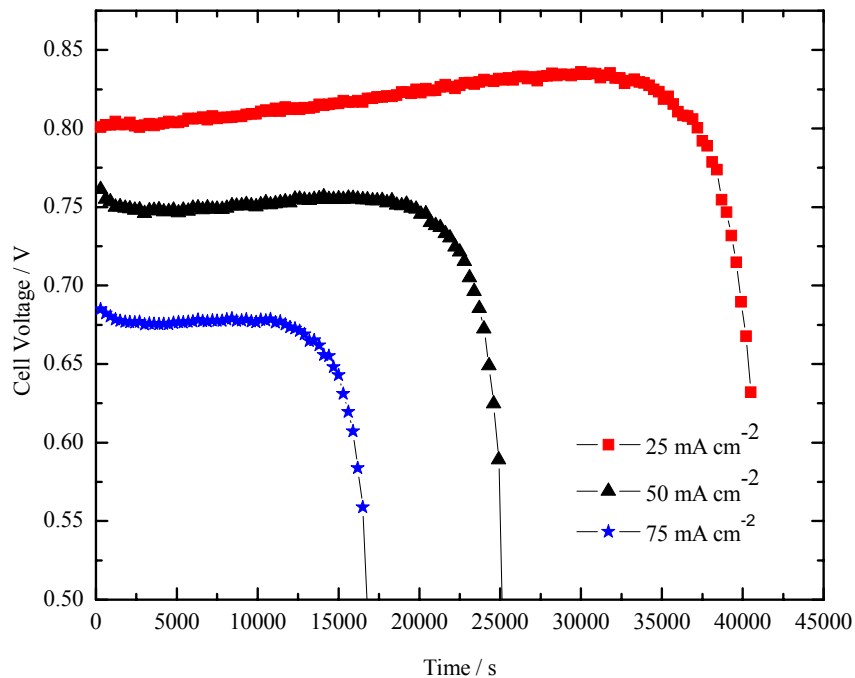


Figure 4.25 Chronopotentiometric data for determination of fuel efficiency in a DBFC based on PVA hydrogel membrane.

Short-term stability of borohydride-oxygen fuel cell using PVA hydrogel membrane was tested by monitoring the cell voltage change during the galvanostatic discharge of 50 mA cm^{-2} of the DBFC in a period of more than 100 h at ambient temperature as shown in Figure 4.26. The DBFC maintained a stable performance over the test period.

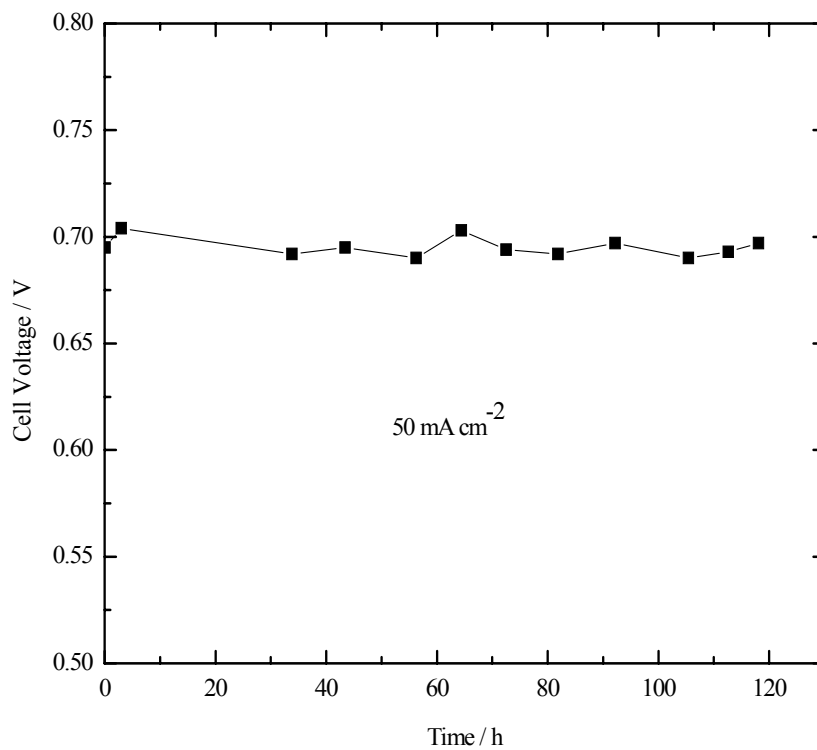


Figure 4.26 Performance stability of a PVA hydrogel membrane-based DBFC operating at current density of 50 mA cm^{-2} at ambient temperature.

4.4 Chitosan hydrogel membrane

In section 4.2, chitosan was employed as a binder material for DBFC electrode. A DBFC based on chitosan chemical hydrogel binder achieved superior power performance as compared to that using Nafion[®] binder. Inspired by this result, a polymer membrane electrolyte was prepared using chitosan material and employed in a DBFC. Preliminary cost estimates for chitosan membranes range from \$20-30/m², which is more than an order of magnitude lower than the current cost of Nafion[®] membranes, which range from \$500-1000/m² depending on the type and quantity ordered [97].

4.4.1 Glutaraldehyde cross-linked chitosan membrane

A chitosan membrane was prepared by homogeneously cross-linking it with an aqueous solution of glutaraldehyde. Pure chitosan membranes are colorless, whereas membranes cross-linked by glutaraldehyde are light yellow in color, which may indicate the presence of conjugated double bonds in the structure.

An electrode prepared by electron beam evaporation was employed as anode. This electrode had a thickness of 480 angstroms of Ni, followed by a thickness of 10 angstroms of Pt on Ni foam electrode substrate. The ratio of Ni and Pt is 20, and the metal loading is 0.45 mg cm⁻². Physical vapor deposition (PVD) methods afford some advantages over traditional means of ink paste method. These include production of thin layer of nano-sized particles with high electrochemical surface area, dramatic reduction in materials required, and the ability to reproducibly form controlled film composition and morphology with

minimal impurity incorporation. Besides, thin layer coating on electrode substrate with cost effective large volume manufacture protocols employing intelligent process controls would provide increased yield and product uniformity. Figure 4.27 shows a picture of a glutaraldehyde cross-linked chitosan membrane and Ni-based composite electrode prepared by electron beam evaporation.

A DBFC was assembled with Ni-based composite anode prepared by PVD, and glutaraldehyde cross-linked chitosan hydrogel membrane. The electrochemical performance of this cell was tested using oxygen as the oxidant. Cathode was Pt electrode (Pt/C, 1 mg Pt cm⁻² on Toray[®] carbon paper). Fuel was 5 wt.% NaBH₄ in 2.5 M NaOH. Flow rate of fuel was 5 mL min⁻¹. Flow rate of gaseous oxidant was 0.15 L min⁻¹. Electrochemical performance of this DBFC was studied for a period spanning over seven days, and the pertinent data are summarized in Table 4.1. Cell polarization and power density curve of the 2nd day was plotted and shown in Figure 4.28. The OCV values for this DBFC remained stable at around 1 V over the aforesaid duration. Peak power density and current density corresponding in the second day test increased significantly as compared to the first day test. During the characterization of this DBFC from 2nd day to 7th day, the DBFC power performance was found to be stable and intact.

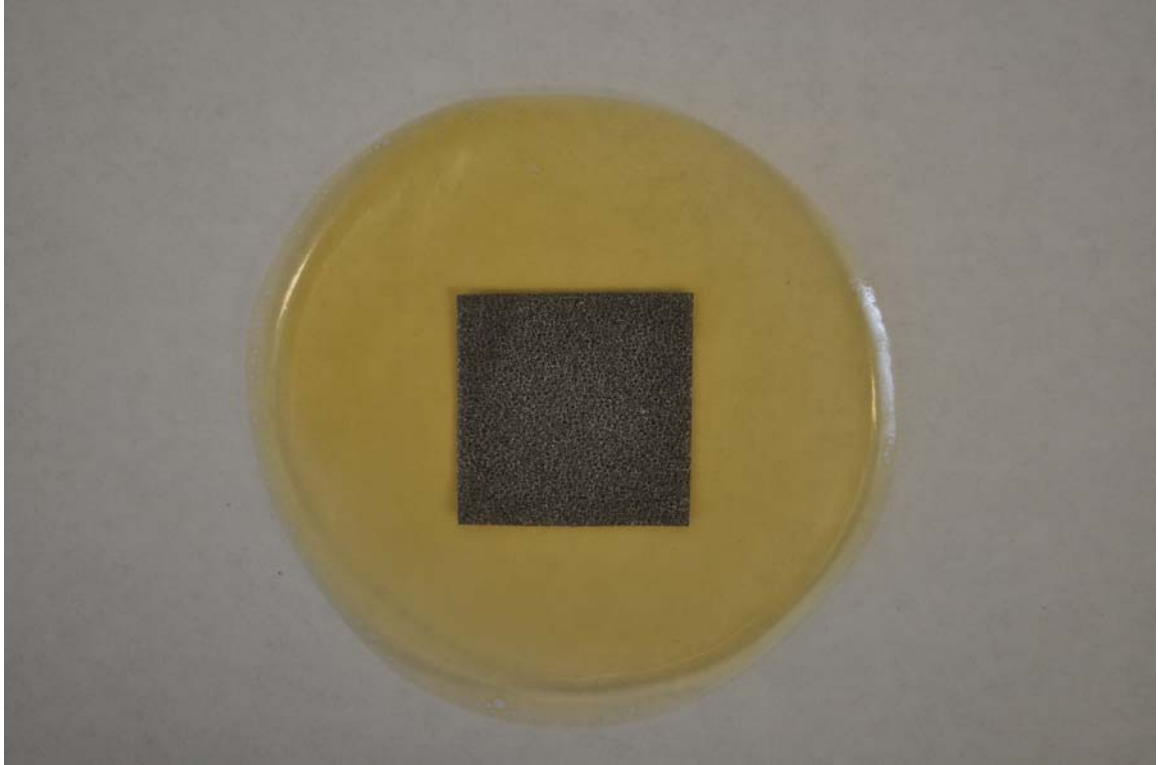


Figure 4.27 A picture of a glutaraldehyde cross-linked chitosan membrane and an electrode prepared by electron beam evaporation on Ni foam substrate.

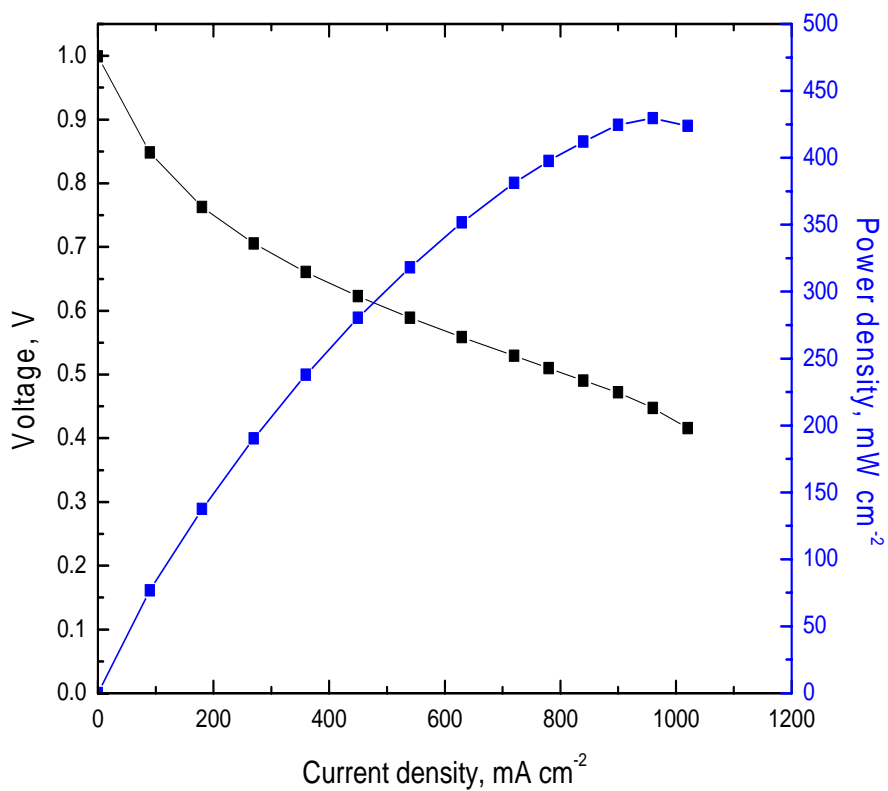


Figure 4.28 Plots of cell polarization and power density versus current density for DBFCs using chitosan membrane cross-linked by glutaraldehyde, and electron beam deposited Ni-based composite anode at 60 °C.

Table 4.1 Electrochemical performance durability data for a DBFC using chitosan membrane cross-linked by glutaraldehyde, and electron beam deposited Ni-based anode at 60 °C.

Day	1 st	2 nd	3 rd	4 th	7 th
OCP, V	1.007	1.004	0.984	1.008	1.000
Peak power density, mW cm ⁻²	333.8	429.7	424.7	425.4	427.3
Corresponding current density, mA cm ⁻²	720.7	960.2	980.2	980.5	980.5

4.4.2 Sulfuric acid/sulfate modified chitosan membrane

Chitosan membrane was prepared and modified by sulfuric acid or sodium sulfate. Use of H_2SO_4 is accompanied by health hazard. Being a corrosive liquid reagent, handling and use of H_2SO_4 as cross-linking agent is cost-intensive. Use of salts such as sodium sulfate overcomes both of the two limitations. A picture of sulfuric acid modified chitosan membrane is shown in Figure 4.29. The ionic interaction between chitosan and sulfate ion is shown in Figure 4.30.



Figure 4.29 A picture of sulfuric acid modified chitosan membrane.

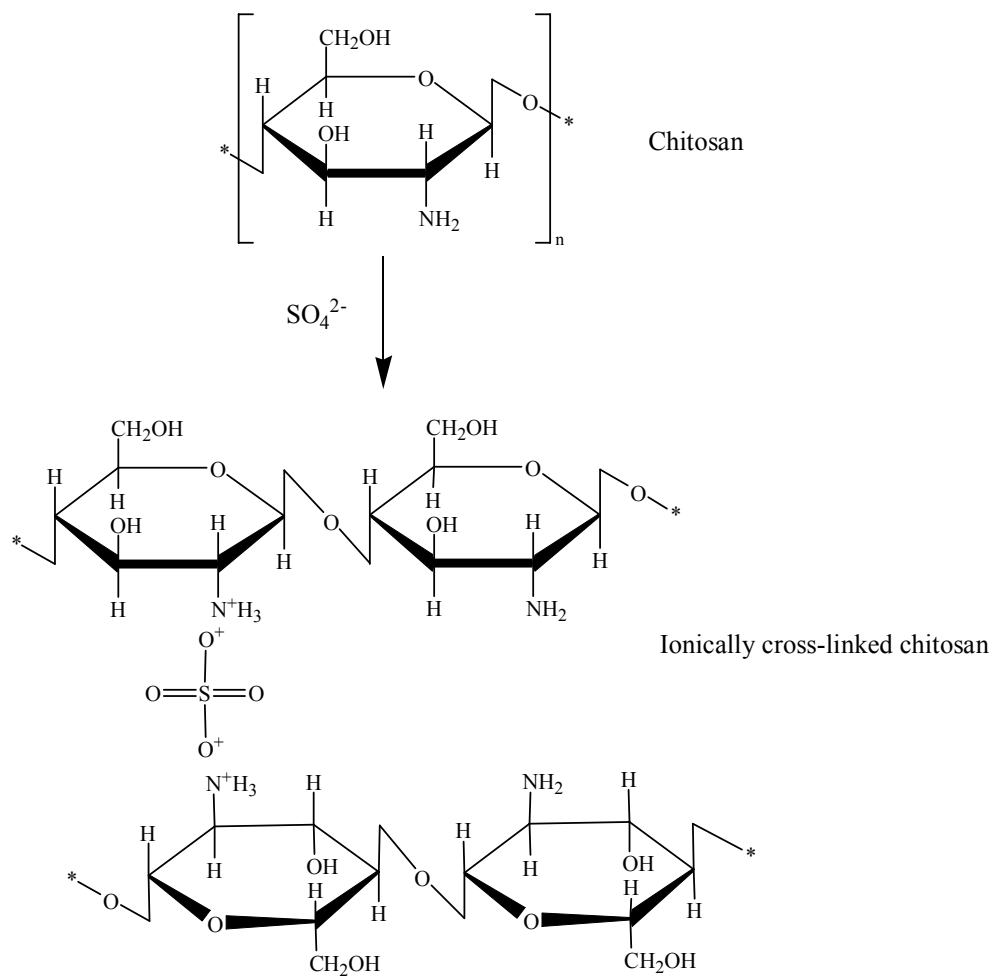


Figure 4.30 Chemical structures of chitosan and sulfate ion cross-linked chitosan.

4.4.2.1 Membrane characterization

To evaluate the mechanical properties of a sulfate chitosan membrane in its swollen state, the membrane was immersed in water for several days, and prior to the test it was taken out of water. The tensile strength at break and Young's modulus values for sulfate chitosan membranes in their swollen state were found to be 4.1 MPa and 8.3 MPa, respectively.

To determine the water uptake at hydration, the membranes were removed from water, blotted dry and quickly weighed to give the initial wet weight. After that, the sulfate modified chitosan membrane pieces were dried at 110 °C in an oven for 48 h to evaporate all the absorbed water. The water-uptake value of the sulfate chitosan membrane has been found to be about 93.5 %. Table 4.2 summarizes some properties of chitosan membrane modified by sulfate salt of sodium.

A dry piece of sulfate modified chitosan membrane was examined under thermogravimetric analysis. As shown in Figure 4.31, the TGA curve for the sulfate chitosan membrane sample exhibited an initial weight loss of about 7 % in the temperature range 30–200 °C. This initial weight loss was attributed to the desorption of physically absorbed water. The second weight loss of 12 % took place in the second stage in the temperature range of 200–240 °C. In the third stage, a weight loss of about 30 % was observed in the temperature range of 240–800 °C. The second and the third stages of weight losses were probably due to the decomposition of polymeric network of chitosan.

Table 4.2 Summary of properties of chitosan membrane modified by sulfate salt of sodium.

Sulfate chitosan hydrogel membrane	Tensile strength (MPa)	Young's modulus (MPa)	Water uptake (%)
	4.1	8.3	93.5

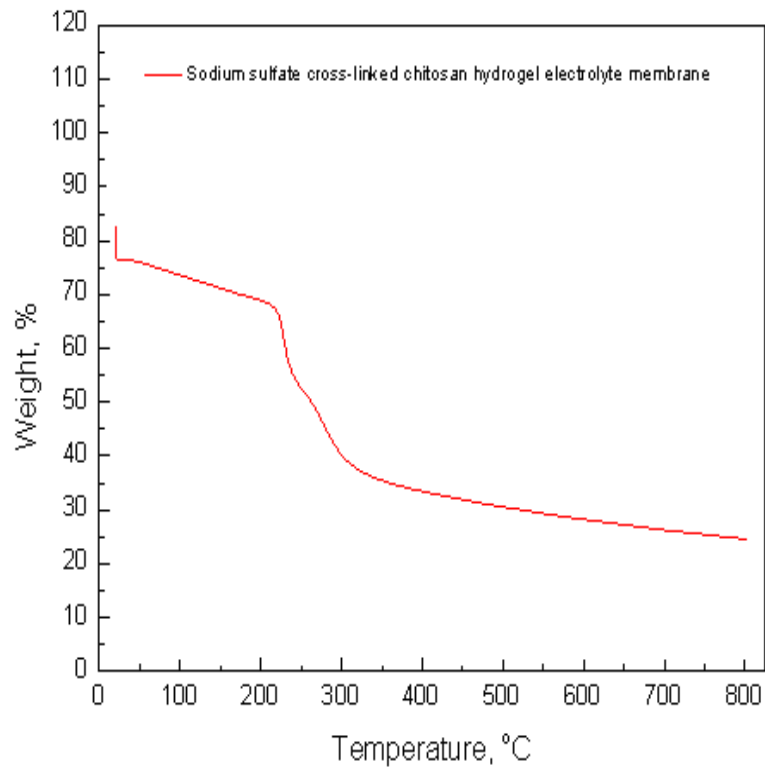


Figure 4.31 Thermogravimetric analysis curve for sulfate modified chitosan membrane.

Chitosan hydrogel membrane was also evaluated in terms of ionic conductivity and its values were compared with a Nafion[®] 212 membrane. Prior to the test, membranes were equilibrated in DI water or aqueous NaOH solution, Nyquist plots were recorded by carrying out impedance spectroscopic measurements, and are shown in Figure 4.32 (a) and (b). The ionic conductivity data derived from Nyquist plots are summarized in Table 4.3. After pretreatment, where the membrane was boiled in 3 wt.% sulfuric acid for 1 h, Nafion[®] 212 membrane was in H⁺-form. The ionic conductivity of Nafion[®] 212 membrane equilibrated with DI water was found to be $7.6 \times 10^{-2} \text{ S cm}^{-1}$, which is close to the reported value [98]. After it was equilibrated in NaOH aqueous solution, Nafion[®] 212 membrane was in Na⁺-form. The ionic conductivity of Nafion[®] 212 membrane in alkaline medium was $7.4 \times 10^{-3} \text{ S cm}^{-1}$, which is one order of magnitude lower than that in acid form. The conduction of H⁺ ions in the acid-form of Nafion[®] 212 membrane takes place by its transport from one anionic site (-SO₃⁻) to another anionic site through water medium by Grotthus type mechanism which contributes to the abnormally high mobility of the proton as compared to other ions. In contrast, the conduction of Na⁺ in NaOH-treated Nafion[®] 212 membrane takes place by its transport from one anionic site to another through water medium by segmental motion-aided diffusion mechanism. As shown in Figure 4.33, in Grotthus type mechanism, conduction of H⁺ through water takes place by alternation of covalent bond into hydrogen bond and vice versa [95]. Contrastingly, conduction of Na⁺ through water medium of Na⁺-form of Nafion[®] 212 membrane takes place by diffusion of hydrated Na⁺ ion as shown in Figure 4.34. Because of the more facile conduction of H⁺

ions as compared to Na^+ ions, acid form of the Nafion[®] 212 membrane exhibits higher ionic conductivity than sodium form one. It has been found that the replacement of proton on the sulfonic group by cations affects the transport characteristics of polymer electrolyte, reducing ionic conductivity, and water uptake [99].

Chitosan film can be cast from dissolving chitosan powder in organic acid aqueous solution. The resulted chitosan film is in acid form ($-\text{NH}_3^+$) which can be converted to $-\text{NH}_2$ form by air drying [100] during which the organic acid is removed by evaporation. After the addition of sulfuric acid to chitosan film, the amino groups are protonated and cross-linking reaction occurs between two negatively charged oxygen moieties of sulfate ion of sulfuric acid and positively charged ammonium groups ($-\text{NH}_3^+$) of two chitosan chains. This type of ionic interaction takes place at multiple points of the chitosan chains, thereby making the chitosan hydrogel membrane stable in aqueous medium. Sulfuric acid modified chitosan membrane demonstrated a conductivity of $6.2 \times 10^{-3} \text{ S cm}^{-1}$ after washing with DI water. The ionic conductivity of chitosan hydrogel membrane is lower than that of Nafion[®] 212 membrane after equilibrated with DI water. The high conductivity of Nafion[®] membrane is due to the linked ionic cluster structure, which enables the protons jump from one sulfonic group to another through water medium [101,102]. In chitosan hydrogel membrane, ionic bonds formed between the $-\text{NH}_2$ group and $-\text{SO}_3\text{H}$ groups consume some of the proton exchange sites, which is unfavorable to proton conduction. It is possible that in chitosan hydrogel membrane the distance between two proton receptor sites is longer

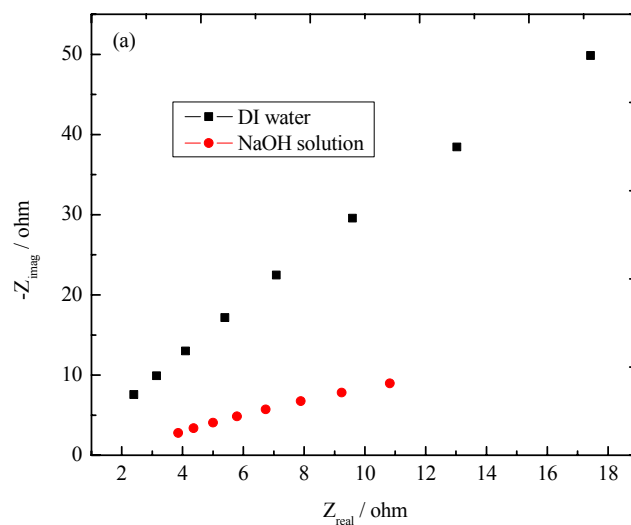
and so electromosis is slower than in the Nafion[®] membrane [103], and as a result, the conductivity of chitosan hydrogel membrane is lower.

The conductivity of chitosan hydrogel membrane in alkaline medium was calculated to be $1.1 \times 10^{-1} \text{ S cm}^{-1}$, which is significantly higher than after dipping in the DI water medium. When chitosan hydrogel membrane is treated with aqueous NaOH solution, Na⁺ and OH⁻ ions penetrate into the matrix of cross-linked chitosan membrane. The hydroxide ion is capable of forming hydrogen bonding in water medium of cross-linked chitosan membrane hydrogel matrix and transports through the matrix by Grotthus type mechanism. The higher ionic conductivity of NaOH-equilibrated chitosan hydrogel membrane is due to the contribution of OH⁻ ion in addition to the contributions from the SO₄²⁻ and Na⁺ ions. The conductivity of chitosan hydrogel membrane is higher than that of Nafion[®] 212 membrane in alkaline medium. Chitosan contains polar functional groups, namely hydroxyl (-OH), primary amine (-NH₂), and ether (C-O-C) groups which have the capability of forming hydrogen bonding with water and trapping water in its polymer matrix. Nafion[®] polymer possesses both hydrophilic and hydrophobic properties. Since the water attracting behavior of Nafion[®] is restricted to its hydrophilic region only, its water retaining capability is not as good as that of chitosan. The high water uptake capability of chitosan hydrogel membrane is demonstrated by the difference between its wet thickness and dry thickness. It is evident from Table 4.3 that the wet thickness of Nafion[®] 212 membrane (60 μm) is only slightly higher than its dry thickness (50 μm). In contrast, the wet thickness of chitosan hydrogel membrane (115 μm) is much higher than its dry thickness (45 μm). Greater water uptake

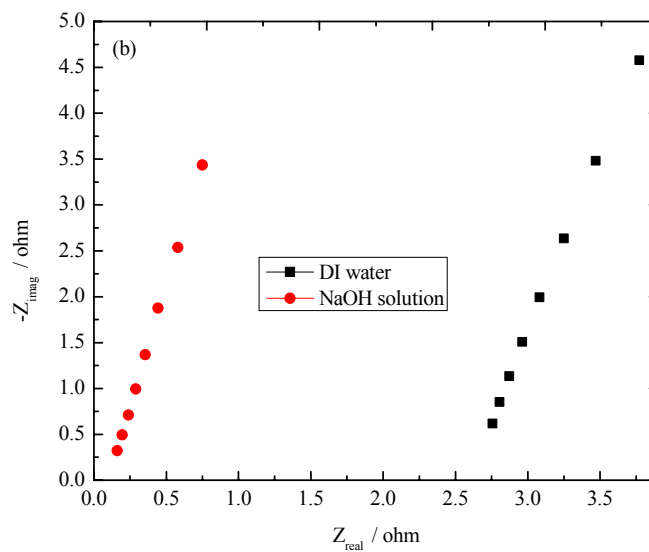
ability of chitosan hydrogel membrane leads to its greater uptake ability of electrolyte solutions such as NaOH, and ultimately contributes to a higher ionic conductivity which is related to the number and mobility of conductive of ions in the polymer complexes [104]. An ideal ionic conductivity of hydrated polyelectrolyte membrane should be close to 10^{-2} S cm⁻¹ or higher for polymer electrolyte fuel cell application [105]. Thus, chitosan hydrogel membrane possesses conductivity high enough to serve as electrolyte in a DBFC.

For application in DBFCs, another important property of membrane electrolyte is borohydride crossover. Therefore, ex-situ studies were carried out to investigate borohydride crossover rate across membrane electrolytes. The calibration plot exhibiting relation between anodic peak current and borohydride concentration is shown in Figure 4.35(a). The plot is linear over a wide concentration range with a root square deviation of 0.9986. Figures 4.35 (b) and (c) show typical linear sweep voltammograms recorded for alkaline solution of NaBH₄ that crossed over during 24 h of test duration through Nafion[®] 212 and chitosan hydrogel membrane, respectively. It can be seen that a lower peak current is observed for Nafion[®] 212 membrane as compared to chitosan hydrogel membrane, which implies a lower rate of borohydride crossover through Nafion[®] 212 membrane. Borohydride crossover rates through chitosan hydrogel membrane and Nafion[®] 212 membrane were calculated to be 4.6×10^{-8} and 4.8×10^{-9} mol s⁻¹ cm⁻², respectively. Borohydride crossover rate through the chitosan hydrogel membrane is higher than that through the Nafion[®] 212 membrane by one order of magnitude. The difference in crossover rates of borohydride fuel through the two membranes can be understood by

considering their structural features. Nafion[®] membrane is a cation exchange membrane with negatively charged $-\text{SO}_3^-$ groups attached to the polymer backbone. Being a negatively charged ion, BH_4^- experiences a repulsive force while crossing over through the Nafion[®] membrane. In contrast, chitosan hydrogel membrane has positively charged $-\text{NH}_3^+$ groups attached to the polymer backbone. Because of the electrostatic attraction with $-\text{NH}_3^+$ group, BH_4^- ion experiences a facilitated crossover through chitosan hydrogel membrane in contrast to Nafion[®] 212 membrane. Therefore, Nafion[®] membrane is more effective in the suppression of BH_4^- crossover as compared to chitosan hydrogel membrane.



(a)



(b)

Figure 4.32 Nyquist plots of (a) Nafion[®] 212, and (b) sulfuric acid modified chitosan hydrogel membrane recorded by electrochemical impedance spectroscopy.

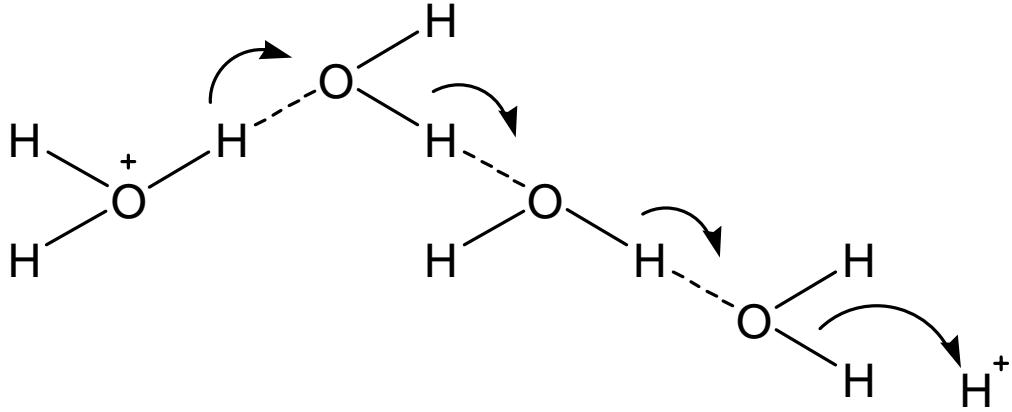


Figure 4.33 Grotthius-type mechanism of proton conduction.

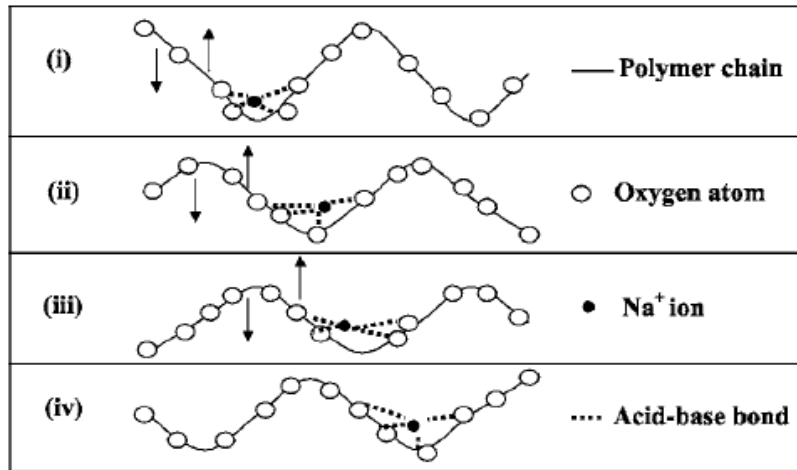
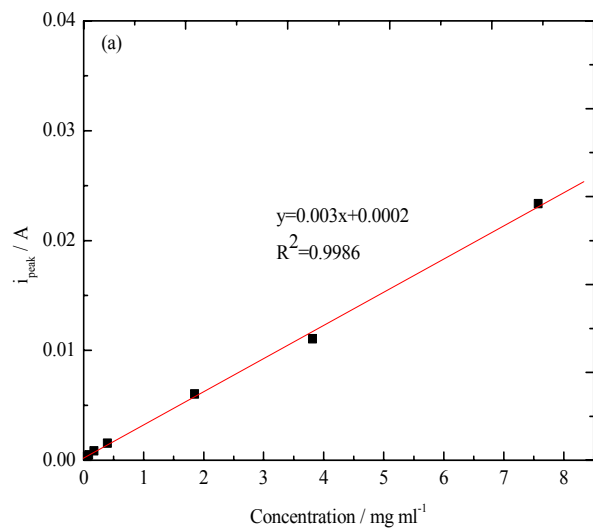
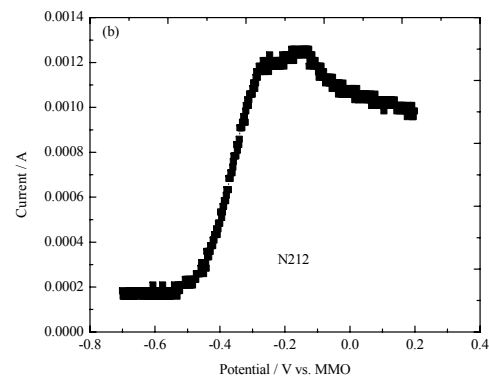


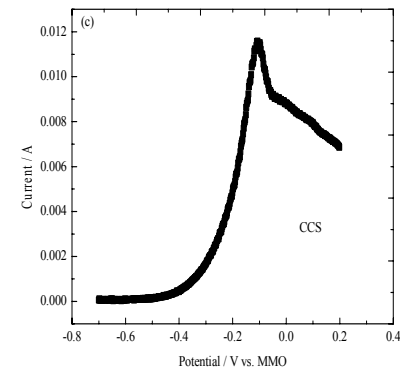
Figure 4.34 Segmental-motion mechanism of ionic conduction in alkaline membrane electrolytes [95].



(a)



(b)



(c)

Figure 4.35 (a) Dependence of peak anodic current at gold electrode on borohydride concentration; a typical linear sweep voltammogram (LSV) recorded during estimation of borohydride crossover through (b)Nafion[®] 212 membrane, and (c) sulfuric acid modified chitosan hydrogel membrane.

Table 4.3 Comparison between properties of chitosan hydrogel membrane and Nafion[®] 212 membrane.

Membrane	Dry thickness (μm)	Wet thickness (μm)	Ionic conductivity measured after dipping in DI water (S cm ⁻¹)	Ionic conductivity measured after dipping in NaOH solution (S cm ⁻¹)	Boro-hydroxide crossover rate (mol s ⁻¹ cm ⁻²)
Nafion [®] 212	50	60	7.6×10^{-2}	7.4×10^{-3}	4.8×10^{-9}
Chitosan membrane modified by sulfuric acid	45	115	6.2×10^{-3}	1.1×10^{-1}	4.6×10^{-8}

4.4.2.2 Power performance of DBFCs using chitosan hydrogel membrane

The electrochemical performance was measured in a DBFC by using either chitosan hydrogel membrane or Nafion[®] 212 membrane. The catalyst anode binder was either chitosan chemical hydrogel (2 wt.% loading) or Nafion[®] solution (12.5 wt.% loading). The anode was Ni+Pd/C on Ni foam (0.5 mm) with 5 mg metal cm⁻². Fuel was 5 wt.% NaBH₄ and 10 wt.% NaOH. Flow rate of the fuel was 5 mL min⁻¹. Cathode was Pt cathode (1 mg Pt cm⁻² on Toray[®] carbon paper). The oxidant was humidified oxygen. Flow rate of the oxidant was 0.15 L min⁻¹. The electrochemical performance data for DBFCs are shown in Figure 4.36. Peak power density for DBFC employing Nafion[®] 212 membrane and Nafion[®] binder increased from 169 mW cm⁻² to 382 mW cm⁻² as the cell temperature was enhanced from 30 to 60 °C. Peak power density for DBFC employing chitosan hydrogel membrane and Nafion[®] binder increased from 172 mW cm⁻² to 402 mW cm⁻² as the cell temperature was increased from 30 to 60 °C. Under the same experimental conditions, the power performance of DBFC using chitosan hydrogel membrane is higher than that of DBFC using Nafion[®] 212 membrane at both 30 and 60 °C. Higher power performance of chitosan hydrogel membrane-based DBFC as compared to Nafion[®] 212 membrane-based DBFC can be understood in terms of the characteristics of the two membranes. As given in Table 4.3, the wet thickness of chitosan hydrogel membrane is about two times that of Nafion[®] 212 membrane whereas the ionic conductivity in alkaline medium of chitosan hydrogel membrane is about fifteen times that of Nafion[®] 212 membrane. Despite the slightly higher wet thickness, significantly higher ionic conductivity leads to lower ohmic

resistance and therefore a higher power density. Interestingly, the superior performance associated with the application of chitosan hydrogel membrane to Nafion[®] 212 membrane is more obvious at elevated temperature. This is likely due to the high water uptake capacity of chitosan hydrogel membrane. Increase in temperature might result in partial dryness of membrane electrolyte. Chitosan hydrogel membrane has higher water holding capacity compared to Nafion[®] 212 membrane. As a result, chitosan hydrogel membrane is more effective in preventing partial dryness of membrane at a high fuel cell temperature. Figure 4.36 also gives DBFC power performance with chitosan binder-based anode and chitosan hydrogel membrane. The peak power densities of this cell are 187 mW cm⁻² and 450 mW cm⁻² at 30 and 60 °C, respectively. Thus, the performance of chitosan hydrogel membrane-based DBFC was further improved by using chitosan binder as compared to Nafion[®] binder, and the superior performance of the said DBFC was more evident at a high temperature.

The electrochemical performance data recorded for DBFC employing sulfate modified chitosan hydrogel membrane and chitosan anode binder at 70 °C are shown in Figure 4.37. A peak power density of 750 mW cm⁻² and a current density corresponding to peak power of 1560 mA cm⁻² were achieved.

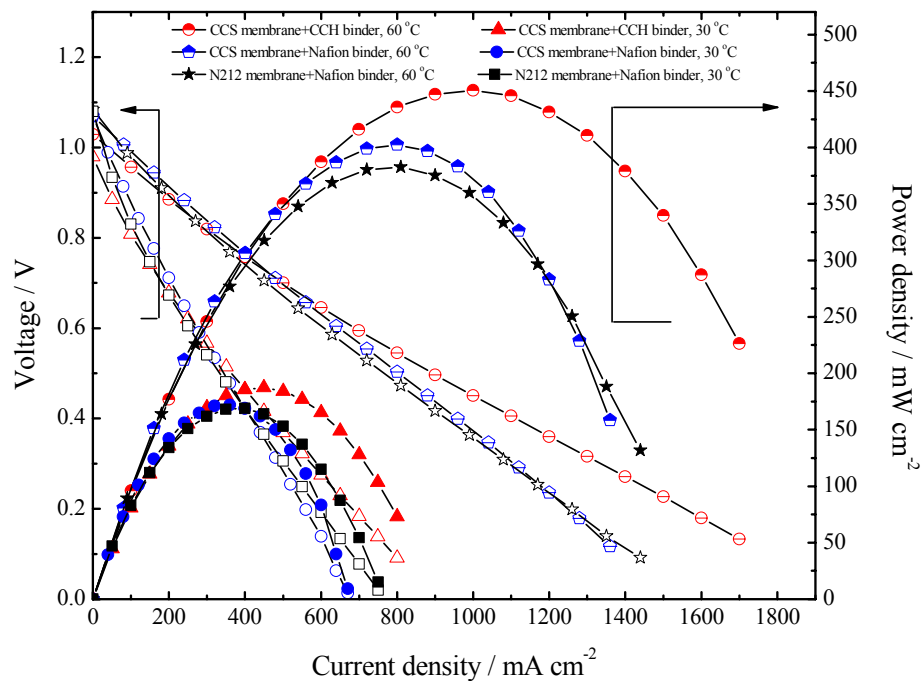


Figure 4.36 Plots of cell polarization and power density versus current density for DBFCs using sulfuric acid chitosan (CCS) hydrogel membrane and Nafion[®] 212 (N212) membrane, chitosan chemical hydrogel (CCH) binder and Nafion[®] binder at 30 and 60 °C.

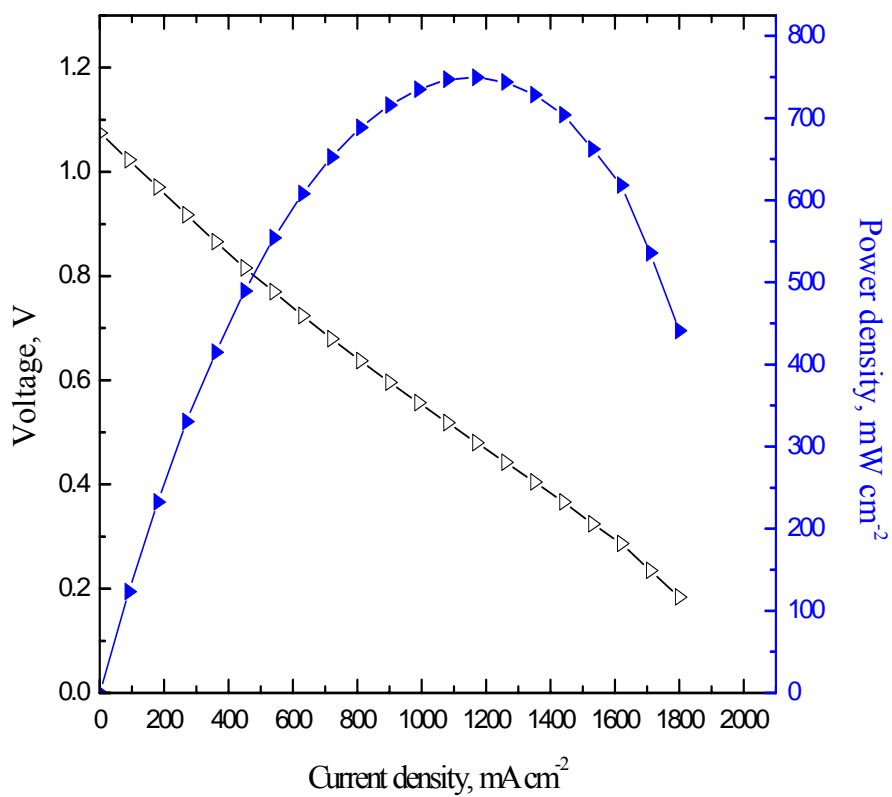


Figure 4.37 Cell polarization and power density plots for DBFC employing sulfate modified chitosan membrane and chitosan anode binder at 70 °C.

Performance stability of a borohydride-oxygen fuel cell using chitosan hydrogel membrane and chitosan anode binder was tested continuously for more than 100 h at 30 °C. As shown in Figure 4.38, the DBFC exhibited a stable performance over the test period. The operating cell voltage was fairly constant at 0.75 V with slight fluctuations over the test period. Thus, chitosan hydrogel membrane and chitosan binder are not only able to achieve high power but also good performance stability in DBFC application. Voltage efficiency of a fuel cell can be expressed as $\varepsilon = E(i)/E_r$, where $E(i)$ is the cell potential at a given applied current density and E_r is the reversible potential. The observed open circuit potential of the present DBFC is about 1 V. The observed OCP is lower than the theoretical value of 1.64 V due to fuel crossover, mixed potential at electrode, and sluggish electrode kinetics. The single fuel cell potential during operation of a fuel cell is diminished by the losses in over-potential at anode, cathode, and electrolyte. The over-potential losses encountered in a fuel cell include activation loss due to slow kinetics of electrochemical reactions at the electrodes, ohmic loss due to resistance of electrolyte membrane, cell components and inter-connects, mass transport loss due to insufficient concentrations of reactants at the electrode/electrolyte interface at high load current condition, and fuel crossover loss due to crossover of fuel through membrane electrolyte. Due to these losses, the operating efficiency of fuel cells is lower than the theoretical value. It is noteworthy that the potential vs. time plot was recorded at a constant load current density of 120 mA cm^{-2} . If the applied load current density is lowered, the observed voltage

will be higher than 0.75 V with the ultimate consequence of increased voltage efficiency of the same DBFC.

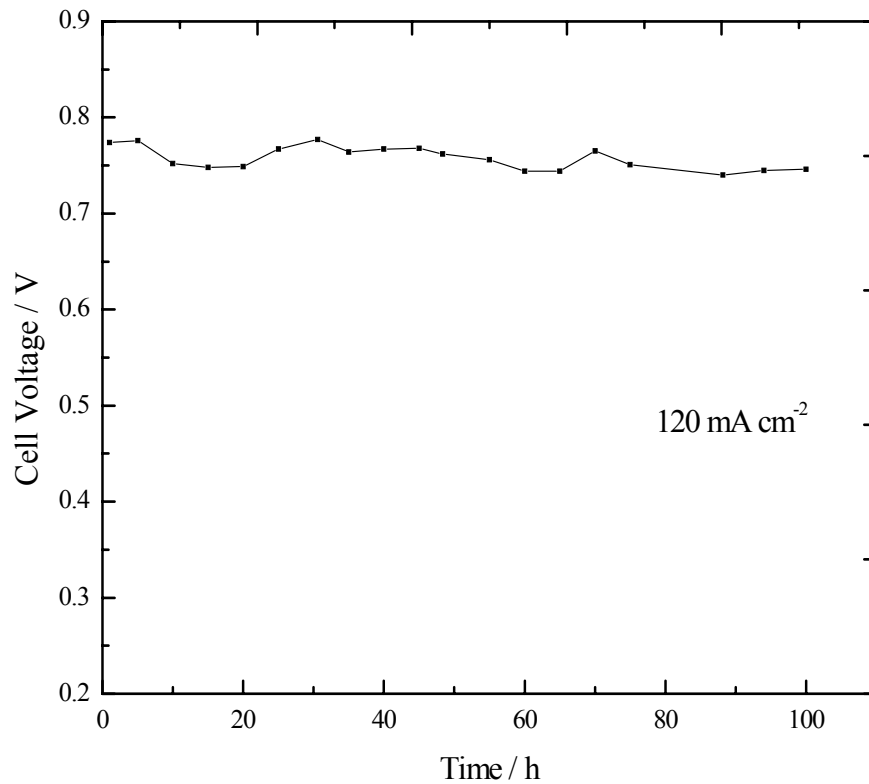
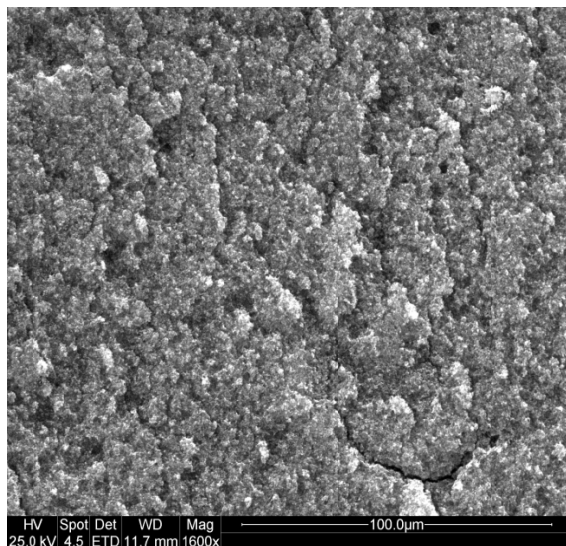


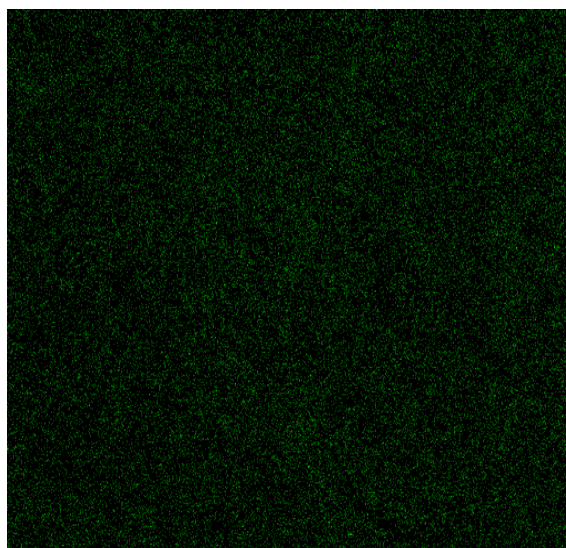
Figure 4.38 Fuel cell performance stability data for a DBFC, which employs chitosan anode binder and chitosan hydrogel membrane, recorded by operating it at a current density of 120 mA cm^{-2} at $30 \text{ }^\circ\text{C}$.

4.4.2.3 Ionic transport through chitosan hydrogel membrane

In DBFC with Nafion[®] membrane, it is known that sodium ions are charge carriers in it [2]. In chitosan hydrogel membranes, it is expected that Na⁺ is also responsible for the ionic charge transfer. To verify that Na⁺ is the ion conducting through the chitosan hydrogel membrane during DBFC operation, the cathode was analyzed by SEM after the fuel cell was operated for 2 h at a current density of 50 mA cm⁻². Figure 4.39(a) shows a scanning electron micrograph of the cathode surface. Figure 4.39(b) is a SEM mapping image which shows the presence of Na (green spot) in the cathode. This result proved that Na⁺ ions migrated from the anode compartment to the cathode compartment through the chitosan hydrogel membrane.



(a)



(b)

Figure 4.39 (a) Scanning electron micrograph of cathode surface, and (b) Na-mapping EDS image of cathode surface after used in a DBFC at a current density of 50 mA cm^{-2} for 2 h.

4.4.3 Multivalent phosphate modified chitosan membrane

Chitosan is polycationic in acidic media (pKa 6.5) and can interact with negatively charged species such as triphosphate (TPP) and phosphate by electrostatic forces as shown in Figure 4.40. Many research explored the potential pharmaceutical usage of chitosan triphosphate or phosphate complex. However, TPP modified chitosan has not been used in any electrochemical energy devices. In the present study, phosphate chitosan (CsP) and triphosphate chitosan (CsTP) hydrogel membranes were prepared, characterized, and fabricated into a MEA for use in a DBFC.

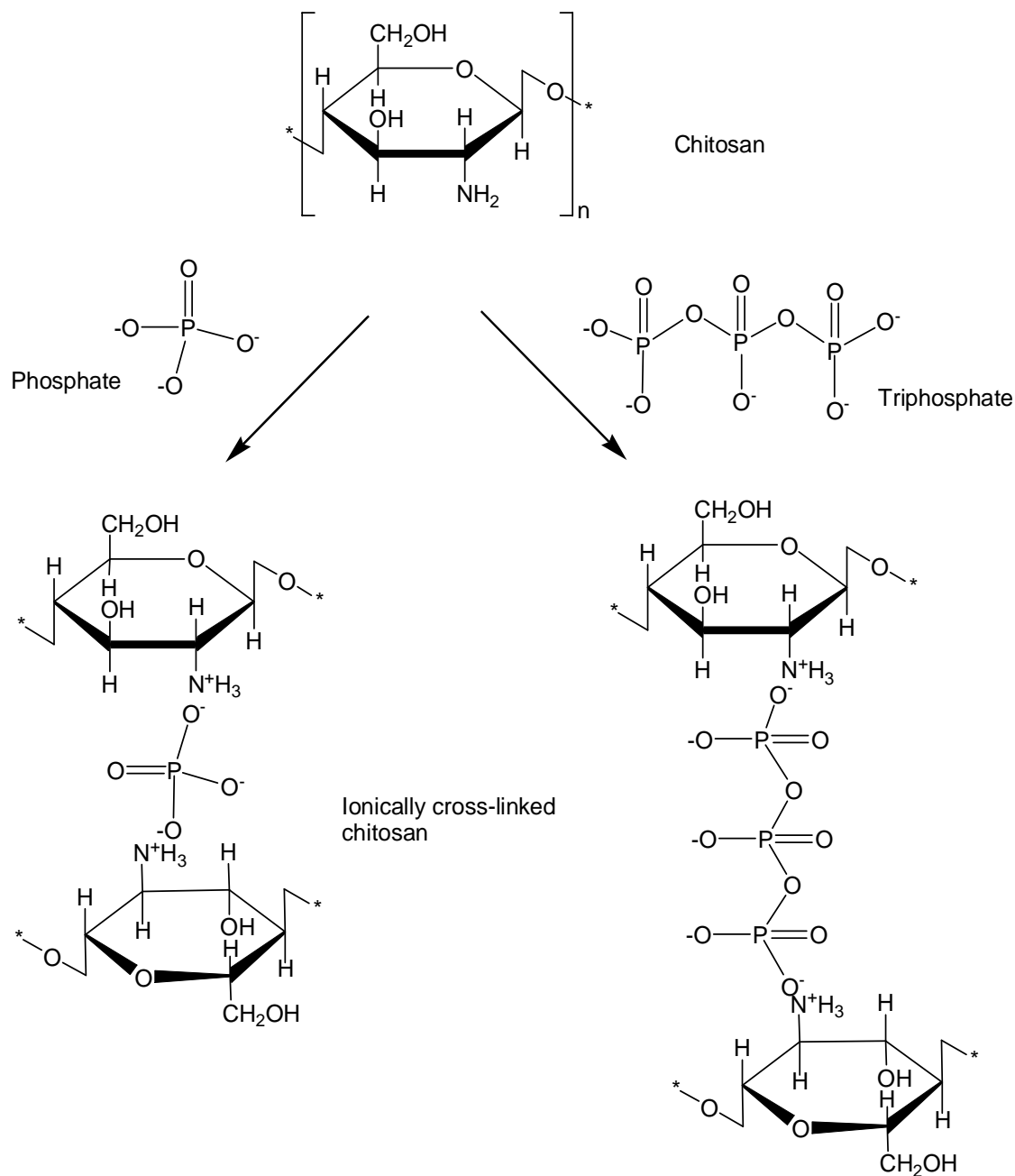


Figure 4.40 Chemical structures of chitosan and phosphate and triphosphate cross-linked chitosan.

4.4.3.1 Membrane characterization

ATR IR study

Table 4.4 lists FTIR bands of chitosan membrane. The FTIR spectra for pristine chitosan membrane and chitosan hydrogel membrane modified with TPP are shown in Figure 4.41. The spectrum of chitosan exhibits strong and broad band centered at about 3543, 3362, and 3310 cm^{-1} that result from overlapping of the O–H and N–H stretching vibrations of functional groups engaged in hydrogen bonds. Absorption bands at 1146, 1070 and 1031 cm^{-1} are characteristic of chitosan saccharide structure. Bands at 2910, 2862 cm^{-1} belong to symmetric and anti-symmetric C-H stretching vibrations. Bands in the range of 1421-1262 cm^{-1} belong to C-H bending vibrations. Amide III band is also possibly present in this range.

In the spectra of TPP modified chitosan, the band characteristic of NH_2 bending vibrations (around 1580 cm^{-1} , amide II) was weakened, and new absorption bands characteristic of NH_3^+ symmetric and asymmetric bending vibrations appeared at 1634 cm^{-1} and 1546 cm^{-1} . These results suggest that the NH_2 groups in the chitosan chains were protonated and had interaction with TPP. In addition, the chitosan O-H and N-H absorption bands became less distinct. The absorption band appeared near 3200 cm^{-1} was broadened as the reaction between TPP and chitosan progressed. The broad band near 3200 cm^{-1} might be assigned to the stretching vibration of $\text{N}^+\text{-H}$. The position of the absorption due to the C-H stretching vibration shifted to higher wavenumbers (from 2862 to 2888 cm^{-1}). Infrared C-H stretching bands shift to lower wavenumbers as crystallinity

increases. Thus this shift was consistent with decreasing crystallinity as the reaction progressed.

Table 4.4 Infrared band assignments for chitosan membrane.

Vibrational mode assignment	Peak position wavenumber, cm^{-1}
O-H stretching	3543
N-H ₂ symm. stretching	3362
N-H ₂ asymm. stretching	3310
C-H symm. stretching	2910
C-H asymm. stretching	2862
Amide I (C=O)	1642
N-H ₂ deformation, amide II	1580
Saccharide structure (-C-O- stretching)	1146, 1070 , 1031

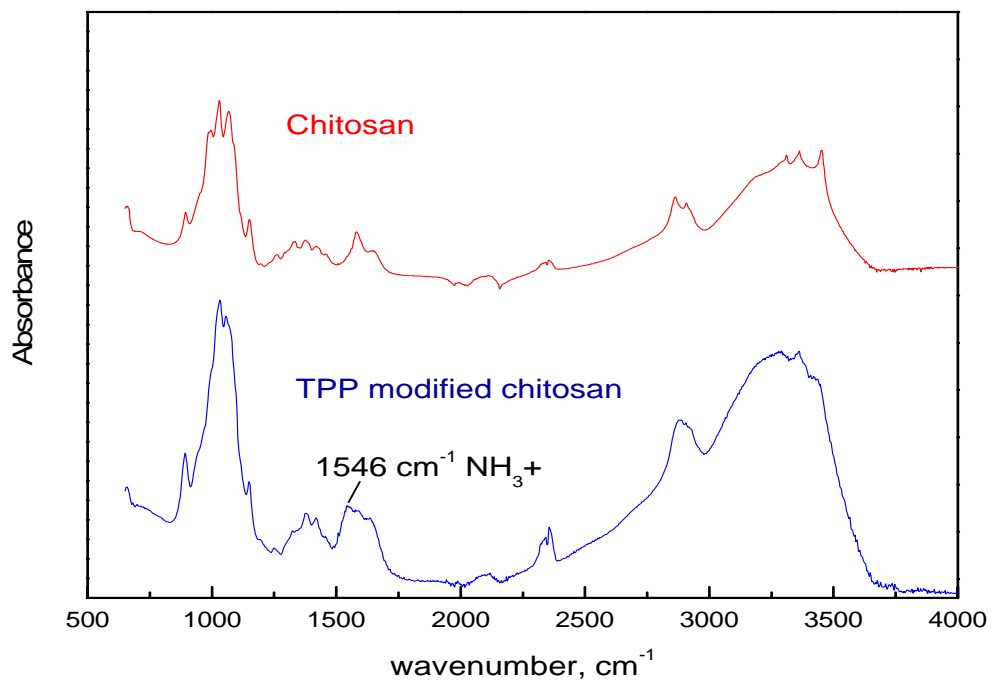
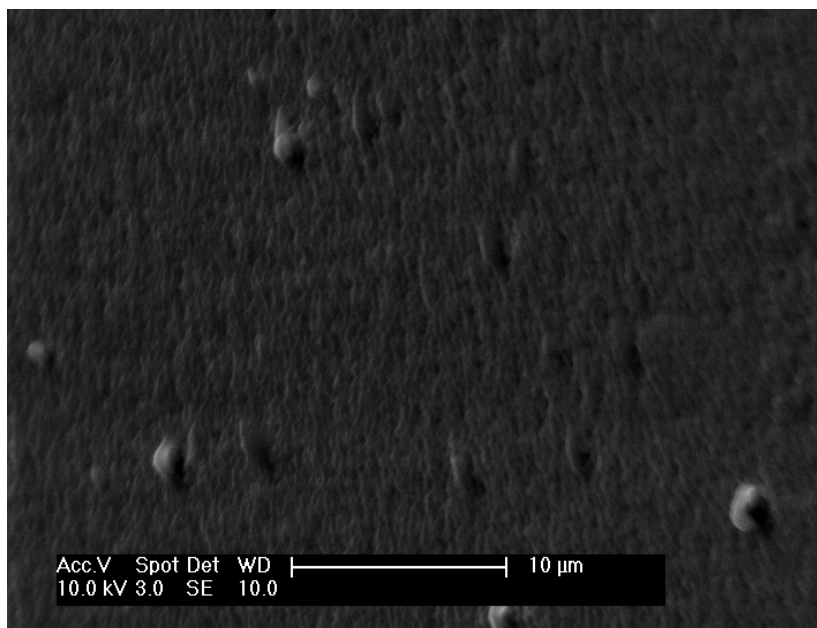


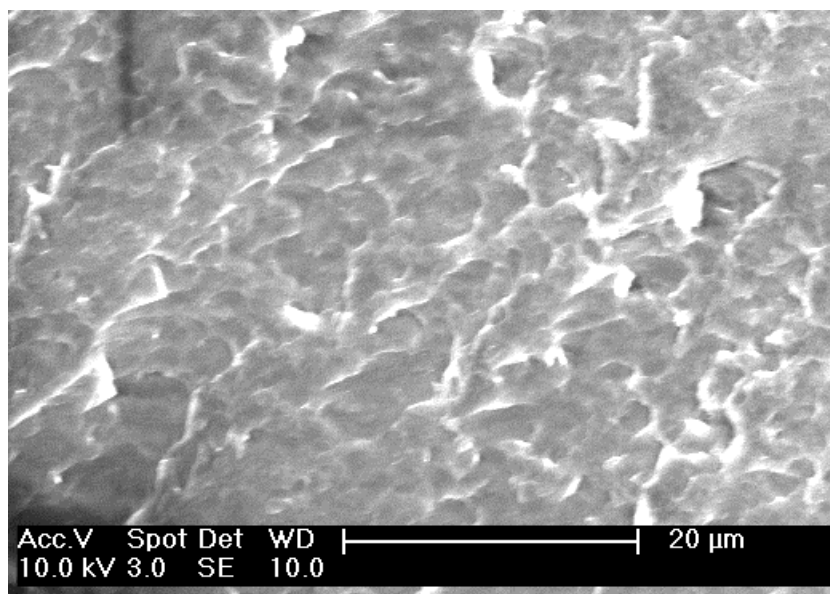
Figure 4.41 The FTIR spectra for uncross-linked chitosan membrane and chitosan membrane modified with TPP.

SEM study

Figure 4.42 shows the surface and cross-sectional morphology of chitosan membrane modified by TPP. The chitosan membrane seems to have a smooth surface morphology, and appears homogeneous and dense. As shown in Figure 4.43, EDX analysis on both surface and cross sectional areas of chitosan membrane modified by TPP shows phosphor element, which provides supporting information of TPP modification.

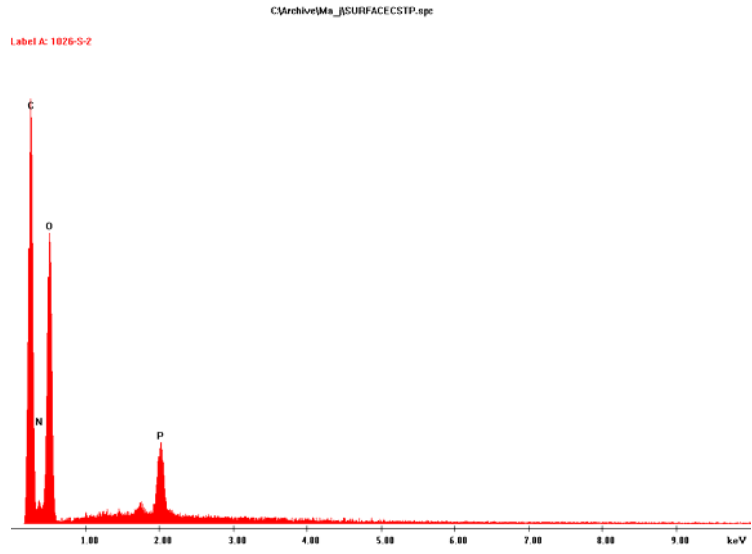


(a)

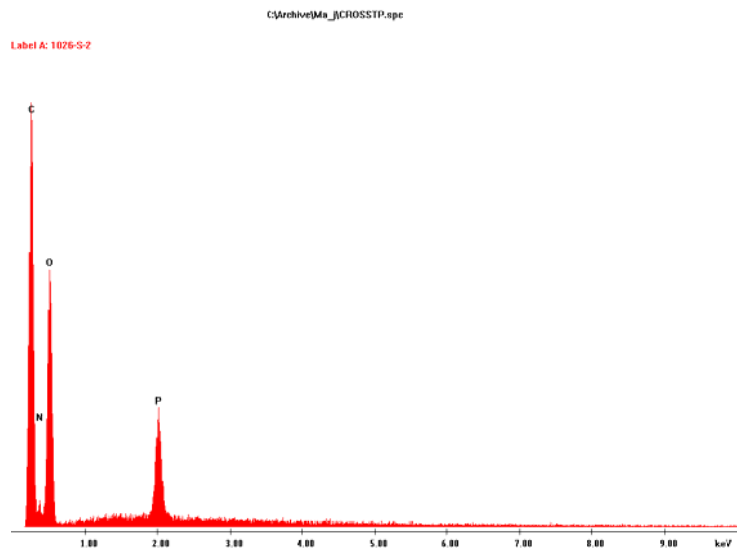


(b)

Figure 4.42 SEM pictures of (a) surface and (b) cross-sectional morphology of chitosan membrane modified by TPP.



(a)



(b)

Figure 4.43 EDX spectra of (a) surface and (b) cross section of chitosan membrane modified by TPP.

Thermal analysis

The weight loss (%) against temperature curves for Nafion[®], pristine chitosan, CsP, and CsTP membranes in the presence of nitrogen are given in Figure 4.44. Pristine chitosan membrane shows a gradual weight loss starting from 25 °C and a major weight loss occurs from 213 to 416 °C. The maximum decomposition rate occurs at 280 °C with a weight loss of 32 %. CsP membrane has two major different stages of weight loss. The first stage ranges between 25 and 126 °C, during which there is a 10 % weight loss corresponding to the loss of adsorbed and bound water. A 38 % weight loss has been observed for CsP membrane from 220 to 330 °C due to chitosan decomposition. Similar to CsP, TGA of CsTP membrane mainly shows two stages of weight loss. The first stage has a 10 % weight loss in the temperature range between 25 and 144 °C, during which CsTP membrane gradually loses water. After 144 °C, CsTP membrane continues to lose weight up to 320 °C. In this range there is a 45 % weight loss due to the degradation of chitosan polymer. Compared with pristine chitosan membrane, both CsP and CsTP membranes have lower degradation temperatures, which indicate a lower thermal stability. The decrease in thermal stability of cross-linked chitosan membranes is associated with reduced hydrogen bonding. Generally speaking, hydrogen bonds between polymer chains contribute to raising the degradation temperature. Cross-linking results in a loss of hydrogen bonding, and hence a lower degradation temperature for cross-linked membranes as compared to uncross-linked membranes [106]. The TGA results have also demonstrated that CsTP membrane has less thermal stability than CsP membrane. This is possibly

because CsTP has a higher degree of cross-linking and thus a larger extent of hydrogen bonding loss. The larger cross-linking density associated with CsTP membrane might be because triphosphate salt ($P_3O_{10}^{5-}$) with more negative charges has a higher ability to ionically cross-link with chitosan than phosphate salt (PO_4^{3-}) with a lower charge number.

Studies on the thermal behavior of Nafion[®] membrane have shown that this membrane is thermally stable up to 260 °C. Below this temperature, there is a gradual weight loss of 4 % which is mainly attributable to water evaporation. A decomposition stage with a weight loss of 12 % has been observed at range between 260 and 352 °C, and is associated with the desulfonation process (i.e. the loss of $-SO_3H$ groups) [107]. At temperatures above 352 °C, Nafion[®] membrane continues to decompose until about 99.9 % was lost at 520 °C. This weight loss is attributed to the decomposition of the perfluoropolyalkylether side chains and the polytetrafluoroethylene chains on its backbone [108]. TGA analysis shows that Nafion[®] membrane has better thermal properties than chitosan membrane, primarily because its main chain decomposes at 352 °C and its initial decomposition occurs at 260 °C, which is a higher decomposition temperature than that of chitosan membranes. However, DBFCs are operated in temperatures below 100 °C, and thus both chitosan hydrogel membranes are stable at desired operating temperatures of DBFCs.

DSC study was performed to understand the behavior of the cross-linked chitosan membranes on application of thermal energy. As presented in Figure 4.45, DSC

thermograms of both CsP and CsTP membranes exhibit broad endothermic peaks that are attributable to water loss at 35–160 °C. Endothermic peak of CsTP membrane is smaller than that of CsP membrane, which indicates a lower water-holding capacity of CsTP membrane as compared to CsP membrane. This might be explained by the difference in cross-linking density of these two membranes. As membranes are cross-linked, the membranes would be more rigid and structurally compact, and thus free volume available for water molecules would be decreased [109,110]. Besides, the number of available water absorption sites might be reduced as a result of cross-linking between amino groups of chitosan chain and phosphate or triphosphate salt. As indicated by TGA results, CsTP membrane might have a higher cross-linking density and thus it can be expected that CsTP membrane would have less free volume and absorption sites for water as compared to CsP membrane.

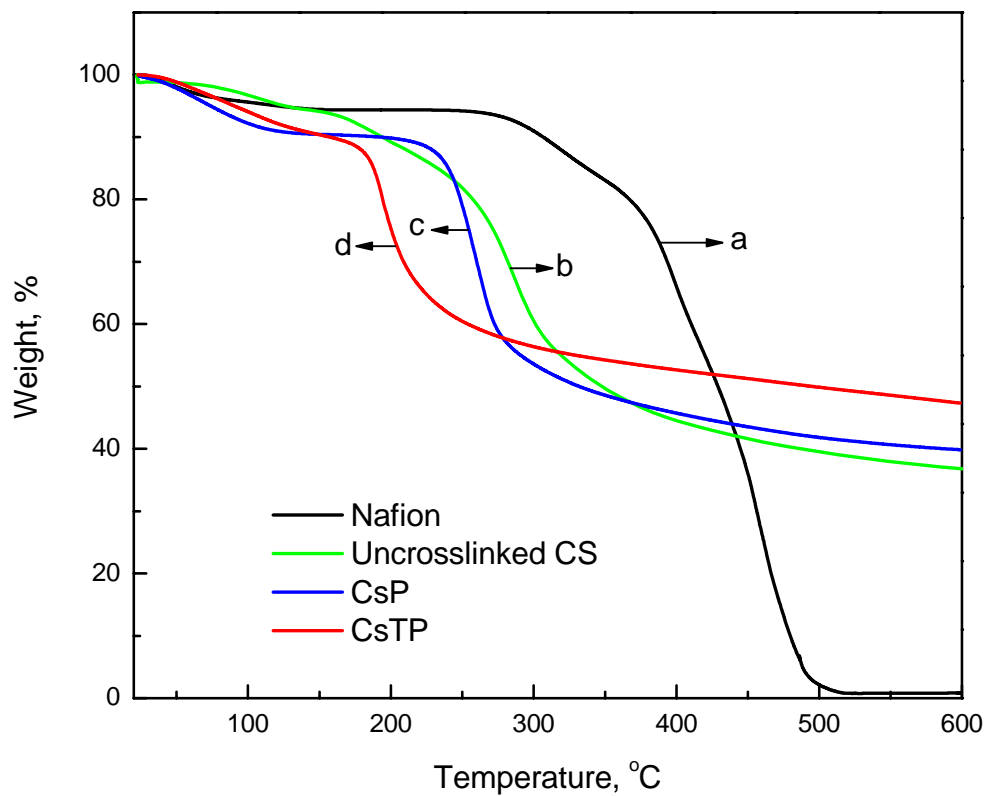


Figure 4.44 TGA thermograms of (a) Nafion[®], (b) pristine chitosan, (c) CsP, and (d) CsTP membranes.

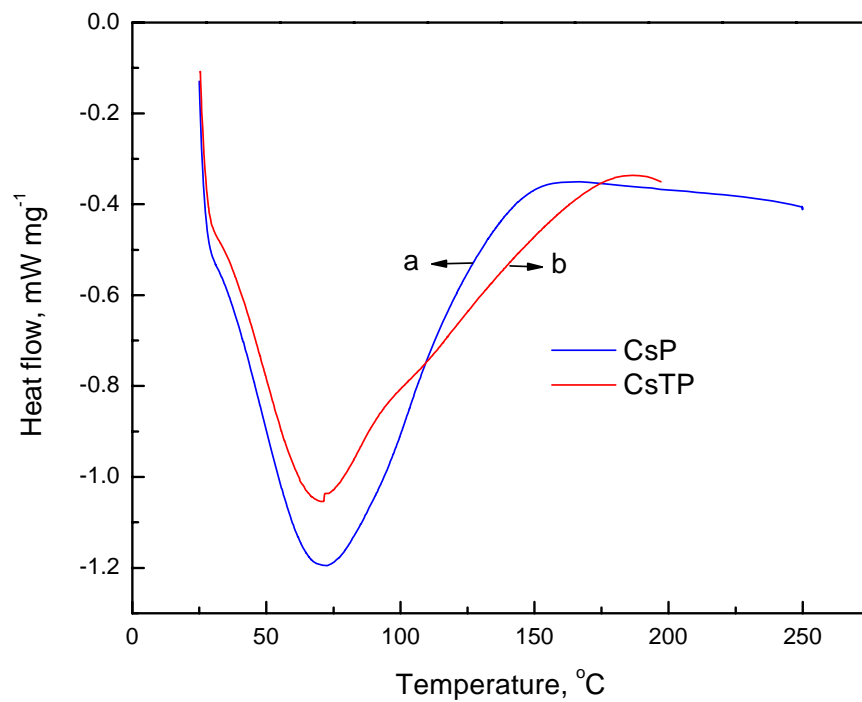


Figure 4.45 DSC thermograms of CsP and CsTP membranes.

Table 4.5 Water uptake values of Nafion[®], CsP, and CsTP membranes.

Membrane	Water uptake %	
	25 °C (step I)	100 °C (step I & II)
Nafion [®]	34	36
CsP	150	199
CsTP	102	144

Water uptake

Table 4.5 gives the results of water uptake for Nafion[®], CsP, and CsTP membranes. The membrane water uptake was determined at two different temperatures. When drying at room temperature for 24 h, the water uptake values of CsP and CsTP membranes were 150 % and 102 %, respectively, remarkably higher than that of Nafion[®] membrane (34 %). Weight losses of 36 %, 199 % and 144 % were observed for Nafion[®], CsP, and CsTP membranes, respectively, after the membranes were further dried at 100 °C for 3 h. Nafion[®] membrane demonstrated about the same weight loss after drying at two different temperatures. In case of chitosan hydrogel membranes, an approximately 40 % increase in water uptake values was found after the membranes were dried at an elevated temperature. From the above discussion, it can be surmised that chitosan membranes possess higher hydrophilic characteristics as compared to Nafion[®] membrane. As also indicated by the DSC study, water uptake results show that CsTP membrane has a lower water uptake capacity than CsP membrane, possibly because of a higher degree of cross-linking associated with CsTP membrane.

Mechanical properties

Since membranes for a DBFC are operated in aqueous environment, mechanical properties of membranes were tested in a water tank. Stress–strain curves of Nafion[®], CsP, and CsTP membranes are shown in Figure 4.46. Nafion[®] membrane demonstrates higher tensile strength at break (4.5 MPa), and lower elongation at break (18.7 %) than chitosan hydrogel membranes. Tensile strength and elongation at break of CsP membrane are 3.2 MPa and 46.7 % respectively. In case of CsTP membrane, tensile strength and elongation at break are 3.8 MPa and 50.7 % respectively. From the results, it can be observed that CsTP membrane exhibits higher strength and larger elongation at break than CsP membrane. When a certain degree of cross-linking is achieved, enough bridges and even a cross-linked network may be set up between the chitosan molecules, and as a result the tensile strength of the chitosan membrane is enhanced [72]. Thus, the higher mechanical strength of CsTP membrane is possible because CsTP membrane has a higher cross-linking density than CsP membrane, which is also indicated by TGA and water uptake studies. Besides, water uptake studies have shown that CsP has a higher degree of water content than CsTP membrane. Excessive high levels of water uptake can result in the dimensional change of the membranes, which leads to loss of mechanical properties [72].

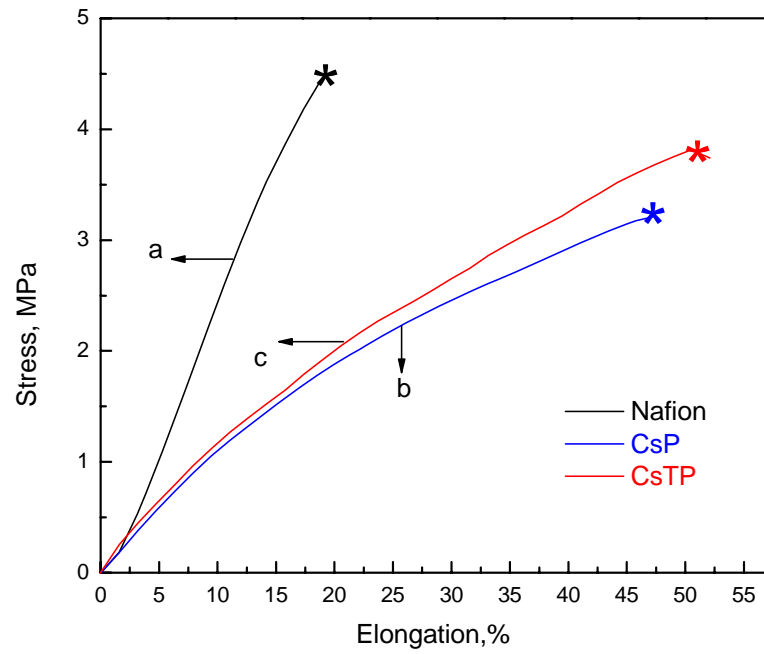


Figure 4.46 Stress–strain curves of (a) Nafion[®], (b) CsP, and (c) CsTP membranes.

Ionic conductivity

As given in Table 4.6, the conductivities of CsP and CsTP membranes after being equilibrated in alkaline medium are 0.089 and 0.114 S cm⁻¹, respectively. These values are higher than the ionic conductivity of Nafion[®] 212 membrane measured under the same conditions. The higher ionic conductivity of chitosan membranes than Nafion[®] membranes in alkaline medium may be attributed to higher water uptake capacity of chitosan. As shown in water uptake studies, chitosan membranes have significantly higher water holding capacity than Nafion[®] membrane. Greater water uptake ability of chitosan membrane leads to its greater uptake ability of electrolyte solutions such as NaOH, and ultimately contributes to a higher ionic conductivity which is related to the number and mobility of ions in the polymer complexes.

Considering the water uptake property, it is interesting to note that CsTP membrane with a lower water uptake value exhibits a higher ionic conductivity than CsP membrane. This is possibly because increased amount of water uptake dilutes ion concentration and extends the distance of ion migration due to membrane swelling [111]. The higher ionic conductivity associated with CsTP membrane might be also due to its larger number of anionic sites for sodium ion conduction, which is the result of its higher degree of cross-linking and larger number of negative charges of triphosphate than phosphate.

Borohydride crossover

As given in Table 4.6, borohydride crossover rates through CsP and CsTP membranes are calculated to be 4.57×10^{-8} and 1.32×10^{-8} mol s⁻¹ cm⁻², respectively. CsTP membrane demonstrates lower BH₄⁻ crossover rate than CsP membrane. This is possibly because, compared with CsP membrane, CsTP membrane has a larger number of anionic sites of negatively charged oxygen moieties, due to its higher degree of cross-linking and large number of negative charges of triphosphate salt, and these anionic sites repel BH₄⁻ of the same charge. As expected, borohydride crossover rate through CsP and CsTP membrane is higher than that through the Nafion[®] membrane by one order of magnitude.

Table 4.6 Ionic conductivity and borohydride crossover values of CsP and CsTP membranes

Membrane	Ionic conductivity measured after dipping in NaOH solution (S cm ⁻¹)	Borohydride crossover rate (mol s ⁻¹ cm ⁻²)
CsP	0.089	4.57×10^{-8}
CsTP	0.114	1.32×10^{-8}

4.4.3.2 Performance of DBFCs

Power Performance

A DBFC was assembled with either Nafion[®] 212 membrane or multivalent phosphate modified chitosan membrane, and its electrochemical performance was recorded. For a chitosan membrane-based DBFC, chitosan chemical hydrogel binder (2 wt.% loading) was used as anode catalyst binder. For a Nafion[®] membrane-based DBFC, Nafion[®] solution (12.5 wt.% loading) was used as anode catalyst binder. The anode was Ni+Pd/C on Ni foam (0.5 mm) with 5 mg metal cm⁻². Fuel was 5 wt.% NaBH₄ and 10 wt.% NaOH. Flow rate of the fuel was 5 mL min⁻¹. Cathode was Pt cathode (1 mg Pt cm⁻² on carbon paper). Oxidant was humidified oxygen. Flow rate of the oxidant was 0.15 L min⁻¹. As shown in Figure 4.47, peak power densities of Nafion[®]-based DBFC were 204 and 448 mW cm⁻² at 30 and 60 °C, respectively. DBFC employing CsP membrane achieved peak power densities of 282 and 657 mW cm⁻² at 30 and 60 °C, respectively. DBFC employing CsTP membrane achieved peak power densities of 295 and 685 mW cm⁻² at 30 and 60 °C, respectively. Significantly higher power performance was achieved by chitosan-based DBFC as compared with Nafion[®]-based one. This can be attributed to the higher ionic conductivity of chitosan hydrogel membrane in alkaline medium than Nafion[®] membrane as demonstrated by the EIS study. Besides, chitosan-based DBFC employed chitosan chemical hydrogel as anode binder which has a larger water retention capacity and thus is more effective in attaining high mobility of ions, fuel within the hydrogel-bonded electrode matrix. CsTP membrane gave slightly superior power performance as compared to CsP

membrane, and this result was consistent with that of EIS study which showed that the ionic conductivity of CsTP membrane was higher than that of CsP membrane in alkaline medium.

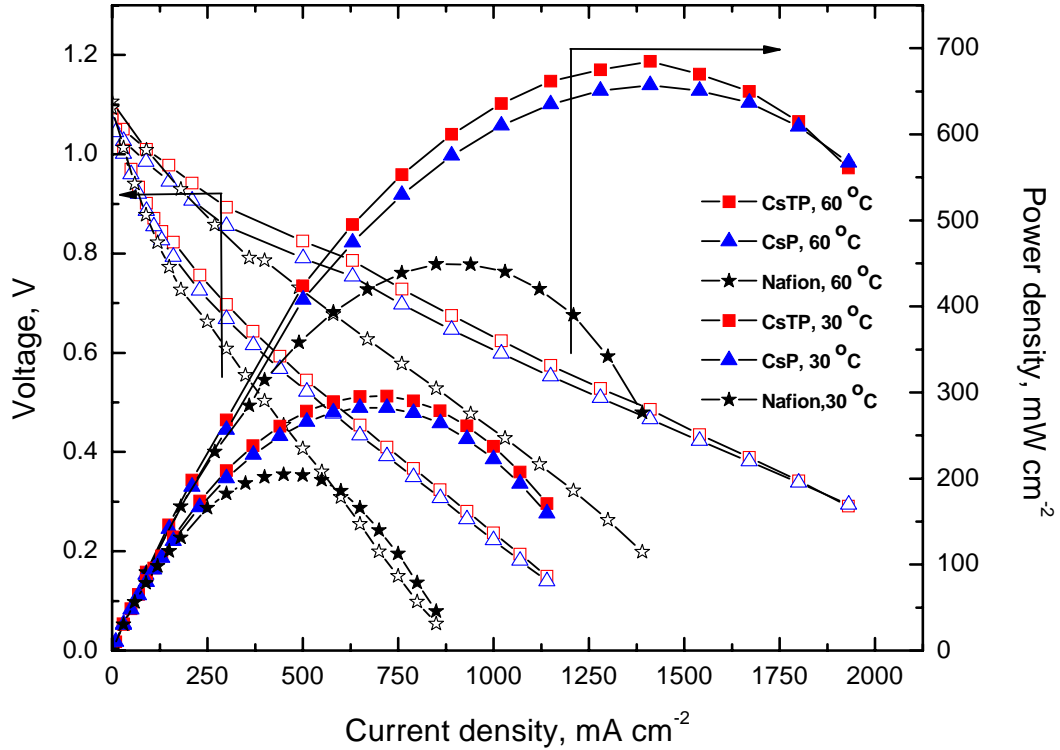


Figure 4.47 Plots of cell polarization and power density versus current density for DBFCs using Nafion[®], CsP, and CsTP membranes at 30 and 60 °C.

Stability

Performance stability of a DBFC using CsP or CsTP membrane was tested by monitoring the cell voltage change during the galvanostatic discharge of 120 mA cm^{-2} in a period of more than 100 h at $30 \text{ }^\circ\text{C}$. For a chitosan membrane-based DBFC, chitosan chemical hydrogel binder (2 wt.% loading) was used as anode catalyst binder. For a Nafion[®] membrane-based DBFC, Nafion[®] solution (12.5 wt.% loading) was used as anode catalyst binder. The anode was Ni+Pd/C on Ni foam (0.5 mm) with $5 \text{ mg metal cm}^{-2}$. Fuel was 5 wt.% NaBH_4 and 10 wt.% NaOH . Flow rate of the fuel was 5 mL min^{-1} . Cathode was Pt cathode (1 mg Pt cm^{-2} on Toray[®] carbon paper). Oxidant was humidified oxygen. Flow rate of the oxidant was 0.15 L min^{-1} . As shown in Figure 4.48 and Figure 4.49, the DBFC exhibited a stable performance over the test period. The operating cell voltage was fairly constant at 0.8 V with slight fluctuations over the test period. In order to evaluate the stability of multivalent phosphate modified chitosan hydrogel membrane at an elevated temperature, stability of a DBFC using CsTP membrane was recorded at $60 \text{ }^\circ\text{C}$ and compared with a Nafion[®]-based DBFC under the same condition. As shown in Figure 4.50, chitosan-based DBFC showed comparable stability as a Nafion[®]-based one. Thus chitosan-based DBFC demonstrated not only high power performance but also reasonable stability at both low and elevated temperatures.

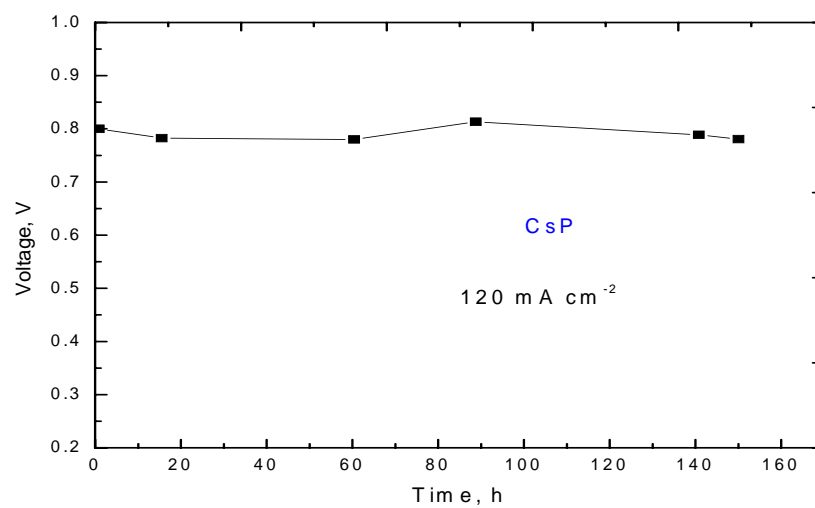


Figure 4.48 Performance stability of a DBFC using CsP membrane at 30 °C.

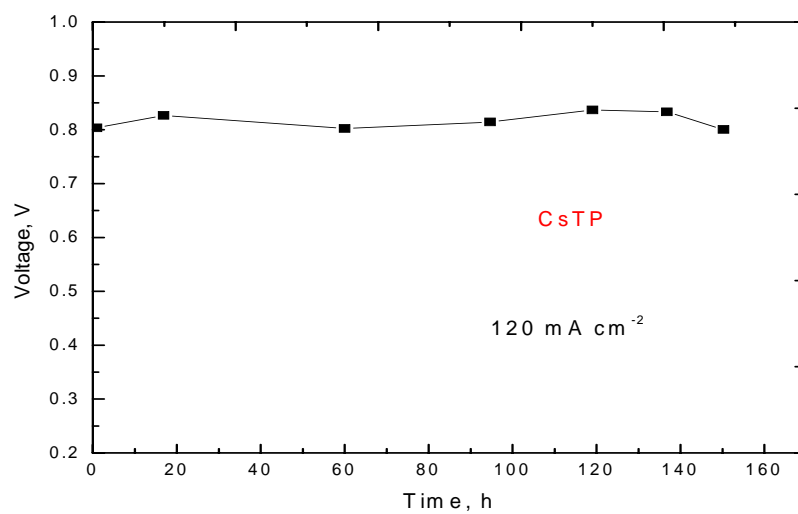


Figure 4.49 Performance stability of a DBFC using CsTP membrane at 30 °C.

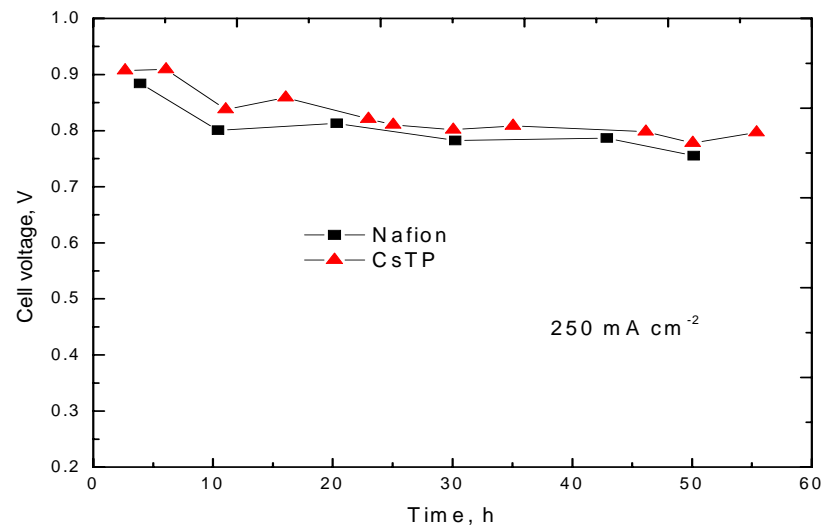


Figure 4.50 Comparative performance stability of chitosan-based DBFC and Nafion[®]-based DBFC at 60 °C.

Coulombic Efficiency

To investigate the fuel utilization, coulombic efficiencies of the chitosan-based and Nafion[®]-based DBFCs were analyzed under a constant current discharge. For a chitosan membrane-based DBFC, chitosan chemical hydrogel binder (2 wt.% loading) was used as anode catalyst binder. For a Nafion[®] membrane-based DBFC, Nafion[®] solution (12.5 wt.% loading) was used as anode catalyst binder. The anode was Ni+Pd/C on Ni foam (0.5 mm) with 5 mg metal cm⁻². Fuel was 5 wt.% NaBH₄ and 10 wt.% NaOH. Flow rate of the fuel was 5 mL min⁻¹. Cathode was Pt cathode (1 mg Pt cm⁻² on Toray[®] carbon paper). Oxidant was humidified oxygen. Flow rate of the oxidant was 0.15 L min⁻¹. As shown in Figure 4.51, Figure 4.52, and Figure 4.53, the cell voltage under these currents stayed almost stable, with slow drop caused by the gradual decrease of NaBH₄ concentration. The final rapid drop of cell voltage was due to the exhaustion of NaBH₄. Based on the chronopotentiometric curves, coulombic efficiencies for DBFCs employing Nafion[®], CsP, and CsTP membrane were estimated to be in the range of 31-42 %, 31-38 %, 31-41 %, respectively. Borohydride undergoes hydrolysis both chemically and electrochemically on various electrode materials of DBFCs. This leads to the evolution of hydrogen at the anode, which limits the coulombic efficiency. The actual number of electron transferred of the anodic reaction depends on the anodic materials, and current etc. The anode catalyst employed in this study was Ni and Pd/C composite. It has been found that the borohydride electro-oxidation on Ni is generally a four-electron process even with changing currents and borohydride concentrations, while in case of Pd and Pt, the coulombic number is

higher than four electrons at high anode currents and low borohydride concentrations. The coulombic efficiency loss is also attributed to borohydride crossover from the anodic side to the cathodic one through membrane, and remaining borohydride in the anode chamber which cannot be used due to mass transfer limitations. It can also be seen that the voltage of chitosan-based DBFC was more stable than that with Nafion[®] materials. This is possible because the use of chitosan hydrogel binder facilitates mass transport of fuel from the anode diffusion layer to anode catalyst layer [112].

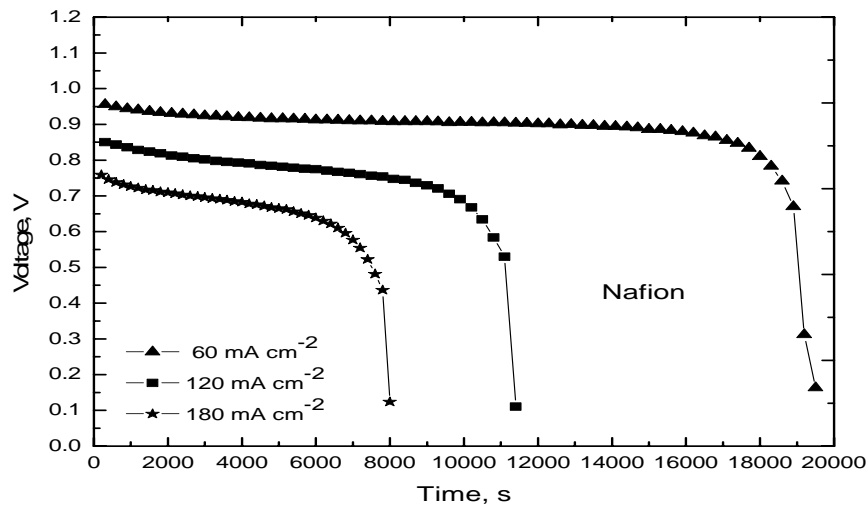


Figure 4.51 Fuel efficiency of a DBFC using Nafion[®] membrane and Nafion[®] binder at 30 °C.

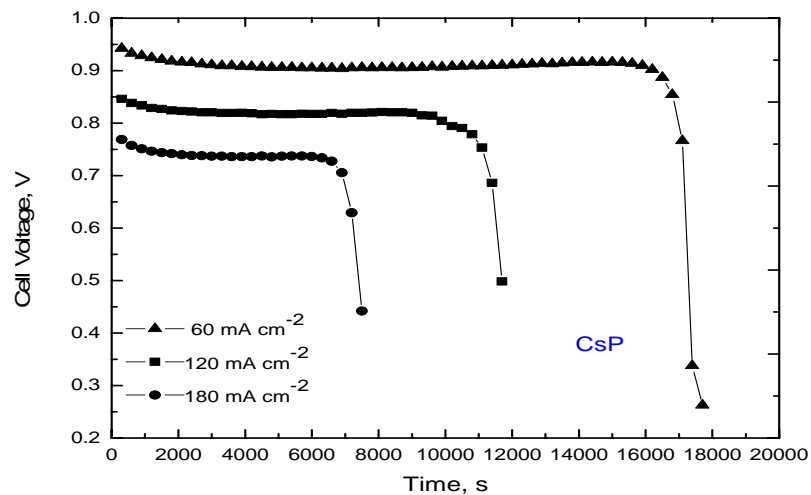


Figure 4.52 Fuel efficiency of a DBFC using CsP membrane and chitosan hydrogel binder at 30 °C.

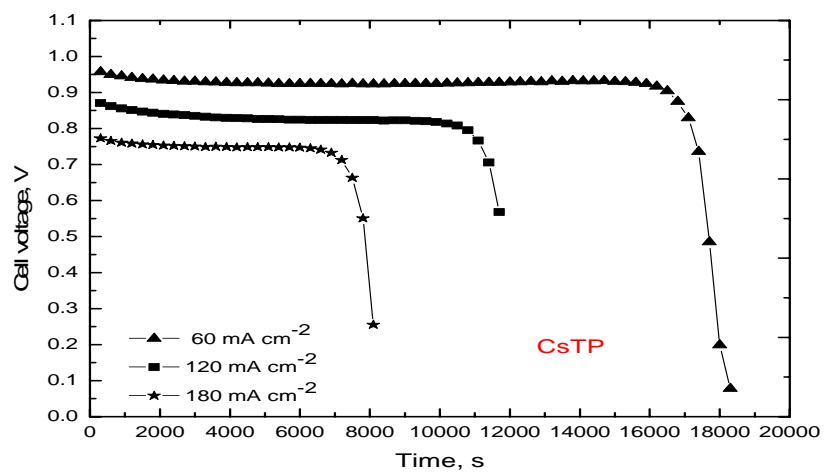


Figure 4.53 Fuel efficiency of a DBFC using CsTP membrane and chitosan hydrogel binder at 30 °C.

Chapter 5 Summary and Future Work

Summary

Cost and performance are two major factors affecting commercialization of various types of fuel cells. Membrane-electrode-assembly is a major cost of a single direct borohydride fuel cell. Thus, the cost of these materials needs to be reduced to produce economical DBFCs. This study focuses on developing high performance and cost-effective membrane-electrode-assembly materials for DBFCs.

First, an active single fuel cell system has been established and various operational parameters such as anolyte and catholyte flow rate, anolyte concentration, gas humidity, have been examined and optimized for this DBFC system. Non-precious electrocatalyst materials are available for the electro-reduction of oxidant and the electro-oxidation of borohydride. This advantage of DBFC over H₂-PEFC and DMFC provides a solution to reduce DBFC costs. The anode electrocatalyst employed in this study was a composite of Ni catalyst with either carbon supported Pd or with carbon supported Pt. The amount of Pd or Pt used was low (weight ratio of Ni and Pt or Pd being 25:1). A small enhanced power density was found by increasing the loading of anodic catalyst. A DBFC with Ni+Pt/C composite anodic catalyst gave higher power density than that using Ni+Pd/C. Ni foam was found to be superior to carbon paper as anode substrate for application in a DBFC since it extends electrochemical active area and facility two-phase transport.

Physical vapor deposition provided a way to reduce catalyst loading and increase uniformity of catalyst coating. Both reasonably good power performance and stability were achieved by a DBFC using Ni-based composite anode. H_2O_2 is a good oxidant for air deficient applications. A borohydride- H_2O_2 fuel cell was assembled with a nickel-based composite anode and an electrodeposited Pd cathode, and this cell achieved peak power densities of 327 mW cm^{-2} and 665 mW cm^{-2} at $28 \text{ }^\circ\text{C}$ and $60 \text{ }^\circ\text{C}$, respectively.

Polymer binder is an important constituent of an electrode. To develop low-cost and effective binders in place of expensive Nafion[®] ionomer, chemical hydrogel based on polyvinyl alcohol (PVA) and chitosan have been prepared. Chitosan chemical hydrogel binder performed better than commercial Nafion[®] binder, whereas PVA chemical hydrogel binder performed as well as Nafion[®] binder in a direct NaBH_4 - H_2O_2 fuel cell. The better electrochemical performance of chitosan binder as compared to that of PVA as well as Nafion[®] binders is due to the better water retention capability of chitosan.

Chemically cross-linked PVA hydrogel membrane has been prepared by a solution casting method and employed in a DBFC. NaBH_4 - H_2O_2 fuel cells using Nafion[®] membranes exhibited higher power densities than those employing PVA hydrogel membrane, possibly due to the higher rate of undesired crossover of PVA hydrogel membrane than Nafion[®] membranes. The peak power densities of the PVA hydrogel membrane-based DBFCs were a little higher than those of DBFCs using Nafion[®] membranes at $60 \text{ }^\circ\text{C}$, indicating the effectiveness of the PVA membrane in DBFCs when

oxygen or air was used as the oxidant. This fuel cell was able to perform a good stability for more than 100 h.

Chitosan is an abundant natural biopolymer. Chitosan membranes were prepared and heterogeneously modified by sulfuric acid/sulfate, phosphate and triphosphate. Chitosan hydrogel membrane was also prepared by homogeneously cross-linking with glutaraldehyde. Chitosan hydrogel membranes were characterized in terms of SEM, FTIR, thermal properties, mechanical properties, water uptake, ionic conductivity, and borohydride crossover rate, and some of these characteristics were compared with commercial Nafion[®] 212 membrane. Thermal stability analysis revealed that chitosan hydrogel membranes could withstand temperature higher than 200 °C in nitrogen atmosphere, which ensures their thermal stability in the operational temperature of DBFCs. Tensile test showed that chitosan hydrogel membranes had higher elongation and lower tensile strength at break in aqueous medium than Nafion[®] membrane. Chitosan hydrogel membranes demonstrated higher water uptake, higher ionic conductivity in alkaline medium and higher borohydride crossover rate than Nafion[®] membrane. Characterization results indicated that triphosphate chitosan hydrogel membrane had higher cross-linking density than tribasic phosphate chitosan hydrogel membrane. Under identical conditions, chitosan hydrogel membrane exhibited better power performance as compared to Nafion[®] 212 membrane in a DBFC at both 30 and 60 °C. The performance of chitosan membrane-based DBFC was further improved by using chitosan chemical hydrogel as anode binder as compared to Nafion[®] binder. A borohydride-oxygen fuel cell employing

triphosphate chitosan membrane and chitosan binder achieved a peak power density of 685 mW cm⁻² at 60 °C, which is over 50 % higher than the power performance of a DBFC using commercial Nafion[®] materials. The chitosan-based DBFC exhibited a stable fuel cell performance for a continuous duration of more than 100 h. Comparable performance stability was achieved by a chitosan-based DBFC as compared to Nafion[®]-based DBFC at an elevated temperature. Various studies show that chitosan is a cost-effective alternative material to Nafion[®] for application in direct borohydride fuel cells. Use of chitosan in DBFC would significantly reduce its cost and may help in its commercialization.

Future work

Despite the rapid development of DBFCs, they are still at the initial stage and many problems remain unsolved. Borohydride hydrolysis lowers coulombic efficiency of the fuel cell. Beside, hydrogen gas evolution from hydrolysis complicates the mass transport and this problem is enlarged in DBFC multi-cell stacks. A key point to solve this problem is to develop anode electrocatalysts which possess high catalytic activity towards borohydride electro-oxidation and capability of making the electro-oxidation of BH₄⁻ via a quasi-eight-electron process or intrinsic eight-electron process. This is, however, difficult to achieve. Thus, instead of completely eliminating hydrogen evolution, keeping a balanced rate of hydrogen generation and consumption might be a more practical way to achieve high power performance as well as high coulombic efficiency. In addition, anode structure needs to be modified to accommodate the two-phase flow in the anode and also

maximize the active reaction area. To achieve optimization of anode electrode pore size, a theoretical modeling study is needed to guide material design, so that the transport of liquid fuel and release of unreacted hydrogen gas are well balanced and also ionic and electronic conductions are both optimal.

Borohydride crossover results in inefficient use of the fuel and deterioration of cathode catalysts, thereby adversely affecting DBFC performance. Development of low-cost polymer membranes with little BH_4^- crossover is a key in bringing DBFC to the level of common usage. Membrane plays an important role in water management in the whole fuel cell. Water uptake of a membrane electrolyte needs to be optimized to achieve ideal ionic conductivity, mechanical strength and other properties. A theoretical model should be established to gain a better understanding the mechanism of ion transfer, and the effect of water uptake in membrane properties. Another attractive solution to borohydride crossover might be to use cathode catalysts with high activity and selectivity to electro-reduction of oxidant and high tolerance to borohydride crossover.

Cost, is the hurdle to commercialization of various types of fuel cells. In addition to the cost of an MEA, cost of borohydride compounds is very high and it needs to be decreased significantly to make DBFC commercially viable. It is expected that the cost of NaBH_4 can be reduced by improving its synthesis techniques and by meta-borate recycling. Stability of DBFC single cell and stack performances have been reported for relatively shorter periods as compared to H_2 -PEFC and DMFC. Stability for long periods tests, 1000 h for instance, are needed for further research. Power performance and stability need to be

considered into cost estimation of membrane and electrode, since short material lifetime or low material performance will reduce cost per time or cost per power, respectively.

References

- [1] Amendola SC, Onnerud P, Kelly MT, Petillo PJ, Sharp-Goldman SL, Binder M. J. Power Sources 1999; 84:130.
- [2] Li ZP, Liu BH, Arai K, Suda S. J. Electrochem. Soc. 2003; 150: A868.
- [3] Indig ME, Snyder RN. J. Electrochem. Soc. 1962; 109: 1104.
- [4] Cost Analysis of Fuel Cell Systems for Transportation Compressed Hydrogen and PEM Fuel Cell System Discussion Fuel Cell Tech Team FreedomCar Detroit. MI, October 20, 2004, TIAX LLC Acorn Park Cambridge, Massachusetts 02140-2390.
- [5] U.S.Ozkan, Course 713 Lecture notes, 2009.
- [6] Demirci UB. J. Power Sources 2007; 172676.
- [7] Santos DMF, Sequeira CAC, Renew. Sust. Energ. Rev. 2011; 15: 3980.
- [8] Morris JH, Gysing HJ, Reed D. Chem. Rev. 1985; 85: 51.
- [9] Gardiner JA, Collat JW. J. Am. Chem. Soc. 1965; 87:1692.
- [10] Liu BH, Suda S. J. Alloys and Compounds 2008; 454: 280.
- [11] Larminie J, Dicks A. (Eds.) Fuel Cell System Explained, Second Edition, Wiley 2003.
- [12] Elder JP, Hickling A. Trans. Faraday Soc. 1962; 58:1852.
- [13] Gyenge E. Electrochim. Acta 2004; 49: 965.
- [14] Mirkin MV, Yang H, Bard AJ. J. Electrochem. Soc. 1992; 139:2212.
- [15] Cheng H, Scott K. Electrochim. Acta 2006; 51:3429.

- [16] Krishnana P, Yang TH, Advani SG, Prasad AK. *J. Power Sources* 2008; 182:106.
- [17] Chatenet M, Micoud F, Roche I, Chainet E. *Electrochim. Acta* 2006; 51:5459.
- [18] Lee SM, Kim JH, Lee HH, Lee PS, Lee JY. *J. Electrochem. Soc.* 2002; 149: A603.
- [19] Raman RK, Choudhury NA, Shukla AK. *Electrochem. and Solid-State Lett.* 2004; 7:A488.
- [20] Greef R, Peat R, Peter L, Pletcher D, Robinson J, *Instrumental methods in electrochemistry*. Chichester, UK: Ellis Horwood; 1985.
- [21] Liu BH, Li ZP, Suda S. *Electrochim. Acta* 2004; 49: 3097.
- [22] Cheng H, Scott K, Lovell K. *Fuel Cells* 2006; 6:367.
- [23] Geng X, Zhang H, Ye W, Ma Y, Zhong H. *J. of Power Sources* 2008; 185: 627.
- [24] Sabatier J, Senderens JB. *Compt. Rend.*, 1899; 128: 1173.
- [25] Liu BH, Li ZP, Suda S. *J. Power Sources* 2008; 185: 1257.
- [26] Gyenge E, Atwan MH, Northwood DO. *J. Electrochem. Soc.* 2006; 153:A150.
- [27] Atwan MH, Northwood DO, Gyenge EL. *Int. J. Hydrogen Energy* 2005; 30:1323.
- [28] Atwan MH, Macdonald CLB, Northwood DO, Gyenge EL. *J. Power Sources* 2006; 158:36.
- [29] Atwan MH, Northwood DO, Gyenge EL. *Int. J. Hydrogen Energy* 2007; 32: 3116.
- [30] Jamard R, Latour A, Salomon J, Capron P, Martinent-Beaumont A. *J. Power Sources* 2008; 176:287.
- [31] Cao D, Chen D, Lan J, Wang G, *J. Power Sources* 2009; 190: 346.
- [32] Feng RX, Dong H, Cao YL, Ai XP, Yang HX. *Int J Hydrogen Energy* 2007; 32:4544.

- [33] Liu BH, Suda S. *J. Alloys and Compounds* 2008; 454: 280.
- [34] Ponce de León C, Walsh FC, Pletcher D, Browning DJ, Lakeman JB. *J. Power Sources* 2006; 155:172.
- [35] Gupta S, Tryk D, Bae I, Aldred W, Yeager E, *J. Appl. Electrochem.* 1989; 19: 19.
- [36] Villers D, Jacques-Bedard X, Dodelet JP, *J. Electrochem. Soc.* 2004; 151: A1507.
- [37] Bashyam R, Zelenay P. *Nature* 2006; 443: 63.
- [38] Chatenet M, Micoud F, Roche I, Chainet E, Vondrák J. *Electrochim. Acta* 2006; 51:5452.
- [39] Wang YG, Xia YY. *Electrochem. Commun.* 2006; 8:1775.
- [40] Ma J, Liu Y, Zhang P, Wang J. *Electrochem. Commun.* 2008; 10:100.
- [41] Ma J, Wang J, Liu Y. *J. Power Sources* 2007; 172: 220.
- [42] Cheng H, Scott K. *J. Electroanal. Chem.* 2006; 596:117.
- [43] Qin HY, Liu ZX, Yin WX, Zhu JK, Li ZP. *J. Power Sources* 2008; 185: 909.
- [44] Ma J, Liu Y, Liu Y, Yan Y, Zhang P. *Fuel Cells* 2008; 8: 394.
- [45] Gu L, Luo N, Miley GH. *J. Power Sources* 2007; 173: 77.
- [46] Cao D, Chao J, Sun L, Wang G, *J. Power Sources* 2008;179:87.
- [47] Raman RK, Shukla AK. *J. Appl. Electrochem.* 2005; 35:1157.
- [48] Selvarani G, Prashant SK, Sahu AK, Sridhar P, Pitchumani S, Shukla AK. *J. Power Sources* 2008; 178: 86.
- [49] Kim JH, Kim HS, Kang YM, Song MS, Rajendran S, Han SC, et al. *J. Electrochem. Soc.* 2004; 151: A103.

- [50] Cheng H, Scott K. *J. Appl. Electrochem.* 2006; 36:1361.
- [51] Ponce de León C, Bavykin DV, Walsh FC. *Electrochem. Commun.* 2006; 8:1655.
- [52] Liu BH, Li ZP, Arai K, Suda S. *Electrochim. Acta* 2005; 50:3719.
- [53] Cheng H, Scott K, Lovell KV, Horsfall JA, Waring SC. *J. Membr. Sc.* 2007; 288: 168.
- [54] Alberti G, Casciola M, *Ann. Rev. Mater. Res.* 2003; 33:129.
- [55] Celik C, San FGB, Sarac HI. *J. Power Sources* 2008; 185:197.
- [56] Jamard R, Latour A, Salomon J, Capron P, Martinent-Beaumont A. *J. Power Sources* 2008; 176:287.
- [57] Li ZP, Liu BH, Zhu JK, Suda S. *J. Power Sources* 2006; 163:555.
- [58] Duteanu N, Vlachogiannopoulos G, Shivhare MR, Yu EH, Scott K. *J. Appl. Electrochem.* 2007; 37: 1085.
- [59] Cheng H, Scott K. *J. Power Sources* 2006; 160: 407.
- [60] Coowar FA, Vitins G, Mepsted GO, Waring SC, Horsfall JA. *J. Power Sources* 2008; 175:317.
- [61] Ponce de León C, Walsh FC, Rose A, Lakeman JB, Browning DJ, Reeve RW. *J. Power Sources* 2007; 164: 441.
- [62] Raman RK, Shukla AK. *Fuel Cells* 2007; 7: 225.
- [63] Raman RK, Prashant SK, Shukla AK. *J. Power Sources* 2006; 162:1073.
- [64] Choudhury NA, Raman RK, Sampath S, Shukla AK. *J. Power Sources* 2005; 143:1.
- [65] Wan Y, Creber KAM, Peppley B, Tam Bui V, *Polymer* 2003; 44: 1057.

- [66] Lo'pez-Cha'vez E,. Marti'nez-Magada'n JM, Oviedo-Roa R, Guzma'n J, Rami'rez-Salgado J, Mari'n-Cruz J, *Polymer* 2005; 46: 7519.
- [67] Singh A, Narvi SS, Dutta PK, Pandey ND, *Bull. Mater. Sci.* 2006; 29: 233.
- [68] Monteiro OAC, Airoidi C, *Int. J. Biol. Macromol.* 1999; 26: 119.
- [69] N.S. Mohamed, R.H.Y. Subban, A.K. Arof, *J. Power Sources* 56 (1995) 153–156.
- [70] Morni NM, Arof AK, *J. Power Sources* 1999;77: 42.
- [71] Osifo PO, Masala A, *J. Power Sources* 2010; 195: 4915.
- [72] Wan Y, Creber KAM, Peppley B, Tam Bui V, *J. Appl. Polym. Sci.* 2003; 89: 306.
- [73] Mukoma P, Jooste BR, Vosloo HCM, *J. Power Sources* 2004; 136: 16.
- [74] DeMerlis CC, Schoneker DR, *Food Chem. Toxicol.* 2003; 41: 319.
- [75] Kim SY, Shin HS, Lee YM, Jeong CN, *J. Appl. Polym. Sci.* 1999; 73: 1675.
- [76] Sahu AK, Selvarani G, Pitchumani S, Sridhar P, Shukla AK, Narayanan N,. Banerjee A, Chandrakumar N, *J. Electrochem. Soc.* 2008; 155:B686.
- [77] Guo R, Hu C, Li B, Jiang Z, *J. Membr. Sci.* 2007; 289:191.
- [78] Sodium Borohydride Digest; Morton International Inc., Specialty Chemical Group: Danvers, MA, 1989.
- [79] Gardiner JA, Collat JW, *J. Am. Chem. Soc.* 1985; 87:1692.
- [80] Lichtenstein IE, Mras JS, *J. Franklin Inst.* 1988; 281: 481.
- [81] Mirkin MV, Bard A, *J. Anal. Chem.* 1991; 63: 532.
- [82] Lakeman JB, Rose A, Pointon KD, Browning DJ, Lovell KV, Waring SC,. Horsfall JA, *J. Power Sources* 2006; 162: 765.

- [83] Celikkan H, Aydin H, Aksu ML, Turk. J. Chem. 2005; 29: 519.
- [84] Liu B, Li Z, Suda S, J. Power Sources 2008; 175: 226.
- [85] Li ZP, Liu BH, Arai K, Asaba K, Suda S, J. Power Sources 2004; 126: 28.
- [86] Raman RK, Choudhury NA, Shukla AK, Electrochem. Solid. St. 2004; 7: A488.
- [87] Kim C, Kim K, Ha MY, J. Power Sources 2008; 154: 161.
- [88] Park KT, Jung UH, Jeong SU, Kim SH, J. Power Sources 2006; 162: 192.
- [89] Peppas NA, Hydrogels in Medicine and Pharmacy: Fundamentals, Vol. 1, CRC Press, 1986.
- [90] Berger J, Reist M, Mayer JM, Felt O, Peppas NA, Gurny R, Eur. J. Pharm. Biopharm. 2004; 57: 19.
- [91] Biffinger JC, Kim HW, DiMagno SG, ChemBioChem 2004; 5: 622.
- [92] Mauritz KA, Moore RB, Chem. Rev. 2004; 104: 4535.
- [93] Yeom CK, Lee KH, J. Membr. Sci. 1996; 109: 257.
- [94] Goto M, Shiosaki A, Hirose T, Sep. Sci. Technol. 1994; 29: 1915.
- [95] Choudhury NA, Shukla AK, Sampath S, Pitchumani S, J. Electrochem. Soc., 2006; 153:A614.
- [96] Choudhury NA, Prashant SK, Pitchumani S, Sridhar P, Shukla AK, J. Chem. Sci. 2009; 121: 1.
- [97] S. Agro, T. DeCarmine, S. DeFelice, L. Thoma, Annual Progress Report for the DOE Hydrogen Program, 2005, p. 790, US Department of Energy (DOE) website: <http://www.hydrogen.energy.gov>.

- [98] Santos DMF, Sequeira CAC, ECS Transactions 2010; 25: 111.
- [99] Bendert JC, Papadias DD, Myers DJ, J. Electrochem. Soc. 2010; 157: B1486.
- [100] Lian Q, Samuels R, Antec '96: Plastics-Racing into the Future 1996; 42: 1709.
- [101] Li JY, Nasser SN, Mech. Mater. 2000; 32: 303.
- [102] Jiang Z, Zheng X, Wu H, Wang J, Wang Y, J. Power Sources 2008; 180:143.
- [103] Ramírez-Salgado J, Electrochim. Acta 2007; 52: 3766
- [104] Du JF, Bai Y, Chu WY, Qiao LJ, J. Polym. Sci. Pol. Phys. 2010; 48: 880.
- [105] Sumner JJ, Creager SE, Ma JJ, Des Marteau DD, J. Electrochem. Soc. 1998; 145: 107.
- [106] Wan Y, Creber KAM, Peppley B, Tam Bui V, Macromol. Chem. Phys. 2003; 204:
- [107] Surowiec J, Bogoczek R, J. Therm. Anal. 1988; 33: 1097.
- [108] Samms SR, Wasmus S, Savinell RF, J. Electrochem. Soc. 1996; 143: 1498.
- [109] Seo JA, Koh JH, Roh DK, Kim JH, Solid State Ionics 2009; 180: 998.
- [110] Jiang Z, Zheng X, Wu H, Wang J, Wang Y, J. Power Sources 2008; 180: 143.
- [111] Wan Y, Peppley B, Creber KAM, Tam Bui V, J. Power Sources 2010; 195: 3785.
- [112] Lai Q, Yin G, Wang Z, Du C, Zuo P, Cheng X, Fuel Cells 2008; 8: 339.